

Jagellonian University

Institute of Physics

# Hadronic interaction of $\eta$ and $\eta'$ mesons with protons

Paweł Moskal

Habilitation thesis prepared at the Department of Nuclear Physics in the Institute of Physics of the Jagellonian University and at the Institute of Nuclear Physics of the Research Centre Jülich, submitted to the Faculty of Physics, Astronomy and Applied Computer Science at the Jagellonian University, for the postdoctoral lecture qualification.

Cracow 2004



## Acknowledgement

Accomplishment of the experiments presented in this treatise was possible only thanks to the joined effort of friends from the COSY-11 group with whom I had the luck to work during many years of my involvement at the Jagellonian University in Poland and the Research Centre Jülich in Germany. I am greatly indebted to all of them for their help.

A person whom I own most and whom I revere and admire is Professor Walter Oelert, inventor of the COSY-11 facility and founder of the COSY-11 collaboration. It is only due to his great open mindedness and understanding that I could devote a lot of my time to study physics while working as a physicist. I thank you from the bottom of my heart for the time devoted, support and patience, the latter so often tried to the utmost.

I am profoundly grateful to Professor Lucjan Jarczyk and Professor Walter Oelert for being my promotors in the truest sense of this word.

Wise and friendly advise, encouragement and direct reprimands of Professor Lucjan Jarczyk I value more highly than I can express in words.

At the last stage of completing this dissertation I was pleased to work together with talented and zealous students: Master of Science Rafał Czyżykiewicz, Master of Science Michał Janusz, Master of Science Paweł Klaja, Master of Science Cezary Piskor-Ignatowicz, and Master of Science Joanna Przerwa. When introducing you to the experimental technique I certainly gained more than yourselves and for an instant I will not regret the time spent together. I am especially thankful to Joanna who kindly agreed to defend our recent experimental proposal and who with her unbelievable charm and serenity made our daily work pleasurable.

One of the many factors which motivated me to conduct this work was the written wish of Master of Science Peter Winter who had wanted to adress me in the acknowledgements of his PhD thesis without a negation in front of the title he had granted me in advance. Although it is probably too late, I did do my best.

For the perusal of parts of this manuscript I owe a great debt to Prof. Lucjan Jarczyk, Prof. Walter Oelert, Dr. Thomas Sefzick, Dr. Dieter Grzonka, Dr. hab. Jerzy Smyrski, Dr. Magnus Wolke, Mgr. Rafał Czyżykiewicz, Prof. Bogusław Kamys, Dr. Christoph Hanhart, Dr. Vadim Baru, and Mrs. Joanna Czekotowska. This treatise benefited immeasurably from your emendations and critical remarks concerning the earlier version. Still it does not make me any less responsible for any mistake I may have made.

For the support of my activities in the Department of Nuclear Physics of the Jagellonian University and for the approval of my work I am grateful to Prof. Reinhard Kulessa, and for the inestimable support of my work in the Nuclear Physics Institute of the Research Centre Jülich I am thankful to Prof. Kurt Kilian.

Last but not least, I do appreciate very much the support, patience and love of Żaneta, Ines and Gabriel.

# Contents

<b>Preface</b>	<b>7</b>
<b>1 Introduction</b>	<b>9</b>
<b>2 Manifestation of hadronic interactions</b>	<b>17</b>
<b>3 Definitions of observables</b>	<b>21</b>
3.1 Cross section . . . . .	21
3.2 Partial waves – selection rules . . . . .	24
3.3 Phase space population . . . . .	30
3.4 Orientation of the emission plane . . . . .	33
<b>4 Low energy interaction within the <math>pp\eta</math> and <math>pp\eta'</math> systems</b>	<b>37</b>
4.1 Range of the dominance of the $^3P_0 \rightarrow ^1S_0 s$ transition . . . . .	37
4.2 Influence of the $pp\eta$ and $pp\eta'$ interaction on the excitation function of the $pp \rightarrow pp\eta(\eta')$ reaction	41
4.3 Phenomenology of the proton-proton initial and final state interaction	49
4.4 Qualitative comparison between $pp\eta$ , $pp\eta'$ , and $pp\pi^0$ interactions . . .	53
4.5 Dalitz plot occupation for the $pp\eta$ system . . . . .	55
4.6 Quasi-bound state . . . . .	61
4.7 Search for a signal from $\eta'$ -proton interaction in the invariant mass distributions	65
<b>5 Dynamics of the near threshold production of <math>\eta</math> and <math>\eta'</math> mesons in collisions of nucleons</b>	<b>67</b>
5.1 Comparison of the production yields . . . . .	67
5.2 Mesonic degrees of freedom . . . . .	70
5.3 Baryonic resonance – a doorway state for the production of the meson $\eta$	72
5.4 Spin degrees of freedom – a tool to study details of the $pp \rightarrow pp\eta$ reaction dynamics	74
5.5 Possible mechanisms responsible for the creation of the $\eta'$ meson . . .	77
5.5.1 Meson exchange models . . . . .	78
5.5.2 Approaches on the quark-gluon level . . . . .	79
5.6 Exploration of isospin degrees of freedom . . . . .	83
5.6.1 Glue content of the $\eta'$ meson . . . . .	84
5.7 Transition probability as a function of particles’ “virtuality” . . . . .	87
5.8 Natural width of mesons – does it depend on the momentum transfer?	88

<b>6</b>	<b>Experiment</b>	<b>91</b>
6.1	Measurement of the total cross section on the example of the $pp \rightarrow pp\eta'$ reaction	91
6.2	Monitoring of beam and target parameters . . . . .	96
6.2.1	Influence of the stochastic cooling on the proton beam quality	101
6.3	Detailed data analysis on the example of the $pp \rightarrow pp\eta$ reaction . . . .	104
6.3.1	Covariance matrix and kinematical fitting . . . . .	107
6.3.2	Multidimensional acceptance corrections . . . . .	110
6.3.3	Angular distributions . . . . .	118
6.4	Usage of the spectator model for the study of the $\eta$ and $\eta'$ mesons via the proton-neutron interaction	121
6.5	Test measurement of the $pn \rightarrow pn\eta$ reaction . . . . .	125
6.6	Double quasi-free production . . . . .	128
<b>7</b>	<b>Conclusion</b>	<b>133</b>
	<b>References</b>	<b>137</b>

## Preface

Experimental results constituting the basis for this dissertation have been published in twelve articles [1–12] and eleven conference proceedings [13–23]. The research has been realized at the cooler synchrotron COSY by means of the COSY-11 facility [24], which was build to a large extent at the Jagellonian University.

Ideas of experiments connected with this treatise, elaborated and formulated as experimental proposals [25–31], have been positively judged and approved for realization by the Programme Advisory Committee of the COSY accelerator, and the measurements have been carried out by the COSY-11 collaboration.

To render the reading of this dissertation more pleasant I have attempted to adduce at the beginnig of each section a few sentences from books of philosophers and scientists whom I immensely admire.





# 1. Introduction

*It is extremely advantageous to be able to bring a number of investigations under a formula of a single problem. For in this manner, we not only facilitate our own labour, inasmuch as we define it clearly to ourselves, but also render it more easy for others to decide whether we have done justice to our undertaking [32].*

Immanuel Kant

Pseudoscalar mesons ( $\pi, K, \eta, \eta'$ ) constitute the lightest (basic) nonet of particles built out of quarks and antiquarks, and the investigation of their interaction with nucleons is one of the key issues in hadron physics.

The interaction of  $\pi$  and  $K$  mesons with nucleons has been deduced from experiments realized by means of charged pion or kaon beams. Such experiments are, however, generally not feasible in the case of flavour neutral mesons due to their too short lifetime. Therefore, although  $\eta$  and  $\eta'$  mesons were discovered over forty years ago [33–35] their hadronic interaction with nucleons has not been established. The scattering length – the very basic quantity describing the low energy interaction potential – in the case of the  $\eta$  meson is poorly estimated and in the case of the  $\eta'$  meson it is entirely unknown. Estimated values of the real part of the proton- $\eta$  scattering length varies from 0.20 fm to 1.05 fm depending on the approach employed for its determination [36–39].

It is the primordial purpose of this treatise to present methods developed in order to study these interactions, to explain the applied experimental techniques and to discuss the progress achieved. We will address also the issue of the quark-gluon structure of these mesons since in analogy to the connection between electromagnetic and Van der Waals potentials, we may perceive the hadronic force as a residuum of the strong interaction that occurs between quarks and gluons – the constituents of hadrons.

In the quark model the  $\eta$  and  $\eta'$  mesons are regarded as the mixture of the singlet ( $\eta_1 = \frac{1}{\sqrt{3}}(u\bar{u} + d\bar{d} + s\bar{s})$ ) and octet ( $\eta_8 = \frac{1}{\sqrt{6}}(u\bar{u} + d\bar{d} - 2s\bar{s})$ ) states of the SU(3)-flavour pseudoscalar nonet. A small mixing angle  $\Theta = -15.5^\circ$  [40] implies that the percentage amount of strange and

non-strange quarkonium in both mesons is almost the same:

$$\eta = 0.77 \frac{1}{\sqrt{2}}(u\bar{u} + d\bar{d}) - 0.63 s\bar{s}, \quad \eta' = 0.63 \frac{1}{\sqrt{2}}(u\bar{u} + d\bar{d}) + 0.77 s\bar{s}.$$

Although, the  $\eta$  and  $\eta'$  mesons possess similar quark structure, their physical properties are unexpectedly different. Let us adduce three examples. The  $\eta'(958)$  meson mass is almost two times larger than the mass of the  $\eta(547)$  meson. The branching ratios for the decays of  $B$  and  $D_s$  mesons into the  $\eta'$  meson exceed significantly those into the  $\eta$  meson and the standard model predictions [41, 42]. There exist excited states of nucleons which decay via emission of the  $\eta$  meson, yet none of the observed baryon resonances decays via the emission of the  $\eta'$  meson [43]. Thus, it is natural to expect that the production mechanisms of these mesons in the collision of nucleons as well as their hadronic interactions with nucleons should also differ from each other.

In spite of the fact that the strange and non-strange quarkonium content of  $\eta$  and  $\eta'$  mesons is similar, the  $\eta$  meson remains predominantly the SU(3)-flavor octet and the  $\eta'$  meson the SU(3)-flavor singlet. This indicates that the  $\eta'$  meson may be mixed with pure gluon states to a much larger extent than the  $\eta$  and all other pseudoscalar and vector mesons. The anomalously large mass of the  $\eta'$  meson [44] and the analysis of the decays of pseudoscalar, vector, and  $J/\psi$  mesons indicate [45], that the  $\eta'$  meson is indeed a mixture of quarkonium and gluonium. The gluonic admixture of  $\eta'$  will influence the  $\eta'$ -nucleon interaction via the U(1) anomaly [44]. The range of the glue induced  $\eta'$ -nucleon interaction, if determined by the two-gluon effective potential, would be in the order of 0.3 fm [12]. This range is large enough to be important in the threshold production of the  $\eta'$  meson e.g. via the  $pp \rightarrow pp\eta'$  reaction which occurs at distances of the colliding nucleons in the order of 0.2 fm. At such small distances the quark-gluon degrees of freedom may play a significant role in the production dynamics of the  $\eta$  and  $\eta'$  mesons. It is essential to realize that the investigation of the interaction between hadrons is inseparably connected with the study of their structure and the dynamics of the processes in which they are created. Therefore, in this treatise we present our study of the interaction between protons and  $\eta$  or  $\eta'$  mesons in strict connection with the investigation of their structure and production mechanism.

The fact that forty years after the discovery of the  $\eta$  and  $\eta'$  mesons, their interaction with nucleons remains so weakly established, in spite of its crucial importance for hadron physics, indicates that it is rather challenging to conduct such research.

From the methodological point of view, the first difficulty needed to be solved was to find a way of how the interaction with nucleons of such short-lived objects like  $\eta$  and  $\eta'$  mesons can manifest itself in a measurable manner. For, even when moving close to the velocity of light, both these mesons disintegrate on the average within a distance of tens of femtometers rendering their direct detection impossible. Not to mention, that it is completely unfeasible to accomplish out of them a beam or a target. However, the creation of these mesons in the vicinity of nucleons with low relative velocities appeared to us to be a promising tool which could facilitate the study of meson-nucleon interactions. For this purpose the best suited is the production close to the kinematical threshold or in kinematical regions where the outgoing particles indeed possess low relative velocities and hence remain in distances of few Fermi long enough to experience the hadronic interaction. Investigations were started with measurements of the excitation function for the  $pp \rightarrow pp\eta$  and  $pp \rightarrow pp\eta'$  reactions, searching for its statistically significant distortion caused by the interacting ejectiles. We scanned the energy region close to the kinematical threshold where the effect was supposed to be most significant and where the interpretation of the results is not burdened by the complexity resulting from contributions of many angular momentum states of initial and final systems. Indeed, we found out that the interaction between protons augments the total production cross section gradually with decreasing volume of the phase space. At the threshold the enhancement is most pronounced and corresponds to an enlargement of the cross section by more than an order of magnitude and it vanishes where the kinetic energy shared by ejectiles in the centre-of-mass system exceeds  $\sim 100$  MeV. It was most fascinating to see that the interaction of the  $\eta$  meson with protons enhanced the cross section by a further factor of two. As it will be demonstrated in this dissertation, we were able to discern this from the effect caused by the overwhelming proton-proton interaction in a model independent manner. This was possible by making a comparison of the excitation functions of the  $pp \rightarrow pp\eta$  and  $pp \rightarrow pp\pi^0$  reactions.

We would like to stress that the revealed phenomenon – viz the interaction of the created object with the outgoing nucleons affects the probability of its very production – is of a purely quantum mechanical nature. Our understanding of this peculiar effect will be presented in chapter 2. However, it is by far easier to imagine that the interaction between ejectiles modifies the distributions of their relative momenta. This appears much more intelligible even on the analogy of the well known

effect that the momentum distributions of  $\beta$  particles are different for positrons and for electrons due to their Coulomb interaction with the residual nucleus. Therefore seeking for another measurable manifestation of the interaction between the  $\eta$  meson and the proton we performed a measurement of the  $pp \rightarrow pp\eta$  reaction with a statistics which permitted to derive distributions of a complete set of differential cross sections. The determined spectra of the invariant mass distributions for the two-particle subsystems of the  $pp\eta$  final state revealed strong deviations from the predictions based on the assumption that all kinematically allowed momentum configurations of ejectiles are equally probable. Deviations at low relative proton-proton momenta can be explained satisfactorily well by the hadronic interaction between protons. Yet, a pronounced discrepancy observed in the region of large relative momentum between protons is by far larger than expected from an influence of the  $\eta$ -proton hadronic potential. This intricate observation will be examined in detail in section 4.5. Its explanation appears to be quite a challenge due to the need for the description of a three-body system subjected to the complex hadronic potentials. Later on in section 4.7 we will outline our ongoing investigations aiming at the determination of the hadronic interaction occurring between the  $\eta'$  meson and the proton. In this case, contrary to the  $\eta$  meson, the excitation function for the  $pp \rightarrow pp\eta'$  reaction did not reveal any statistically significant signal which could have been assigned to the  $\eta'$ -proton interaction. At present we are continuing these studies by determining distributions of the invariant masses for two-particle subsystems of the  $pp\eta'$  final state which might deliver the first ever experimental evidence for this still unknown potential. Such investigations constitute a much more difficult experimental task compared to the study of the  $\eta$  meson. This is mostly due to the fact that the cross section for the  $pp \rightarrow pp\eta'$  reaction is by about a factor of thirty smaller than the one of the  $pp \rightarrow pp\eta$  reaction at the corresponding excess energy.

Thorough theoretical investigations have shown that in order to understand how the energy of motion is converted into a meson, it is of utmost importance to take into account also an interaction between nucleons before the very collision. We will demonstrate in section 4.3 that the interaction between nucleons in the initial channel reduces the total cross section drastically. For the  $pp \rightarrow pp\eta$  reaction it is decreased by a factor of four and in the case of the  $pp \rightarrow pp\eta'$  reaction by a factor of three!

As an essence of the above part of the introduction we would like to emphasize that the inferences about the hadronic interaction of  $\eta$  and  $\eta'$

with nucleons will be based on comparisons of both the differential cross sections and the close-to-threshold excitation functions for the  $pp \rightarrow pp\eta$  and  $pp \rightarrow pp\eta'$  reactions with predictions based on the assumption that the kinematically available phase space is homogeneously populated.

It cannot be, however, a priori excluded that possible deviations of the experimental distributions from the phase space governed calculations may also be due to other physical effects caused by the specific production mechanism. Therefore, the discussion of the dynamics of the considered reactions, embodied in chapter 5, constitutes a part of this thesis. We will show that at threshold the entire production dynamics manifests itself in a value of a single constant which determines the magnitude of the total cross section. Consequently, the measurements of one reaction channel (eg.  $pp \rightarrow ppX$ ) is by far not sufficient for a full understanding of the reaction mechanism, since having only one observable at disposal it is impossible to establish contributions from many plausible production currents (as an example let us mention mesonic, nucleonic, or resonance currents). Therefore, an exploration of isospin and spin degrees of freedom is mandatory if we like to corroborate or refute the hypotheses proposed. In addition, the question of the reaction mechanism is connected with the very basic problem of whether hadronic or quark-gluon degrees of freedom are more appropriate for the description of phenomena occurring in the energy regime relevant to our studies. We address this issue in chapter 5, which comprises the description of currently considered production models and gives account of present and planned future experimental studies of spin and isospin observables. For example, we will discuss to what extent one can infer a gluonic component of the  $\eta'$  wave function from a comparison of its creation in collisions of nucleons with different isospin combination.

Consideration of the quasi-free meson creation on virtual nucleons bound inside a nucleus led us to the idea of studying the dependence of the meson production cross section on the virtuality of colliding baryons. The idea will be elucidated in section 5.7, and a method for the measurement of the close-to-threshold production of mesons in the quasi-free proton-neutron and even neutron-neutron collisions will be demonstrated in chapter 6.

From the experimental point of view, measuring the energy dependence of the total cross section for the production of mesons close to the kinematical threshold was quite a challenge. First of all, because these cross sections are by more than seven orders of magnitude smaller compared to the total yield of pp reactions, and secondly because they vary

by few orders of magnitude in a few MeV range of the excess energy. The afore mentioned relations are demonstrated in figure 1.1. It shows recently determined excitation functions for the close-to-threshold production of some of the pseudoscalar mesons, and in particular it shows the data for the  $\eta$  and  $\eta'$  mesons, which constitute an experimental basis of this treatise.

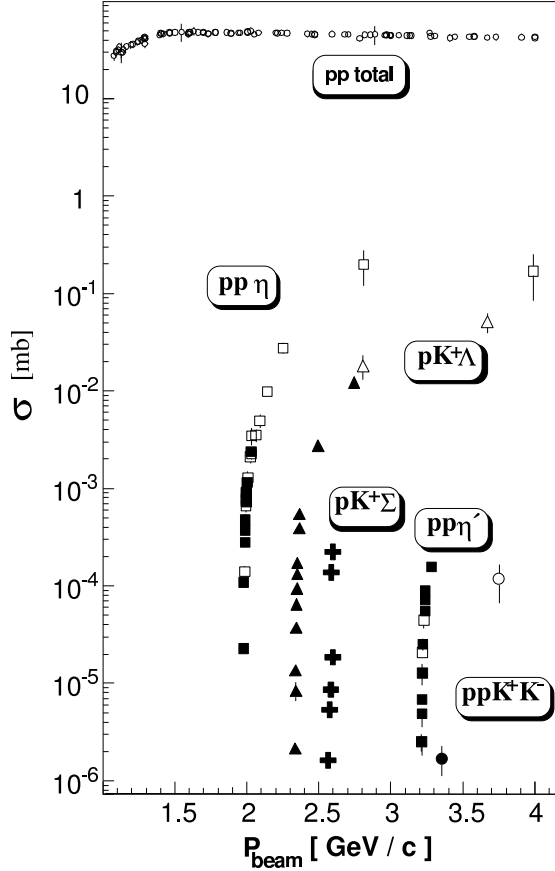


**Figure 1.1:** Close-to-threshold cross section for the proton-proton interaction leading to the production of mesons whose wave function comprises a significant amount of strangeness. For comparison, the total cross section of proton-proton collisions is also shown. The filled points depict data taken at COSY [3, 10, 11, 18, 46–49], and open symbols show results from other laboratories [50–60].

Conclusive inferences concerning the interaction between ejectiles could be drawn only due to the unprecedented experimental precision obtained using proton beams available at storage ring facilities and in particular at the cooler synchrotron COSY. These beams are characterized by low emittance, small momentum spread, and well defined absolute momentum. Experiments which will be discussed in this dissertation have been carried out by means of the COSY-11 facility [24, 61] installed at COSY [62]. Details of the experimental method are elucidated in chapter 6. In short, the technique is based on the determination of the four momentum vectors of colliding and outgoing nucleons, and on the deriva-

tion of the mass of the produced meson or group of mesons employing the principle of energy and momentum conservation. The registered particles are identified by independent measurements of their velocity and momentum, where the former is determined from the time-of-flight between scintillation detectors and the latter is deduced from the curvature of the particle trajectories in a magnetic field. Figure 1.2 presents an example of the mass spectrum determined for a system  $X$  produced via the  $pp \rightarrow ppX$  reaction at an excess energy of 1.5 MeV with respect to the kinematical threshold for the production of the  $\eta'$  meson. A signal from the creation of the  $\eta'$  meson can be well recognized and its width of 0.7 MeV (FWHM) indicates the precision achieved using the stochastically cooled proton beam of COSY and the COSY-11 detection setup. When examining the error bars, it is evident that if the accuracy was twice worse the signal would be disputable. The method invented to monitor the beam geometry at internal target facilities [8, 23], which is described in section 6.2, enabled us to improve the accuracy of mass determination by correcting for variations of the average beam characteristics. On the cognitive side, its application led to the understanding of to what extent the stochastic cooling improves the quality of the beam.

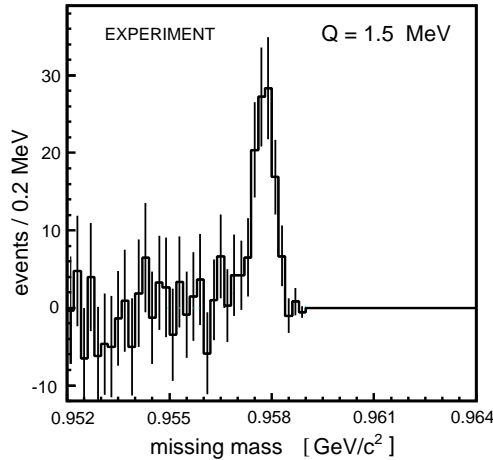


**Figure 1.2:** Missing mass spectrum for the  $pp \rightarrow ppX$  reaction measured by means of the COSY-11 detection facility at the cooler synchrotron COSY. The measurement was performed at a beam momentum corresponding to an excess energy of 1.5 MeV for the  $pp \rightarrow pp\eta'$  reaction. More details concerning the evaluation of the data will be explained in section 6.1. It is worth noting that the attained experimental mass resolution is comparable with the natural width of the  $\eta'$  meson ( $\Gamma_{\eta'} = 0.202$  MeV [43]).

Necessary corrections for a non-ideal detection geometry were performed in an utterly model independent manner. To arrive at this aim we expressed the experimental acceptance as a function of a complete set of mutually orthogonal variables describing the reaction, and to facilitate calculations we digitized the phase space volume into a few thousand partitions in which the acceptance could be safely regarded as constant. In the analysis, we assigned to each measured event a weight equal to the inverse of the acceptance according to the phase space bin to which it

belonged. This allowed us to elaborate the differential distributions independently of the reaction model used in simulations. Employing the missing mass technique it is in principle impossible to discern between the multi-pion and  $\eta$  or  $\eta'$  meson production on the event-by-event basis. Therefore, to derive the differential distributions we divide the range of the studied variable into bins with a width corresponding to the achieved experimental resolution and separate the multi-pion background from the  $\eta$  or  $\eta'$  meson signal for each bin. The effort was undertaken in order to determine background- and model-free distributions of differential cross sections which in turn enable to test various hypotheses without an obscurity due to unnecessary assumptions. Hence we can benefit thoroughly from simplifications gained due to the threshold kinematics. The most crucial facilitation and attractiveness when interpreting the meson production at the vicinity of the threshold is the fact that the relative angular momenta larger than  $l = 0 \hbar$  play no role due to the short range of the strong interaction and small relative momenta of the produced particles. It can be inferred from parity and angular momentum conservation laws that the production of a nucleon-nucleon-meson system (for pseudoscalar or vector mesons) in relative S-waves may only occur if the nucleons collide in P-wave. Thus at threshold the transition  $P \rightarrow Ss$  is the only possible one, with capital letters denoting the angular momentum between nucleons and the small letter describing the meson angular momentum with respect to the pair of nucleons. Section 3.2 will be devoted to the circumstantial discussion of this issue. At this stage we would only like to note, that the dominance of the  $P \rightarrow Ss$  transition at threshold will not be unquestioningly assumed but rather the energy range of its applicability – which varies strongly with the mass of the created meson – will be established in section 4.1.

The present work is divided into seven chapters. After this introduction we will elucidate our understanding of the manifestation of the hadronic interaction via the excitation function and the phase space abundance of the studied reactions. Further, in the third chapter we will introduce the definitions of observables used throughout this work. The fourth chapter comprises a discussion of the experimental evidence concerning the interaction between the pseudoscalar isosinglet mesons ( $\eta$ ,  $\eta'$ ) and the proton. In the fifth chapter we explain the reaction dynamics and discuss the relevance for the production process of hadronic and quark-gluon degrees of freedom. The final conclusion is preceded by the sixth chapter which contains the detailed description of the experimental method.



## 2. Manifestation of hadronic interactions

*... what it can mean to ask what is the probability of past event given a future event! There is no essential problem with this, however. Imagine the entire history of the universe mapped out in space-time. To find the probability of  $p$  occurring, given that  $q$  happens, we imagine examining all occurrences of  $q$  and counting up the fraction of these which are accompanied by  $p$ . This is the required probability. It does not matter whether  $q$  is the kind of event that would normally occur later or earlier in time than  $p$  [63].*

Roger Penrose

The interaction of hadrons – being the reflection of the strong force acting between their constituents – provides information about their structure and the strong interaction itself. In the frame of the optical potential model the hadronic interaction can be expressed in terms of phase-shifts, which in the zero energy limit are described by the scattering length and effective range parameters. These are quite well known for the low-energy nucleon-nucleon interaction [64,65], yet they are still poorly established in the case of meson-nucleon or meson-meson interactions. This is partly due to the absorption of mesons when scattering on a baryon. To account for this effect the scattering length becomes a complex quantity where the imaginary part – e.g. in case of the nucleon- $\eta$  interaction – describes the  $\eta N \rightarrow \pi N$  and  $\eta N \rightarrow \text{multi-}\pi N$  processes. Moreover, the short life-time of all *neutral* ground state mesons prohibits their direct utilization as secondary beams and therefore the study of their interaction with hadrons is accessible only via their influence on the cross section of the reactions in which they were produced (eg.  $NN \rightarrow NN \text{ Meson}$ ). When created close to the kinematical threshold with the relative kinetic energy being in the order of a few MeV, the final state particles remain much longer in the range of the strong interaction than the typical life-time of  $N^*$  or  $\Delta$  baryon resonances with  $10^{-23}$  s, and hence they can easily experience a mutual interaction before escaping the area of an influence of the hadronic force. This – as introduced by Watson [66] – final state interaction (FSI) may significantly modify both the original distributions of relative momenta of the outgo-

ing reaction products and the magnitude of the production cross section. Although it is easy to understand that the FSI changes the distributions of the differential cross sections it is rather difficult to cope with the influences on the magnitude of the total reaction rate, since one tends to separate the primary production from the final state interaction in space as well as in time [66]. The influence of the FSI on the absolute scale of the cross section is a pure quantum mechanical effect and our classical imagination must inevitably fail in this respect. However even when considering the primary production as a separate process it is well worth trying to understand the phenomenon qualitatively. If there were no final state interactions the total cross section would be fully determined by the kinematically available phase space volume  $V_{ps}$ , where each interval is populated with a probability governed by the primary production amplitude only:

$$\sigma = \frac{1}{F} \int dV_{ps} |M|^2 \approx \text{const.} \cdot V_{ps}. \quad (2.1)$$

The approximation in the equation results from the assumption that  $|M|^2 = \text{constant}$  in a few MeV range above the production threshold [67–69].  $F$  denotes the flux factor of the colliding particles.

In the classical picture we might imagine that the reaction particles are created together with their appropriate force field and when escaping the interaction region they acquire a potential energy increasing or decreasing their kinetic energy depending whether the interaction is repulsive or attractive. For an attractive interaction they could be created also in those phase space partitions which are not available for non-interacting particles and subsequently be “pulled down” to the energetically allowed regions by final state interaction. The temporary growth of the primary production phase space would then increase the reaction rate. Contrary, in the case of a repulsive interaction the particles must be produced in the lower phase space volume since leaving the interaction area they will acquire additional kinetic energy. The reduction of the total cross section, for example in case of the repulsive Coulomb force, can easily be understood when considering the production in a coordinate space of point-like objects. Here – in contrast to non-interacting particles – a strongly repulsive object cannot be produced at appropriately small distances since their later acceleration would violate energy conservation and thus the space available to primary production is reduced.

Another more commonly anticipated presupposition of changes of the reaction yield due to the final state interaction is based on the time

invariance principle. It asserts that the cross section for the production of repulsive particles is smaller in comparison to non-interacting particles, all other features being equal, because in the time inversed process the repulsive interaction hinders the slow particles from reaching distances at which a particular reaction may occur.

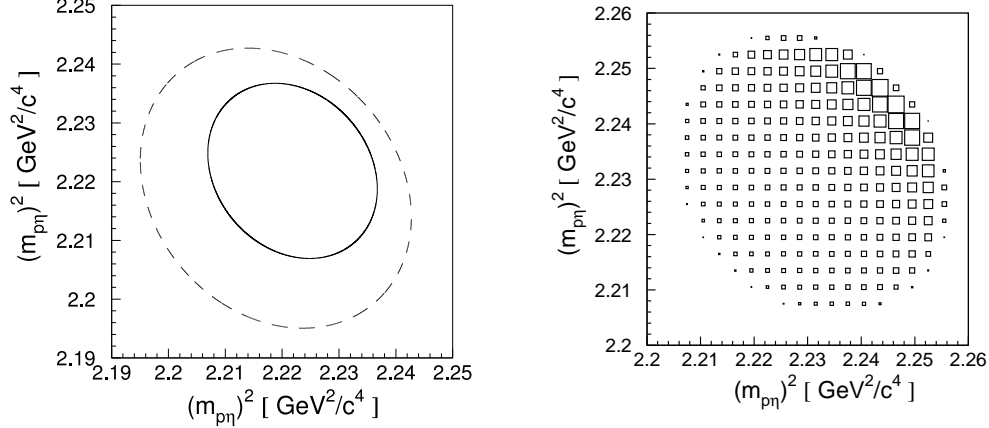


**Figure 2.1:** (left) The solid line indicates the kinematically available area for the  $pp\eta$  system with a total centre-of-mass energy  $\sqrt{s} = 2433.8$  MeV (excess energy  $Q \approx 10$  MeV). The dashed line depicts the range assuming a reduction of the proton and  $\eta$ -meson masses by 2 MeV. The phase space volume results from an integral over the closed area:  $V_{ps} = \frac{\pi^2}{4s} \int \int dm_{p_1\eta}^2 dm_{p_2\eta}^2$ . (Terms of  $(2\pi)^n$  are skipped here and will be included in the flux factor  $F$  according to the convention introduced by Byckling and Kajantie [70]). (right) Distribution of the phase space for the  $pp\eta$  system modified by the proton-proton interaction and calculated for an excess energy of  $Q = 16$  MeV. The area of the squares is proportional to the number of entries and is shown in a linear scale.

One can also argue, that relativistically the primary mechanism creates the particles off the mass shell and subsequently they are lifted onto the mass shell by the final state interaction. The solid line in figure 2.1 (left) depicts the boundary of the Dalitz plot in case of the  $pp \rightarrow pp\eta$  reaction calculated at the total centre-of-mass energy  $\sqrt{s} = 2433.8$  MeV exceeding the threshold energy by 10 MeV. The area surrounded by that curve is a direct measure of the kinematically available phase space volume. The dashed line shows the corresponding plot at the moment of the primary creation if the mass of each particle was reduced by 2 MeV, demonstrating that now the available phase space grows significantly. Indeed, as shall be inferred from the experimental results presented in subsequent sections, at excess energies of a few MeV above threshold, the mutual interaction among the outgoing particles enhances drastically – by more than an order of magnitude – the total cross section and modifies appreciably the occupation of the phase space. Figure 2.1 (right) indicates the phase space distribution expected for the  $pp\eta$  system at an

excess energy of  $Q = \sqrt{s} - 2m_p - m_\eta = 16 \text{ MeV}$ , assuming a homogeneous primary production and taking into account the S-wave interaction between the protons. The proton-proton FSI modifies the homogeneous Dalitz plot distribution of “non-interacting particles”, enhancing its population at a region where the protons have small relative momenta. The interaction of the proton- $\eta$  system would manifest itself at low invariant masses  $m_{p\eta}^2$  corresponding to small relative momenta between the proton and the  $\eta$  meson. Such effects observed in the experiments are presented in section 4.5.

The effect of the nucleon-nucleon FSI diminishes with increasing excess energy since it significantly influences only that partition of the phase space at which the nucleons have small relative momenta. While this fraction stays constant, the full volume of the phase space grows rapidly: An increase in the excess energy from  $Q = 0.5 \text{ MeV}$  to  $Q = 30 \text{ MeV}$  corresponds to a growth of  $V_{ps}$  by more than three orders of magnitude. As a result the S-wave nucleon-nucleon FSI is of less importance for higher excess energies where it affects a small fraction of the available phase space volume only. A more quantitative discussion about the influence of the FSI and ISI (initial state interaction) effects at close-to-threshold production cross sections will be presented in section 4.1.

In this section we would only like to state that an interaction of the nucleons in the entrance channel, similarly to that among ejectiles, influences the production process noticeably [71]. For example, for  $\eta$  production in the  $pp \rightarrow pp\eta$  reaction the initial state interaction reduces the total cross section by a factor of about 3–5 [71, 72] due to the repulsive proton-proton  $^3P_0$ -wave potential. This factor remains rather constant in the range of a few tens of MeV [72] and hence, does not influence the energy dependence of the total cross section of the meson production, which is mostly determined by the final state interaction. In particular, the dominant S-wave nucleon-nucleon final state interaction is by far stronger than any of the low-energy meson-nucleon ones. The reduction of the cross section by the initial state interaction we may intuitively conceive as a loss of the initial flux in favour of elastic, and a plethora of other – than the studied one – inelastic reactions, which may occur when the colliding nucleons approach each other.

The above considerations point out that the hadronic interaction between nucleons and the short-lived mesons like  $\eta$  and  $\eta'$  may be investigated by the observation of the excitation function for the production of these mesons off nucleons, as well as by the studies of the phase space abundance.

### 3. Definitions of observables

**Hermogenes.** *Suppose that we make Socrates a party to the argument?*

**Cratylus.** *If you please.*

...

**Socrates.** *Then the argument would lead us to infer the names ought to be given according to a natural process, and with a proper instrument, and not at our pleasure: in this and no other way shall we name with success.*

**Hermogenes.** *I agree.*

**Socrates.** *But again, that which has to be cut has to be cut with something?*

**Hermogenes.** *Yes.*

**Socrates.** *And that which has to be woven or pierced has to be woven or pierced with something?*

**Hermogenes.** *Certainly.*

**Socrates.** *And that which has to be named has to be named with something?*

**Hermogenes.** *True [73].*

Plato

#### 3.1 Cross section

*Why is it that, in most cases, the definitions which satisfy scientists mean nothing at all to children? [74]*

Henri Poincaré

Investigations of the production of mesons and their interactions with nucleons are based on measurements determining the total and differential production cross sections and their dependence on the energy of the interacting nucleons. Therefore, to enable a quantitative discussion on the mechanisms leading to the transformation of the energy-of-motion of nucleons into matter in the form of mesons let us recall the formula of the reaction cross section. In the case of the  $NN \rightarrow NN \text{ Meson}$  process – with the four-momenta of the colliding nucleons denoted by  $\mathbb{P}_a$  and  $\mathbb{P}_b$

and with  $n = 3$  particles in the exit channel – it reads:

$$\begin{aligned} \sigma &= \frac{1}{F} \int dV_{ps} |M_{ab \rightarrow 123}|^2 = \\ &= \frac{1}{F} \int \prod_{i=1}^n d^4\mathbb{P}_i \cdot \delta(\mathbb{P}_i^2 - m_i^2) \cdot \Theta(\mathbb{P}_i^2) \cdot \delta^4(\mathbb{P}_a + \mathbb{P}_b - \sum_{j=1}^n \mathbb{P}_j) \cdot |M_{ab \rightarrow 123}|^2, \quad (3.1) \end{aligned}$$

where  $|M_{ab \rightarrow 123}|^2$  denotes the square of the Lorentz-invariant spin averaged matrix element describing the probability to create two nucleons and a meson with four-momenta of  $\mathbb{P}_i = (E_i, \vec{p}_i)$  and  $i = 1..n$ , respectively. The energy and momentum conservation as well as the on-shellness of the created particles is ensured by the Dirac- $\delta$  and the Heaviside- $\Theta$  functions. The formula holds also for  $n \neq 3$ .

The total cross section is then defined as an integral of the probabilities to populate a given phase space interval over the whole kinematically available range – determined by energy and momentum conservation – normalized to the flux factor  $F$  of the colliding nucleons. In the case of non-interacting final state particles the matrix element close to threshold  $|M_{ab \rightarrow 123}|^2$  is nearly constant [67–69] and hence the allowed phase space volume,  $V_{ps}$ , is the decisive quantity which governs the growth of the cross section with increasing excess energy  $Q$ . The latter – defined as the total kinetic energy – is shared among the outgoing particles in the reaction centre-of-mass frame <sup>1</sup>:

$$Q = \sqrt{s} - \sum_{i=1}^n m_i, \quad (3.2)$$

where  $s = |\mathbb{P}_a + \mathbb{P}_b|^2 = |\sum_{i=1}^n \mathbb{P}_i|^2$  denotes the square of the total centre-of-mass energy. Exactly at threshold, where the particles' kinetic energy in the centre-of-mass system equals zero ( $Q = 0$  MeV), the total reaction energy  $\sqrt{s}$  amounts to:  $\sqrt{s_{th}} = \sum_{i=1}^n m_i$ . Before writing explicitly the formula for  $V_{ps}$  let us introduce the kinematical triangle function  $\lambda$  defined as [70]:

$$\lambda(x, y, z) = x^2 + y^2 + z^2 - 2xy - 2yz - 2zx. \quad (3.3)$$

It enables to formulate many useful kinematical variables in a very compact and Lorentz-invariant form. In particular, the momenta of particles

---

<sup>1</sup> Traditionally by the centre-of-mass system we understand a frame in which the momenta of all particles add to zero, called sometimes more explicitly centre-of-momentum frame.

$i$  and  $j$  in their centre-of-mass frame may be expressed as follows:

$$p_i^* = p_j^* = \frac{\sqrt{\lambda(s_{ij}, m_i^2, m_j^2)}}{2\sqrt{s_{ij}}}, \quad (3.4)$$

where  $s_{ij} = |\mathbb{P}_i + \mathbb{P}_j|^2$  stands for the square of the invariant mass of the  $ij$  system considered as one quasi-particle. The above relation gives an expression for the flux factor  $F$  from equation (3.1) in terms of the colliding masses of the nucleons and the total energy  $s$  only, namely:

$$F = 4\sqrt{s} (2\pi)^{3n-4} p_a^* = 2(2\pi)^{3n-4} \sqrt{\lambda(s, m_a^2, m_b^2)}, \quad (3.5)$$

where we have chosen the convention introduced by Byckling and Kajantie [70] and included the  $(2\pi)$  factors for the phase space  $(2\pi)^{3n}$  and for the matrix element  $(2\pi)^{-4}$  into the definition of  $F$ . It is important to note that at threshold, for an excess energy range of a few tens of MeV, the small fractional changes of total energy ( $\frac{Q}{\sqrt{s}} = \frac{Q}{m_1 + m_2 + m_3 + Q}$ ) causes weak variations of the flux factor and influences the shape of the energy dependence of the total cross section only slightly.

For a two-particle final state  $ab \rightarrow 12$  (for instance for the reaction  $pn \rightarrow d\eta$ ) the phase space integral defined in equation (3.1) reduces to  $V_{ps} := \int dV_{ps} = \frac{\pi}{\sqrt{s}} p_1^* = \frac{\pi}{2s} \sqrt{\lambda(s, m_1^2, m_2^2)}$  and the total cross section for such reactions (when neglecting variations due to dynamical effects ( $|M_{ab \rightarrow 12}| = \text{const.}$ )) should increase linearly with the centre-of-mass momentum of the produced meson in the vicinity of the reaction threshold. The total cross section can be expressed analytically as a function of the masses of the particles participating in the reaction and the square of the total reaction energy  $s$ :

$$\sigma_{ab \rightarrow 12} = \text{const} \cdot \frac{V_{ps}}{F} = \frac{\text{const} p_1^*}{16\pi s p_a^*} = \frac{1}{16\pi s} \frac{\sqrt{\lambda(s, m_1^2, m_2^2)}}{\sqrt{\lambda(s, m_a^2, m_b^2)}}. \quad (3.6)$$

Near threshold, at a given excess energy  $Q = \sqrt{s} - m_1 - m_2$ , the emission of the reaction products in the centre-of-mass frame is isotropic and the whole dynamics of the process manifests itself in the absolute value of the transition matrix element  $|M_{ab \rightarrow 12}|$ . The underlying production mechanisms can also be extracted from the deviations of the total cross section energy dependence following the prediction of relation (3.6). A visualization of possible differences in the dynamics of the production of various mesons can be obtained by comparing the total cross sections of

the studied reactions at the same value of the phase space volume normalized to the flux factor ( $V_{ps}/F$ ). It is important to recognize that the comparison at the same centre-of-mass meson momentum ( $p_2^*$ ) gives direct information about the amplitude differences only if the production of mesons with the same masses is concerned (for example  $pp \rightarrow d\pi^+$  and  $nn \rightarrow d\pi^-$ ), yet the reactions  $pn \rightarrow d\eta$  and  $pn \rightarrow d\pi^0$  have by far different  $V_{ps}$  at the corresponding  $p_2^*$ .

Prior to the comparative analysis of the transition amplitudes for the  $pp \rightarrow pp\eta$ ,  $pp \rightarrow pp\eta'$ , and  $pp \rightarrow pp\pi^0$  reactions, a corresponding formula of the phase space volume  $V_{ps}$  for the three particle final state will be introduced in section 3.3.

### 3.2 Partial waves – selection rules

*Not for nothing do we call the laws of nature 'laws':  
the more they prohibit the more they say [75].*

Karl Raimund Popper

If one is interested in the decomposition of the production amplitude according to the angular momenta of the final state particles then indeed the appropriate variable for a qualitative comparison even for particles with different masses is the meson momentum in the reaction centre-of-mass frame. Correspondingly, for the more than two-body final state, the adequate variable is the maximum meson momentum, since it is directly connected with the maximum angular momentum by the interaction range. In the case of a three-body exit channel ( $ab \rightarrow 123$ ) the meson ( $m_3$ ) possesses maximum momentum ( $q_{max}$ ) when the remaining two particles are at rest relative to each other. Hence, employing definition (3.4) one obtains:

$$q_{max} = \frac{\sqrt{\lambda(s, (m_1 + m_2)^2, m_3^2)}}{2\sqrt{s}}. \quad (3.7)$$

Contrary to the two-body final state, at a fixed excess energy the dynamics of the meson production associated with two or more particles reflects itself not only in the absolute value of the square of the matrix element but also in distributions of variables determining the final state kinematics. Usually, in non-relativistic calculations of the total cross section, one takes the Jacobi momenta, choosing as independent variables the 'q'-meson momentum in the reaction centre-of-mass frame and 'k'-momentum of either nucleon in the rest frame of the nucleon-nucleon



subsystem. By means of the  $\lambda$  function they can be expressed as:

$$q = \frac{\sqrt{\lambda(s, s_{12}, m_3^2)}}{2\sqrt{s}}, \quad \text{and} \quad k = \frac{\sqrt{\lambda(s_{12}, m_1^2, m_2^2)}}{2\sqrt{s_{12}}}, \quad (3.8)$$

with  $s_{12} = |\mathbb{P}_1 + \mathbb{P}_2|^2$  denoting the square of the invariant mass of the nucleon-nucleon subsystem. In a non-relativistic approximation the expression of the total cross section defined by formula (3.1) for a meson production reaction in nucleon-nucleon interactions of the type  $NN \rightarrow NN \text{ Meson}$  simplifies to:

$$\sigma \propto \int_0^{q_{max}} k q^2 |M_{ab \rightarrow 123}|^2 dq. \quad (3.9)$$

Denoting by  $L$  and  $l$  the relative angular momenta of the nucleon-nucleon pair and of the meson relative to the  $NN$  system, respectively, and approximating the final state particles by plane waves (case of non-interacting objects), whose radial parts  $\psi_l(q, r)$  are given by the spherical Bessel functions:

$$\psi_l(q, r) \propto j_l(qr) \xrightarrow{qr \rightarrow 0} \frac{(qr)^l}{(2l+1)!}, \quad (3.10)$$

an expansion of the transition amplitude  $|M_{Ll}|^2$  for the  $Ll$  partial wave around  $qr = 0$  leads to

$$|M_{Ll}|^2 \propto |M_{Ll}^0|^2 k^{2L} q^{2l}, \quad (3.11)$$

where,  $M_{Ll}^0$  denotes the matrix elements responsible for the primary production with the angular momenta  $L$  and  $l$ . Thus, the total cross section can be expressed as the following sum of the partial cross sections  $\sigma_{Ll}$ :

$$\sigma = \sum_{L,l} \sigma_{Ll} \propto \sum_{L,l} \int_0^{q_{max}} |M_{Ll}^0|^2 k^{2L+1} q^{2l+2} dq \quad (3.12)$$

Furthermore, if the strength of the the primary production partial amplitudes  $|M_{Ll}^0|$  were constant over the phase space then the energy dependence of the partial cross sections, obtained by solving the above equation, would be given by:

$$\sigma_{Ll} \propto q_{max}^{2L+2l+4} \propto \eta_M^{2L+2l+4}, \quad (3.13)$$

where  $\eta_M = q_{max}/m_M$  with  $m_M$  denoting the mass of the created meson<sup>2</sup>. Thus – at threshold – for the Ss partial wave the cross section for

---

<sup>2</sup> In former works [76, 77] dealing only with pions this parameter is denoted by  $\eta$ , here in order to avoid ambiguities with the abbreviation for the eta-meson, we introduce an additional suffix  $M$ .

the  $NN \rightarrow NN \text{ Meson}$  reaction should increase with the fourth power of  $\eta_M$ . The dimensionless parameter  $\eta_M$  was introduced by Rosenfeld [76] as a variable allowing for qualitative estimations of the final state partial waves involved in pion production. He argued that if the phenomenon of pion production takes place at a characteristic distance  $R$  from the centre of the collision, with  $R$  in the order of  $\hbar/Mc$ , then the angular momentum of the produced meson is equal to  $l = Rq = \hbar q/Mc$ . Hence,  $\eta_M$  denotes the classically calculated maximum angular momentum of the meson relative to the centre-of-reaction. The same arguments one finds in the work of Gell-Mann and Watson [77], where the authors do not expect the range of interaction to be larger than the Compton wavelength of the produced meson ( $\hbar/Mc$ ). However, it is rather a momentum transfer  $\Delta p$  between the colliding nucleons which determines the distance to the centre of the collision  $R \approx \hbar/\Delta p$  at which the production occurs. Based on indications from data, it is emphasized in the original article of Rosenfeld [76] that  $R$  is slightly less than  $\hbar/(2Mc)$ , which is numerically close to the value of  $\hbar/\Delta p$ . Directly at threshold, where all ejectiles are at rest in the centre-of-mass frame,  $\Delta p$  is equal to the centre-of-mass momentum of the interacting nucleons and hence, exploring equation (3.4) it can be expressed as:

$$\Delta p_{th} = \frac{\sqrt{\lambda(s_{th}, m_a^2, m_b^2)}}{2\sqrt{s_{th}}} \xrightarrow{\text{for } pp \rightarrow ppX} \sqrt{m_p m_X + \frac{m_X^2}{4}}. \quad (3.14)$$

Though the present considerations are limited to the spin averaged production only, it is worth noting that very close-to-threshold – due to the conservation laws and the Pauli excluding principle – for many reactions there is only one possible angular momentum and spin orientation for the incoming and outgoing particles. The Pauli principle for the nucleon-nucleon system implies that

$$(-1)^{L+S+T} = -1, \quad (3.15)$$

where  $L$ ,  $S$ , and  $T$  denote angular momentum, spin, and isospin of the nucleon pair, respectively. For example if the nucleon-nucleon wave function is symmetric in the configuration-space ( $L = 0$ ) as well as in the spin-space ( $S = 1$ ) then it must be antisymmetric in the isospin-space ( $T = 0$ ) to be totally antisymmetric.

In the conventional notation [78, 79] the transition between angular momentum parts of the initial and final states of the  $NN \rightarrow NNX$  reactions are described in the following way:

$$^{2S^i+1}L_{J^i}^i \rightarrow ^{2S+1}L_J, l \quad (3.16)$$

where, superscript  $i$  indicates the initial state quantities,  $l$  denotes the angular momentum of the produced meson with respect to the pair of nucleons, and  $J$  stands for the total angular momentum of the N-N system. The values of angular momenta are commonly being expressed using the spectroscopic notation ( $L = S, P, D, \dots$  and  $l = s, p, d, \dots$ ). The parity conservation implies that  $L^i + L + l$  must be an even number if the parity of the produced meson is positive or odd if this parity is negative. Employing additionally the conservation of the total angular momentum and Pauli principle one can deduce that at threshold the  $NN \rightarrow NNX$  reactions will be dominated by the transitions listed in table 3.1.

**Table 3.1:** Partial wave transitions for the  $pp \rightarrow pp \text{ Meson}$  and  $nn \rightarrow nn \text{ Meson}$  reactions at threshold

type	meson	spin and parity	transition
pseudoscalar	$\pi, \eta, \eta'$	$0^-$	${}^3P_0 \rightarrow {}^1S_0 s$
vector	$\rho, \omega, \phi$	$1^-$	${}^3P_1 \rightarrow {}^1S_0 s$
scalar	$a_0, f_0$	$0^+$	${}^1S_0 \rightarrow {}^1S_0 s$

For example, the production of neutral mesons with negative parity – as pseudoscalar or vector mesons – may proceed in the proton-proton collision near threshold only via the transition between  ${}^3P_0$  and  ${}^1S_0 s$  partial waves. This means that only the collision of protons with relative angular momentum equal to  $1\hbar$  may lead to the production of such mesons. Moreover, an inspection of the corresponding Clebsch-Gordan coefficients reveals that it is four times more probable that the orientation of spins of the colliding nucleons is parallel than anti-parallel.

In the case of the production of neutral scalar mesons, the protons or neutrons must collide with anti-parallel spin orientations which remains unchanged after the reaction. These simple considerations imply that in close-to-threshold measurements with polarized beam and target one should see a drastic effect in the reaction yield depending whether the polarization of the reacting protons is parallel or anti-parallel. Indeed, in reality, strong differences in the yield for various combinations of beam and target polarization have been determined in the pioneering measurements of the reaction  $\vec{p}\vec{p} \rightarrow pp\pi^0$  at the IUCF facility [80].

Although close-to-threshold higher partial waves are not expected, detailed studies of meson-nucleon interaction require a careful determination of their contributions, in order to avoid false assignment of the

observed signals. If we allow for the production of protons with the relative angular momentum  $L = 0$  or 1 and confine the  $\eta$  meson production to the  $l = 0$  only, then the  $pp \rightarrow pp\eta$  reaction may proceed via three possible transitions listed in table 3.2.

**Table 3.2:** Transitions for the  $pp \rightarrow pp\text{Meson}(0^-)$  reaction in the case where  $l = 0$  and  $L = 0$  or 1. More comprehensive list of allowed transitions for the low partial waves in the  $NN \rightarrow NNX$  reaction can be found in references [81, 82]

$2S^i+1L_J^i$	$\rightarrow$	$2S+1L_J, l$
$^3P_0$	$\rightarrow$	$^1S_0 s$
$^1S_0$	$\rightarrow$	$^3P_0 s$
$^1D_2$	$\rightarrow$	$^3P_2 s$

It is worth to note that the conservation rules mentioned above forbid the production of the  $\eta$  meson with  $l = 1$  if the protons are in the S-wave ( $^1S_0 p$ ). In other words, the  $\eta$  meson can be produced in the p-wave only if  $L$  is larger than zero. This suggests that with an increase of the excess energy the higher partial waves in the  $pp\eta$  system should first appear in the proton-proton subsystem. In fact such an effect was already observed in experiments at the SATURN laboratory in the case of the  $\phi$  meson production via the  $pp \rightarrow pp\phi$  reaction [83]. Since the  $\eta$  production is dominated by the formation and deexcitation of the S-wave baryonic resonance ( $S_{11}(1535)$ ) this supposition becomes even more plausible.

Another important feature of the  $pp \rightarrow ppX$  and also  $nn \rightarrow nnX$  reactions, pointed out in reference [82], is the fact that the interference terms between the transitions with odd and even values of the angular momentum  $L$  of the final state baryons are bound to vanish. This characteristic is due to the invariance of all observables under the exchange of identical nucleons in the final state. Thus, for instance, out of three possible interference terms for transitions listed in table 3.2 only one – namely the interference between the  $^3P_0 s$  and  $^3P_2 s$  final states – will contribute to the production process significantly simplifying an interpretation of the experimental data. In general, conservation of the basic quantum numbers leads – as derived in reference [81] – to the following selection rule for the  $NN \rightarrow NNX$  reaction:

$$(-1)^{(\Delta S + \Delta T)} = \pi_X (-1)^l, \quad (3.17)$$

where  $\pi_X$  describes the intrinsic parity of meson X,  $\Delta S$  denotes the change in the spin, and  $\Delta T$  in isospin, between the initial and final

$NN$  systems. A possible non-zero angular momentum between the outgoing particles can manifest itself in an unisotropic population of the appropriate angles. In particular, the angular distribution of the  $\eta$  meson observed in the overall centre-of-mass frame should reflect a possible non-zero value of  $l$ . However, for the study of the angular momentum  $L$  we need to use another reference system, since for a three body final state the beam axis is not a good reference direction to look for the angular distributions relevant for the relative angular momenta of the two particles [84]. This is because for the fixed relative settings of the two protons the angle between the beam and the vector of relative protons momentum may acquire any value. Searching for an appropriate variable let us consider a two body scattering. In this case, the beam line, which is at the same time the line along which the centre-of-mass system is moving, constitutes a reference frame for the angular distributions. Therefore, by analogy to the two body system, an instructive reference axis for angular distributions in the proton-proton subsystem is now the momentum of the recoil  $\eta$  meson, since the direction of that meson is identical to the direction of the movement of the proton-proton centre-of-mass subsystem.

Figure 3.1 visualises both above introduced angles  $\theta_\eta^*$  and  $\theta_{pp}^{**}$ , the latter

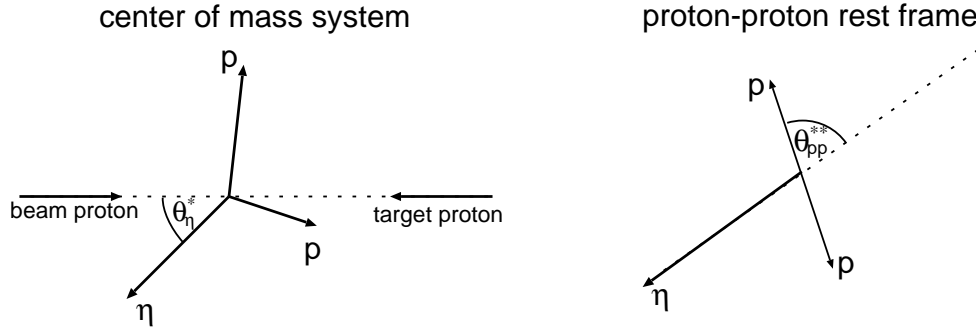


**Figure 3.1:** Definition of the angles used in the text. Throughout the whole work the angles in the overall centre-of-mass frame will be denoted by one asterisk, those in the two-particle subsystems by two asterisks, and the angle in laboratory system will be left without any superscript.

being defined as the angle between the relative proton-proton momentum and the recoil particle ( $\eta$ ) seen from the di-proton rest system [84].

### 3.3 Phase space population

*It is essential to science that its matter should be in a space, but the space in which it is cannot be exactly the space we see or feel [85].*

Bertrand Russell

Due to both the strong nucleon-nucleon low-energy interaction in the  $^1S_0$  state and the meson-nucleon forces in the exit channel, the assumption of non-interacting plane waves leading to equation (3.13) failed when confronted with the experimental data. However, these deviations offer the possibility to determine still poorly known nucleon-meson interactions. The interaction between particles depends on their relative momenta. Consequently, for investigations of final state interactions, more instructive coordinates than the  $q$  and  $k$  momenta are the squared invariant masses of the two-body subsystems [84]. These are the coordinates of the Dalitz plot. In the original paper [86] Dalitz has proposed a representation for the energy partitions of three bodies in an equilateral triangle whose sides are the axes of the centre-of-mass energies. He took advantage of the fact that the sum of distances from a point within the triangle to its sides is a constant equal to the height. Therefore, the height of the triangle measures the total energy  $\sqrt{s} = E_1^* + E_2^* + E_3^*$  and interior points – fulfilling four-momentum conservation – represent energy partitions. For a constant  $\sqrt{s}$ , due to the energy conservation, without losing any information, it is enough to consider the projection on any of the  $E_i E_j$  planes. The linear relation between  $E_i^*$  and  $s_{jk}$  ( $s_{jk} = s + m_i^2 - 2\sqrt{s}E_i^*$ ) allows to use  $s_{jk} s_{ik}$  or  $E_i E_j$  coordinates equivalently, with the following relation between the phase space intervals:  $dE_i^* dE_j^* = \frac{1}{4s} ds_{jk} ds_{ki}$ . According to Kilian's geometrical representation [84] a Dalitz plot lies on a plane in the three dimensional space  $(s_{12}, s_{13}, s_{23})$  orthogonal to the space diagonal. The plane including a Dalitz plot corresponding to a fixed total energy  $\sqrt{s}$  is then given by the following scalar product [84]:

$$(1, 1, 1)(s_{12}, s_{13}, s_{23}) = s_{12} + s_{13} + s_{23} = s + m_1^2 + m_2^2 + m_3^2. \quad (3.18)$$

The second equality of equation (3.18) means that there are only two independent invariant masses of the three subsystems and therefore a projection onto any of the  $s_{ij} s_{jk}$  planes still comprises the whole principally accessible information about the final state interaction of the three-particle system. In the case of no dynamics whatsoever and the absence of any final state interaction the occupation of the Dalitz plot would be

fully homogeneous since the creation in each phase space interval would be equally probable. The final state interaction would then appear as a structure in that area.

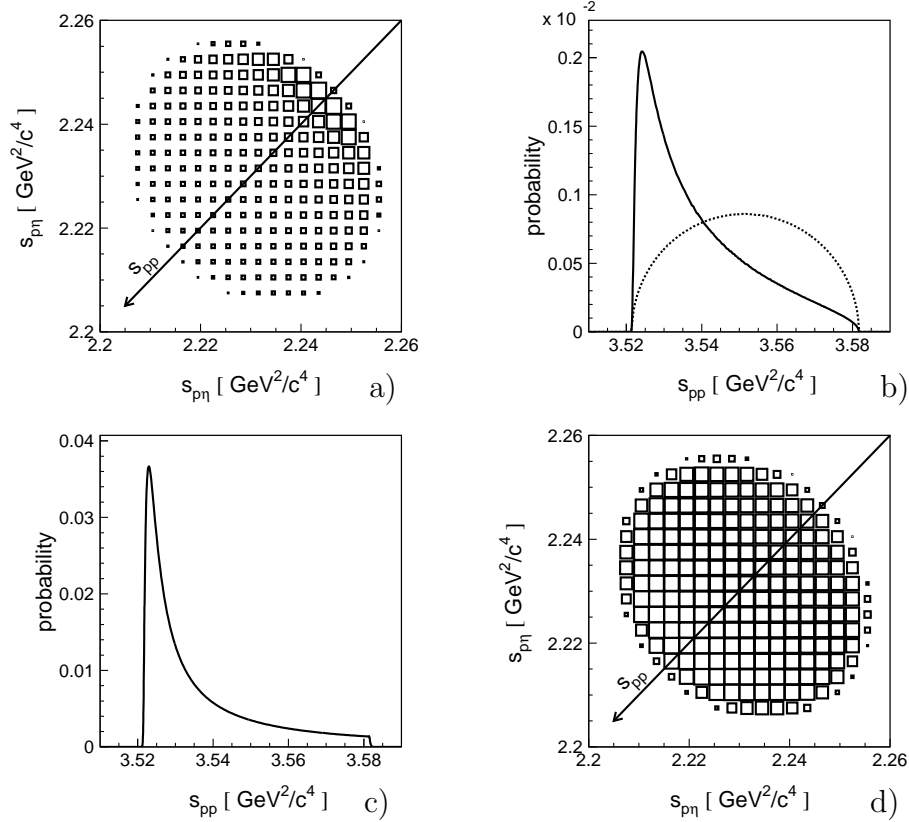


**Figure 3.2:** Monte-Carlo simulations: (a) Phase-space distribution for the  $pp \rightarrow pp\eta$  reaction at  $Q = 16$  MeV modified by the proton-proton final state interaction. (b) The dotted line shows the projection of the pure phase space density distribution onto the  $s_{pp}$  axis and the solid curve presents its modification by the proton-proton FSI. (c) The square of the scattering amplitude for the  $pp \rightarrow pp$  elastic scattering as a function of the proton-proton invariant mass in the range  $2m_p < \sqrt{s_{pp}} < 2m_p + Q$ , calculated according to formula (4.6) of section 4.2. (d) Phase-space density distribution modified by the proton- $\eta$  interaction, with a scattering length equal to  $a_{p\eta} = 0.7 \text{ fm} + i0.3 \text{ fm}$ . The proton- $\eta$  scattering amplitude has been calculated according to equation (4.9). A detailed discussion of the nucleon-nucleon and nucleon-meson interaction will be presented in section 4.2.

Figure 3.2a shows – for the example of the  $pp \rightarrow pp\eta$  reaction – how the uniformly populated phase space density is modified by the S-wave ( $^1S_0$ ) interaction between outgoing protons. An enhancement in the range corresponding to low relative momenta between protons is clearly visible. A steep decrease of the occupation density with increasing invariant mass of

the proton-proton subsystem is even better seen in figure 3.2b presenting the projection of the phase space distribution onto the  $s_{pp}$  axis indicated by an arrow in figure 3.2a. This is a direct reflection of the shape of the proton-proton ( $^1S_0$ ) partial wave amplitude shown in figure 3.2c. Figure 3.2d shows the Dalitz plot distribution simulated when switching off the proton-proton interaction but accounting for the interaction between the  $\eta$ -meson and the proton. Due to the lower strength of this interaction the expected deviations from the uniform distributions are by about two orders of magnitude smaller, but still one recognizes a slight enhancement of the density in the range of low invariant masses of proton- $\eta$  subsystems. However, due to weak variations of the proton- $\eta$  scattering amplitude the enhancement originating from the  $\eta$ -meson interaction with one proton is not separated from the  $\eta$ -meson interaction with the second proton. Therefore an overlapping of broad structures occurs. It is observed that the occupation density grows slowly with increasing  $s_{pp}$  opposite to the effects caused by the S-wave proton-proton interaction, yet similar to the modifications expected for the P-wave one [87]. From the above example it is obvious that only in high statistics experiments signals from the meson-nucleon interaction can appear over the overwhelming nucleon-nucleon final state interaction. It is worth noting, however, that the Dalitz plot does not reflect any possible correlations between the entrance and exit channels [84].

The Dalitz plot representation allows also for a simple interpretation of the kinematically available phase space volume as an area of that plot. Namely, equation (3.1) becomes:

$$\sigma = \frac{1}{F} \frac{\pi^2}{4s} \int_{(m_1+m_2)^2}^{(\sqrt{s}-m_3)^2} ds_{12} \int_{s_{23}^{min}(s_{12})}^{s_{23}^{max}(s_{12})} ds_{23} |M_{ab \rightarrow 123}|^2, \quad (3.19)$$

where the limits of integrations defining the boundaries of the Dalitz plot can be expressed as [70]:

$$s_{23}^{max}(s_{12}) = m_2^2 + m_3^2 - \frac{(s_{12} - s + m_3^2)(s_{12} + m_2^2 - m_1^2) - \sqrt{\lambda(s_{12}, s, m_3^2)\lambda(s_{12}, m_2^2, m_1^2)}}{2s_{12}}$$

$$s_{23}^{min}(s_{12}) = m_2^2 + m_3^2 - \frac{(s_{12} - s + m_3^2)(s_{12} + m_2^2 - m_1^2) + \sqrt{\lambda(s_{12}, s, m_3^2)\lambda(s_{12}, m_2^2, m_1^2)}}{2s_{12}}.$$



Thus, the phase space volume kinematically available for the three-body final state can be written by means of only one integral:

$$\begin{aligned}
 V_{ps} &= \int dV_{ps} = \frac{\pi^2}{4s} \int_{(m_1+m_2)^2}^{(\sqrt{s}-m_3)^2} ds_{12} \int_{s_{23}^{min}(s_{12})}^{s_{23}^{max}(s_{12})} ds_{23} = \\
 &= \frac{\pi^2}{4s} \int_{(m_1+m_2)^2}^{(\sqrt{s}-m_3)^2} \frac{ds_{12}}{s_{12}} \sqrt{\lambda(s_{12}, s, m_3^2) \lambda(s_{12}, m_2^2, m_1^2)}, \quad (3.20)
 \end{aligned}$$

whose solution leads, in general, to elliptic functions [70]. However, in the nonrelativistic approximation it has the following closed form:

$$V_{ps} = \frac{\pi^3}{2} \frac{\sqrt{m_1 m_2 m_3}}{(m_1 + m_2 + m_3)^{\frac{3}{2}}} Q^2, \quad (3.21)$$

where the substitution of the non-relativistic relation between  $\eta_{m_3}$  and  $Q$

$$Q = \frac{m_3^2 + 2m_3^2(m_1 + m_2)}{2(m_1 + m_2)} \eta_{m_3}^2$$

gives the  $Ss$  partial cross section of equation (3.13). On the basis of formula (3.21) the kinematically available phase space volume ( $V_{ps}$ ) can be as easily calculated as the excess energy  $Q$ . Close-to-threshold – in the range of few tens of MeV – the non-relativistic approximation differs only by a few per cent from the full solution given in equation (3.20), which in fact with an up-to-date computer can be solved numerically with little effort. Therefore, in the following chapters we will describe the data as a function of  $V_{ps}$  as well as of  $Q$  or  $\eta_M$ , if it is found to be appropriate.

### 3.4 Orientation of the emission plane

*Angles are the invention of Man;  
God uses vectors! [88]*

Colin Wilkin

For the full description of the three particle system five independent variables are required. In the center-of-mass frame, due to the momentum conservation, the momentum vectors of the particles are lying in one plane often referred to as the emission-, reaction-, or decay plane. In this plane (depicted in figure 3.3) a relative movement of the particles can be

described by two variables only. As anticipated in the previous section, the square of the invariant masses of the di-proton and proton- $\eta$  system denoted as  $s_{pp}$  and  $s_{p\eta}$ , respectively, constitute a natural choice for the study of the interaction within the  $pp\eta$  system. This is because in the case of non-interacting objects the surface spanned by these variables is homogeneously populated. The interaction among the particles modifies that occupation density and in consequence facilitates an easy qualitative interpretation of the experimental results.

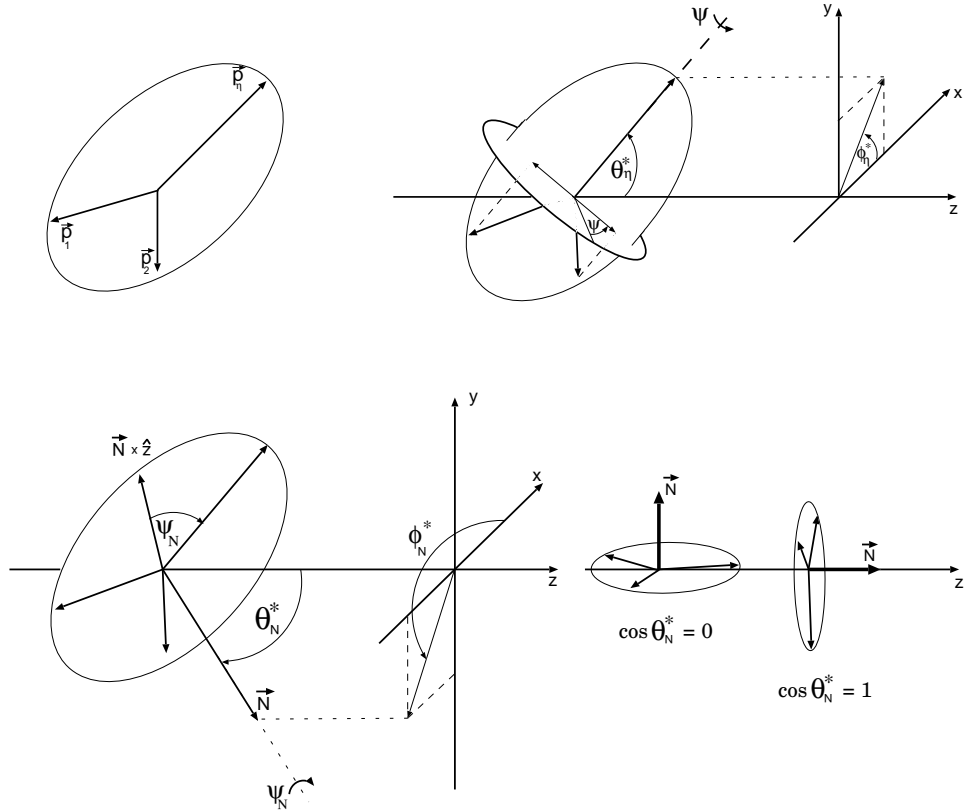


**Figure 3.3:** Definition of the centre-of-mass kinematical variables used for the description of the  $pp\eta$  system. In the centre-of-mass frame, the momenta of ejectiles lie in an emission plane. Within this plane the relative movement of the particles is fixed by the square of the invariant masses  $s_{pp}$  and  $s_{p\eta}$ . As the remaining three variables needed to define the system uniquely we use either  $\phi_\eta^*$ ,  $\theta_\eta^*$ , and  $\psi$  shown in the upper panel or  $\phi_N^*$ ,  $\theta_N^*$ , and  $\psi_N$  defined in the lower panel.  $\vec{N}$  is a vector normal to the emission plane, which can be calculated as the vector product of the centre-of-mass momentum vectors of the outgoing protons. As an example two extreme orientations of the emission plane are shown in the right-lower panel. For further descriptions see the text.

The remaining three variables must define an absolute orientation of the emission plane in the distinguished coordinate system. This may be attained – for example – by defining the orientation for the momentum of the arbitrarily chosen particle in the center-of-mass frame and the angle which describes the rotation around the direction fixed by that particle. In one of our choices (following references [83,89]) the corresponding variables are the polar and the azimuthal angle of the  $\eta$  momentum vector, depicted in figure 3.3 as  $\phi_\eta^*$  and  $\theta_\eta^*$ , respectively, and the angle  $\psi$  describing the rotation around the direction established by the momentum of the  $\eta$  meson. Figure 3.3 demonstrates that such rotation neither affects the  $\eta$  meson momentum nor changes the configuration of the momenta in the emission plane. For experiments with unpolarized beams and targets the only favoured direction is the one of the beam. Therefore, as a zero value of the  $\psi$  angle we have chosen the projection of the beam direction on the plane perpendicular to the momentum vector of the  $\eta$  meson. Note that we identify the z-axis with the beam direction. The  $\phi_\eta^*$ ,  $\theta_\eta^*$ , and  $\psi$  variables can also be interpreted as Euler angles allowing for the rotation of the emission plane into a xz-plane. The angle  $\psi$  may be calculated as an angle between the emission plane and the plane containing momentum vectors of the  $\eta$  meson and the beam proton, or correspondingly as an angle between the vectors normal to these planes. The angle  $\psi$  is equal to zero when these two normals are parallel.

As a second possibility we will describe an orientation of the emission plane by the azimuthal and polar angle of the vector normal to that plane [261]. These angles are shown in figure 3.3 as  $\phi_N^*$  and  $\theta_N^*$ , respectively. Further the absolute orientation of the particles momenta in the emission plane will be described by  $\psi_N$ , the angle between the  $\eta$  meson and the vector product of the beam momentum and the vector  $\vec{N}$ .

Obviously, the interaction between particles does not depend on the orientation of the emission plane, and therefore, it will fully manifest itself in the occupation density of the Dalitz plot which in our case will be represented in terms of the square of the invariant masses of the two particle subsystems. Yet, the distribution of the orientation of the emission plane will reflect the correlation between the initial and final channels and hence its determination should be helpful for the investigation of the production mechanism.



## 4. Low energy interaction within the $pp\eta$ and $pp\eta'$ systems

*It frequently happens that, when particles are produced in a nuclear or elementary particle reaction, some of these interact among themselves so strongly that they influence appreciably the properties of the reaction cross section. **These interactions we shall call “final state interaction”** [66].*

Kenneth Watson

In general, for a three-body exit channel one expects an energy dependence of the total cross section which can be described by the linear combination of partial cross sections from equation (3.13). Therefore, to extract information about the final state interaction of the outgoing particles the contributions originating from different partial waves have to be known precisely. Appropriately, close-to-threshold there is only one important combination of angular momenta of emitted particles (Ss) and in this region the energy dependence of the total cross section is uniquely determined and hence the interpretation of results is significantly simplified. This is one of the most important advantages of the meson creation at its production threshold, however, in order to exploit this fact properly it is essential to determine the range of its applicability, which – as will be demonstrated in the next section – changes significantly with the mass of the produced meson.

### 4.1 Range of the dominance of the ${}^3P_0 \rightarrow {}^1S_0 s$ transition

*... the most exact of sciences are those which are most concerned with primary considerations: for sciences based on few assumptions are more exact than those which employ additional assumptions ... [90].*

Aristotle

Investigations with polarized beams and targets [78,91] of the  $\vec{p}\vec{p} \rightarrow pp\pi^0$  reaction allowed to deduce that the Ss partial-wave accounts for more than 95 % of the total cross section up to  $\eta_M \approx 0.4$ , as can be seen in figure 4.1a, where the Ss contribution is indicated by the dotted line. The

Ss contribution was inferred assuming the  $\eta_M^6$  and  $\eta_M^8$  dependence for Ps and Pp partial waves, respectively. These are power-laws taken from proportionality (3.13), which was derived under the assumption of non-interacting particles. Relatively small values of  $^3P_0$ -wave nucleon-nucleon phase-shifts at low energies (compared to  $^1S_0$  phase-shifts in figure 4.1b) and similarly weak low-energy interactions of P-wave protons in other spin combinations [92] justify this assumption.

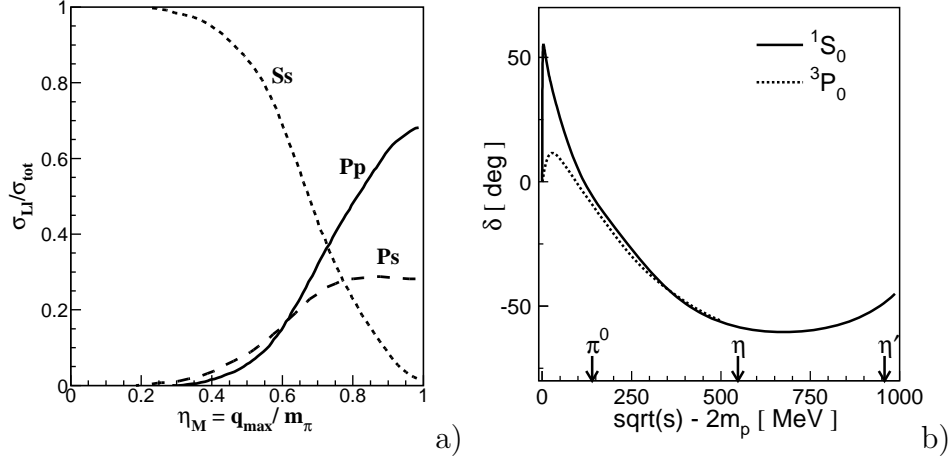


**Figure 4.1:** (a) Decomposition of the total cross section of the  $pp \rightarrow pp\pi^0$  reaction into Ss, Ps, and Pp final state angular momenta. The dashed and solid lines represent the  $\eta_M^6$  and  $\eta_M^8$  dependence of Ps and Pp partial cross sections, respectively. The remainder is indicated as the dotted line. The Sp partial wave is forbidden by the conservation laws and the Pauli excluding principle. Note that at  $\eta_M = 1$  the Pp and Ps partial waves seem to dominate. However, the analysis of the differential cross section measured at CELSIUS at  $\eta_M = 0.449$  [93, 117] showed that also a d-wave pion production – due to the interference between Ss and Sd states – constitutes 7 % of the total cross section, when a meson-exchange model is assumed. The figure has been adapted from [78]. (b) The  $^1S_0$  and  $^3P_0$  phase-shifts of the nucleon-nucleon potential shown versus the centre-of-mass kinetic energy available in the proton-proton system. The values have been extracted from the SAID data base [94] (solution SM97). For higher energies the S- and P-wave phase-shifts are nearly the same. This is because the collision parameter required to yield the angular momentum of  $1\hbar$  diminishes significantly below 1 fm with increasing energy and consequently the interaction of nucleons – objects of about 1 fm size – becomes almost central.

In accordance with the phenomenology of Gell-Mann and Watson [77] described in section 3.2 one expects that also in the case of heavier mesons the Ss partial wave combination will constitute the overwhelming fraction of the total production cross section for  $\eta_M$  smaller than 0.4. This implies – as can be deduced from the relation between  $\eta_M$  and Q illustrated in figure 4.2a – that mesons heavier than the pion are produced exclusively via the Ss state in a much larger excess energy range and hence larger phase space volume (see figure 4.2b). Thus, whereas for  $\pi^0$  production

the onset of higher partial waves is observed at  $Q$  around 10 MeV it is expected only above 100 MeV and above  $\approx 40$  MeV for  $\eta'$  and  $\eta$  mesons, respectively.

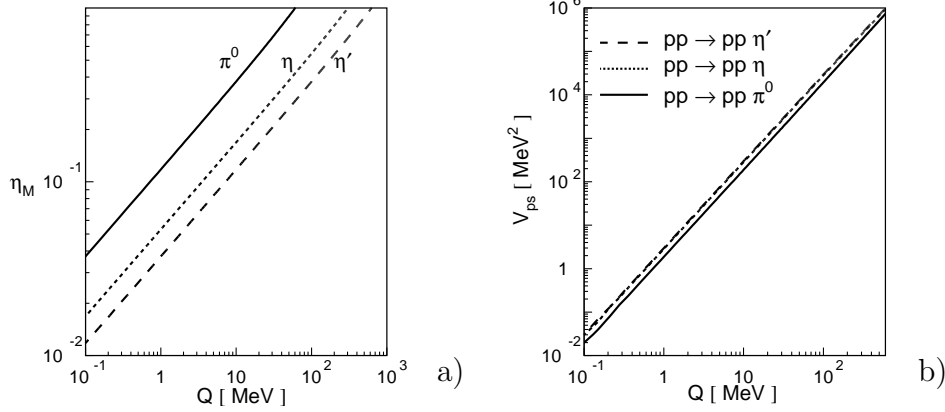


**Figure 4.2:** (a) The variable  $\eta_M$  as a function of the excess energy for  $\pi^0$ ,  $\eta$ , and  $\eta'$  mesons produced via  $pp \rightarrow pp \text{ Meson}$  reactions. (b) The phase space volume  $V_{ps}$  (defined by equation (3.20)) versus the excess energy  $Q$ . The picture indicates that for the production of “heavy mesons” in the nucleon-nucleon interaction at a given  $Q$  value there is only a slight difference of the available phase space volume on the produced meson mass, which is larger than that of  $\pi^0$  production by about 30 % only. Therefore, for the comparative studies of the production dynamics of different mesons,  $Q$  is as much a suitable variable as  $V_{ps}$ . Note, that the dashed and dotted lines are almost undistinguishable.

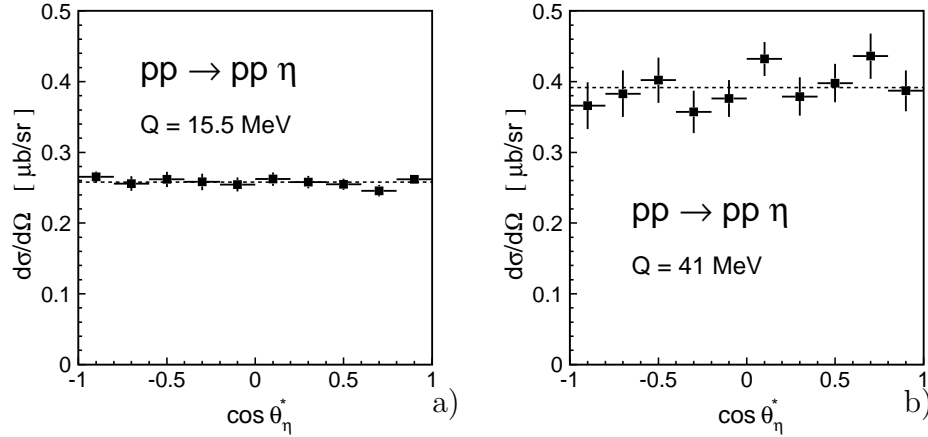


**Figure 4.3:** Differential cross section of the  $pp \rightarrow pp\eta$  reaction as a function of the meson centre-of-mass polar angle. Dashed lines indicate the isotropic distribution. Shown are results of measurements for  $Q = 15.5$  MeV [1, 18] (a) and  $Q = 41$  MeV [95] (b). Only statistical errors are plotted, which in figure (a) are smaller than the size of symbols. The distribution presented in picture (a) is consistent with a measurement performed at an excess energy of  $Q = 16$  MeV by means of the PROMICE/WASA detector [96], whereas the data at  $Q = 37$  MeV also from reference [96] deviate significantly from isotropy. However, data shown in picture (b) have been taken with a detector of much higher angular acceptance.

Figures 4.3a and 4.3b present the angular distributions of the created  $\eta$  meson in proton collisions. It is evident that at  $Q = 15.5$  MeV and still at  $Q = 41$  MeV the production of the  $\eta$  meson is completely isotropic within the shown statistical errors. Although at  $Q = 41$  MeV the accuracy of the data does not exclude a few per cent of contributions originating from higher partial waves, the dominance of the s-wave creation is evident. Similarly, the measurements of the differential cross section (figure 4.4) for the  $pp \rightarrow pp\eta'$  reaction performed at SATURNE [97] at  $Q = 143.8$  MeV and at COSY [5] at  $Q = 46.6$  MeV are still consistent with pure Ss-wave production, though the relatively large error bars would allow for other contributions on a few per cent level ( $\approx 10\%$ ). The observation, reported in section 6.3, that distributions of the orientation of the emission plane (fig. 6.23) and angle  $\psi$  (fig. 6.20) are anisotropic, also suggests a small contribution of higher order partial waves. Specifically, the modulus of the cosine of the po-

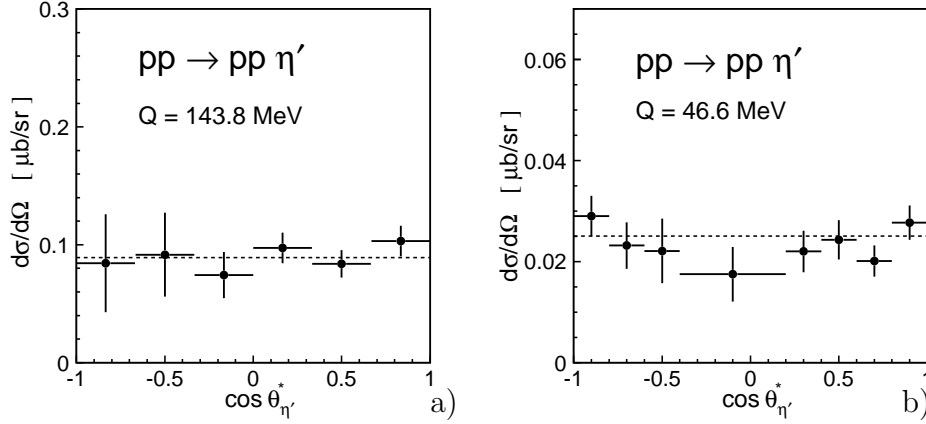


**Figure 4.4:** Differential cross section of the  $pp \rightarrow pp\eta'$  reaction as a function of the meson centre-of-mass polar angle. Dashed lines indicate the isotropic distribution. Shown are results of measurements for the  $pp \rightarrow pp\eta'$  reaction taken at  $Q = 143.8$  MeV [97] (a) and at  $Q = 46.6$  MeV [5] (b).

lar angle of the vector normal to the emission plane, whose distribution is found to be anisotropic, is a function of the sixth power of the final momenta ( $|\cos(\theta_N^*)| \sim \sqrt{|(\vec{p}_{proton_1} \times \vec{p}_{proton_2}) \cdot \vec{p}_{beam}|^2}$ ), and even more peculiar the sine of the angle  $\psi$ , which is a function of the eighth power of the final momenta ( $|\sin(\psi)| \sim \sqrt{|(\vec{p}_{proton_1} \times \vec{p}_{proton_2}) \cdot (\vec{p}_\eta \times \vec{p}_{beam})|^2}$ ), is found to be anisotropic too. This could be a sign of an interference between partial waves higher than Ss-wave <sup>1</sup>.

<sup>1</sup> We are grateful to Colin Wilkin for sharing with us this astonishment.



## 4.2 Influence of the $pp\eta$ and $pp\eta'$ interaction on the excitation function of the $pp \rightarrow pp\eta(\eta')$ reaction

*The only proof capable of being given that an object is visible, is that people actually see it. The only proof that a sound is audible, is that people hear it: and so of the other sources of our experience [98].*

John Stuart Mill

Let us now consider to what extent the energy dependence of the total cross section in the estimated range of the dominance of the Ss partial waves can be understood in terms of the phase space variation and the interaction between the particles participating in the reaction. Watson [66] and Migdal [99] proposed the factorization of the amplitude when the production is of short- and the interaction among the outgoing particles of long range. This requirement is well fulfilled for the close-to-threshold meson production due to the large momentum transfer ( $\Delta p$ ) between the interacting nucleons needed to create the considered mesons ( $\pi, \eta, \dots, \phi$ ).

**Table 4.1:** Momentum transfer  $\Delta p$  calculated according to equation 3.14 and the corresponding distance  $R \approx \hbar/\Delta p$  probed by the  $NN \rightarrow NN \text{ Boson}$  reaction at the kinematical threshold for different particles produced. The table has been adapted from [100].

particle	mass [MeV]	$\Delta p$ [ $\text{fm}^{-1}$ ]	R [fm]
$\gamma$	0	0.0	$\infty$
$\pi$	140	1.9	0.53
$\eta$	550	3.9	0.26
$\rho, \omega$	780	4.8	0.21
$\eta'$	960	5.4	0.19
$\phi$	1020	5.6	0.18

According to the Heisenberg uncertainty relation the large momentum transfer brings about a small space in which the primary creation of the meson takes place. In table 4.1 the distance probed by the  $NN \rightarrow NN \text{ Meson}$  reaction at threshold is listed for particular mesons. It ranges from 0.53 fm for pion production to 0.18 fm for the  $\phi$  meson, whereas the typical range of the strong nucleon-nucleon interaction at

low energies determined by the pion exchange may exceed a distance of a few Fermi and hence is by one order of magnitude larger than the values listed in table 4.1. Thus in analogy to the Watson-Migdal approximation for two-body processes [66] the complete transition matrix element of equation (3.1) may be factorized approximately as <sup>2</sup>

$$|M_{pp \rightarrow ppX}|^2 \approx |M_{FSI}|^2 \cdot |M_0|^2 \cdot F_{ISI}, \quad (4.1)$$

where  $M_0$  represents the total short range production amplitude,  $M_{FSI}$  describes the elastic interaction among particles in the exit channel and  $F_{ISI}$  denotes the reduction factor accounting for the interaction of the colliding protons. Further, in the first order approximation one assumes that the particles are produced on their mass shell and that the created meson does not interact with nucleons. This assumption implies that the  $|M_{FSI}|^2$  term can be substituted by the square of the on-shell amplitude of the nucleon-nucleon elastic scattering:

$$|M_{FSI}|^2 = |M_{NN \rightarrow NN}|^2. \quad (4.2)$$

Effects of this rather bold assumption will be considered later, when comparing the estimation with the experimental data.

In the frame of the optical potential model the scattering amplitude is determined by phase-shifts. Particularly, the  $^1S_0$  proton-proton partial wave – relevant for further considerations – can be expressed explicitly as follows [102]:

$$M_{pp \rightarrow pp} = \frac{e^{-i\delta_{pp}(^1S_0)} \cdot \sin \delta_{pp}(^1S_0)}{C \cdot k}, \quad (4.3)$$

where  $C$  denotes the square root of the Coulomb penetration factor.  $C^2$  determines the ratio of the probability of finding two particles close together to the probability of finding two uncharged particles together, all other things being equal [103] and can be expressed as [104]:

$$C^2 = \frac{2\pi\eta_c}{e^{2\pi\eta_c} - 1}, \quad (4.4)$$

where  $\eta_c$  is the relativistic Coulomb parameter, which for the collision of particles  $i, j$  reads:

$$\eta_c = \frac{q_i q_j \alpha}{v} = q_i q_j \alpha \frac{s_{ij} - m_i^2 - m_j^2}{\sqrt{\lambda(s_{ij}, m_i^2, m_j^2)}},$$

---

<sup>2</sup> For a comprehensive discussion of the FSI and ISI issue including a historical overview and a criticism of various approaches the reader is referred to [101].

with the fine structure constant  $\alpha$ , the relative velocity  $v$  of the colliding particles and with  $q_i, q_j$  denoting their charges <sup>3</sup>.

The variable  $k$  in equation 4.3 stands for either proton momentum in the proton-proton rest frame and the phase-shift is indicated by  $\delta_{pp}$ . The phase-shifts  $\delta_{pp}(^1S_0)$  can be extracted from the SAID data base (see fig. 4.1b) or, alternatively, can be calculated according to the modified Cini-Fubini-Stanghellini formula including the Wong-Noyes Coulomb correction [107–109]

$$C^2 k \operatorname{ctg}(\delta_{pp}) + 2k\eta_c h(\eta_c) = -\frac{1}{a_{pp}} + \frac{b_{pp}k^2}{2} - \frac{P_{pp}k^4}{1+Q_{pp}k^2}, \quad (4.5)$$

where  $h(\eta_c) = -\ln(\eta_c) - 0.57721 + \eta_c^2 \sum_{n=1}^{\infty} \frac{1}{n \cdot (n^2 + \eta_c^2)}$  [103].

The phenomenological quantities  $a_{pp} = -7.83 \text{ fm}$  and  $b_{pp} = 2.8 \text{ fm}$  denote the scattering length and effective range [107], respectively. The parameters  $P_{pp} = 0.73 \text{ fm}^3$  and  $Q_{pp} = 3.35 \text{ fm}^2$  are related to the detailed shape of the nuclear potential and derived from a one-pion-exchange model [107]. Substituting equation (4.5) into equation (4.3) allows to calculate the low-energy amplitude for the proton-proton elastic scattering <sup>4</sup>:

$$|M_{pp \rightarrow pp}|^2 = \frac{C^2}{C^4 k^2 + \left( -\frac{1}{a_{pp}} + \frac{b_{pp}k^2}{2} - \frac{P_{pp}k^4}{1+Q_{pp}k^2} - 2k\eta_c h(\eta_c) \right)^2}. \quad (4.6)$$

The result is presented as a solid line in figure 4.5a and is in good agreement with the values obtained from the phase-shifts of the VPI partial wave analysis [94], shown as solid circles and with the phase-shifts of the Nijmegen analysis [110], shown as open squares. The factor  $C^2$  is always less than unity due to the Coulomb repulsion between protons. At higher energies, where  $C^2$  is close to unity, the nuclear scattering will be predominant and for the very low energies the Coulomb and nuclear interactions are competing. The Coulomb scattering dominates approximately up to about 0.8 MeV of the proton energy in the rest frame of the other proton, where  $C^2$  equals to one-half [103]. In the case of the  $pp \rightarrow pp \text{ Meson}$  reaction the maximum possible energy of a proton seen from another proton is equal to 0.8 MeV already at an excess energy of about  $Q = 0.4 \text{ MeV}$ . Therefore, a significant influence of the Coulomb

<sup>3</sup> For collisions at an angular momentum  $l$  larger than  $0\hbar$  the  $C^2$  of equation (4.4) needs to be multiplied by a factor of  $\prod_{n=1}^l (1 + (\eta_c/n)^2)$  [105, 106].

<sup>4</sup> In principle the formula is valid for  $k \leq 133 \text{ MeV}/c$  [108].  $|M_{pp \rightarrow pp}|^2$  is taken to be constant for larger values of  $k$ .

repulsion on the energy dependence of the total production cross section is expected only at very low excess energies, i.e. conservatively for  $Q \leq 2$  MeV.

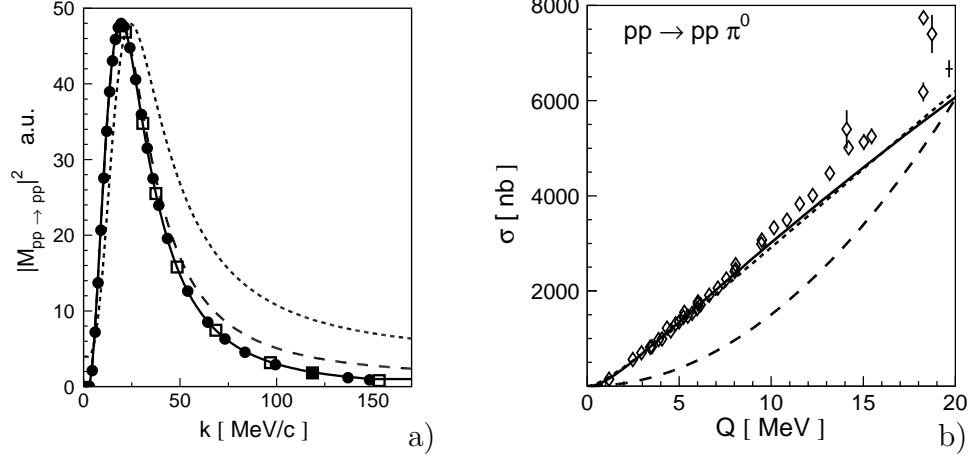


**Figure 4.5:** (a) Square of the proton-proton scattering amplitude versus  $k$ , the proton momentum in the proton-proton subsystem from [102, 107] (solid line), [111] (dashed line), and [112, 113] (dotted line). The filled circles are extracted from [94] and the opened squares from [110]. The curves and symbols have been arbitrarily normalized to be equal at maximum to the result from reference [111], shown as the dashed line. (b) Total cross section for the  $pp \rightarrow pp\pi^0$  reaction as a function of the centre-of-mass excess energy  $Q$ . Data are from refs. [114–117]. The dashed line indicates a phase space integral normalized arbitrarily. The phase space distribution with inclusion of proton-proton strong and Coulomb interactions fitted to the data at low excess energies is shown as the solid line. The dotted line indicates the parametrization of reference [118] written explicitly in equation (4.7), with  $\epsilon = 0.3$ .

Assuming that the on-shell proton-proton amplitude determines exclusively the phase space population one can obtain the total cross section energy dependence substituting equation (4.6) into formula (3.19). The solid line in figure 4.5b represents the determined dependence for the  $pp \rightarrow pp\pi^0$  reaction. The absolute scale of the calculations has been fixed by normalizing to the data. One recognizes the good agreement with the experimental points in the excess energy range up to  $Q \approx 10$  MeV in agreement with the previous conclusions based on the polarisation observables.

The dotted line in figures 4.5b which is practically indistinguishable from the solid line, presents the excess energy dependence of the total cross section taking into account the proton-proton FSI effects according to the model developed by Fäldt and Wilkin [118, 119]. Representing the scattering wave function in terms of a bound state wave function the authors derived a closed formula which describes the effects of the

nucleon-nucleon FSI as a function of the excess energy  $Q$  only. This approach is specifically useful for the description of the spin-triplet proton-neutron FSI, due to the existence of a bound state (deuteron) with the same quantum numbers. Though a bound state of the proton-proton system does not exist, the model allows to express the total cross section energy dependence for a  $pp \rightarrow pp \text{ Meson}$  reaction by a simple and easily utilizable formula:

$$\begin{aligned} \sigma &= \text{const} \cdot \frac{V_{ps}}{F} \cdot \frac{1}{\left(1 + \sqrt{1 + \frac{Q}{\epsilon}}\right)^2} = \\ &= \text{const}' \cdot \frac{Q^2}{\sqrt{\lambda(s, m_p^2, m_p^2)}} \cdot \frac{1}{\left(1 + \sqrt{1 + \frac{Q}{\epsilon}}\right)^2}, \end{aligned} \quad (4.7)$$

where the parameter  $\epsilon$  has to be settled from the data. The flux factor  $F$  and the phase space volume  $V_{ps}$  are given by equations (3.5) and (3.21), respectively. The normalization can be determined from the fit of the data which must be performed for each reaction separately.

The determined energy dependences of the total cross section for  $\eta'$  [3, 5, 11, 53, 97, 120] and  $\eta$  [10, 50–53, 121] mesons production in proton-proton collisions are presented in figure 4.6. Comparing the data to the arbitrarily normalized phase space integrals (dashed lines) reveals that the proton-proton FSI enhances the total cross section by more than an order of magnitude for low excess energies.

One recognizes also that in the case of the  $\eta'$  the data are described very well (solid line) assuming that the on-shell proton-proton amplitude exclusively determines the phase space population. This indicates that the proton- $\eta'$  interaction is too small to manifest itself in the excitation function within the presently achievable accuracy. In the case of  $\eta$  meson production the interaction between nucleons is evidently not sufficient to describe the increase of the total cross section for very low and very high excess energies, as can be concluded from the comparison of the data and the upper solid line in figure 4.6. This line was normalized to the data at an excess energy range between 15 MeV and 40 MeV. The enhancement of the total cross section for higher energies can be assigned to the outset of higher partial waves. As expected from the previous considerations, this is indeed seen at  $Q \approx 40$  MeV where the energy dependence of the total cross section starts to change its shape. On the contrary, the close-to-threshold enhancement – being by about a factor of two larger than in the case of the  $\pi^0$  and  $\eta'$  mesons – can be assigned neither to the

contribution from other than Ss partial waves nor to the variation of the primary production amplitude  $|M_0|$ . The latter is expected to change at the most by a few per cent for excess energies below 20 MeV [124]. Instead, this discrepancy can be plausibly explained by the influence of the attractive interaction between the  $\eta$  meson and the proton.

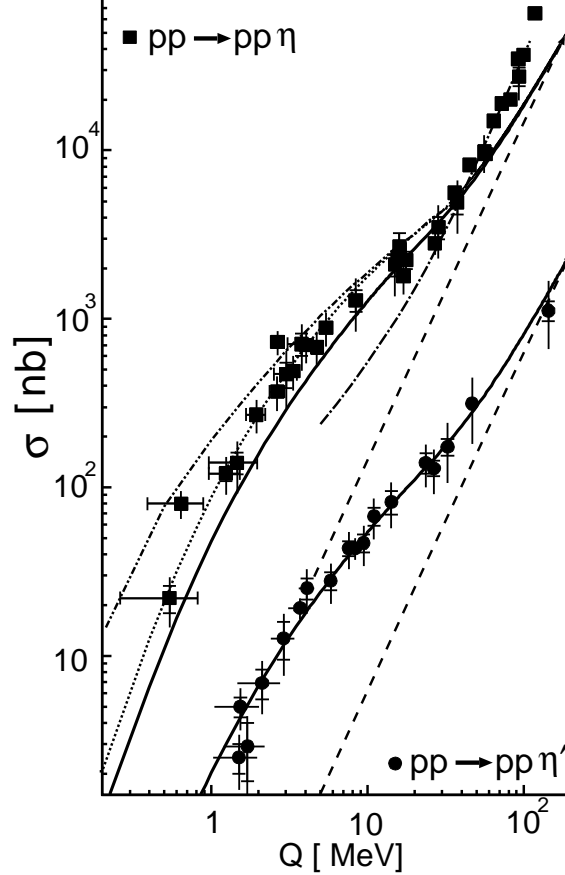


**Figure 4.6:** Total cross section for the reactions  $pp \rightarrow pp\eta'$  (circles) and  $pp \rightarrow pp\eta$  (squares) as a function of the centre-of-mass excess energy  $Q$ . Data are from refs. [3, 5, 10, 11, 50–53, 97, 120, 121]. The dashed lines indicate a phase space integral normalized arbitrarily. The solid lines show the phase space distribution with inclusion of the  $^1S_0$  proton-proton strong and Coulomb interactions. In case of the  $pp \rightarrow pp\eta$  reaction the solid line was fitted to the data in the excess energy range between 15 and 40 MeV. Additional inclusion of the proton- $\eta$  interaction is indicated by the dotted line. The scattering length of  $a_{p\eta} = 0.7 \text{ fm} + i 0.4 \text{ fm}$  and the effective range parameter  $b_{p\eta} = -1.50 \text{ fm} - i 0.24 \text{ fm}$  [36] have been chosen arbitrarily. The dashed-dotted line represents the energy dependence taking into account the contribution from the  $^3P_0 \rightarrow ^1S_0s$ ,  $^1S_0 \rightarrow ^3P_0s$  and  $^1D_2 \rightarrow ^3P_2s$  transitions [79]. Preliminary results for the  $^3P_0 \rightarrow ^1S_0s$  transition with full treatment of three-body effects are shown as a dashed-double-dotted line [122, 123]. The absolute scale of dashed-double-dotted line was arbitrarily fitted to demonstrate the energy dependence only.

Note, that the real part of the scattering length of the  $\eta$ -proton potential – depending on the analysis method and the studied reaction – is 3 to 10 times [38, 125] larger than the scattering length for  $\pi^0$ -proton scattering ( $a_{p\pi} \approx 0.13$  fm) [126]. Hence, the modifications of the total cross section energy dependence due to  $\pi^0$ -proton and  $\eta'$ -proton interaction are too weak to be observed within the up-to-date accuracy of measurements and calculations. However, the influence of the  $\eta$ -proton interaction presented in figure 4.6 is evident and hereafter it will be considered whether it may serve for the estimation of the  $\eta$ -proton scattering parameters.

A strict quantitative calculation requires the evaluation of the three-body Faddeev equation which is out of the scope of the present work<sup>5</sup>. Here, we will rather present a simple phenomenological treatment which shall lead to the qualitative understanding how the mutual interaction among three outgoing particles affects the excitation function. One of the simplest possibilities based on the naive probabilistic interpretation of the incoherent pairwise interaction would be to factorize the overall enhancement factor into corresponding pair interactions [68, 130]:

$$|M_{FSI}|^2 = |M_{12 \rightarrow 12}|^2 \cdot |M_{13 \rightarrow 13}|^2 \cdot |M_{23 \rightarrow 23}|^2, \quad (4.8)$$

where  $|M_{ij \rightarrow ij}|^2$  denotes the square of the elastic scattering amplitude of particles  $i$  and  $j$ . The  $|M_{pp \rightarrow pp}|^2$  term can be evaluated according to the formula (4.6), which for the s-wave  $\eta$ -proton scattering, after substitution of  $C^2 = 1$  and  $\eta_c = P_{pp} = 0$ , reduces to <sup>6</sup>:

$$|M_{p\eta \rightarrow p\eta}|^2 = \left| \frac{1}{\frac{1}{a_{p\eta}} + \frac{b_{p\eta} k_{p\eta}^2}{2} - i k_{p\eta}} \right|^2, \quad (4.9)$$

where

$$k_{p\eta} = \frac{\sqrt{\lambda(s_{p\eta}, m_\eta^2, m_p^2)}}{2\sqrt{s_{p\eta}}}$$

denotes the  $\eta$  momentum in the proton- $\eta$  rest frame. The scattering length  $a_{p\eta}$  and effective range  $b_{p\eta}$  are complex variables with the imaginary part responsible e.g. for the  $p\eta \rightarrow p\pi^0$  conversion.

<sup>5</sup> An exact derivation of the Faddeev equation can be found for example in [127]. Presently few theory groups are carrying on the corresponding calculations [82, 122, 123, 128, 129].

<sup>6</sup> Note that the sign of the term  $-1/a$  from equation (4.6) was changed because the imaginary part of the proton- $\eta$  scattering length is positive [36], as we also adopted here, whereas in the majority of works concerning nucleon-nucleon interaction, the scattering length is negative [64]. We are grateful for this remark to A. Gasparyan.

The factorization of both i) the overall production matrix element (eq. (4.1)) and ii) the three particle final state interactions (eq. (4.8)) applied to formula (3.19) gives the following expression for the total cross section of the  $pp \rightarrow pp\eta$  reaction:

$$\sigma = \frac{F_{ISI} |M_0|^2}{F} \frac{\pi^2}{4s} \int_{(m_p+m_p)^2}^{(\sqrt{s}-m_\eta)^2} ds_{pp} |M_{pp \rightarrow pp}(s_{pp})|^2 \int_{s_{p_2\eta}^{min}(s_{pp})}^{s_{p_2\eta}^{max}(s_{pp})} ds_{p_2\eta} |M_{p_1\eta \rightarrow p_1\eta}(s_{p_1\eta})|^2 \cdot |M_{p_2\eta \rightarrow p_2\eta}(s_{p_2\eta})|^2, \quad (4.10)$$

where the protons are distinguished by subscripts. Exploring formulae (4.6) and (4.9) gives the results shown as the dotted line in figure 4.6. Evidently, the inclusion of the proton- $\eta$  interaction enhances the total cross section close-to-threshold by about a factor of 1.5 and leads to a better description of the data. A similar effect close-to-threshold is also observed in the data of photoproduction of  $\eta$  via the  $\gamma d \rightarrow pn\eta$  reaction [131] indicating to some extent that the phenomenon is independent of the production process but rather related to the interaction among the  $\eta$  meson and nucleons in the  $S_{11}(1535)$  resonance region. However, although a simple phenomenological treatment [4, 68, 130] – based on the factorization of the transition amplitude into the constant primary production and the on-shell incoherent pairwise interaction among outgoing particles – describes the enhancement close-to-threshold (dotted line) very well, it fails to describe the invariant mass distribution of the proton-proton and proton- $\eta$  subsystems determined recently at  $Q = 15$  MeV by the COSY-TOF [95] and at  $Q = 15.5$  MeV by the COSY-11 [1] collaborations. Though the groups utilized entirely different experimental methods the obtained results agree very well with each other. The structure of these invariant mass distributions may indicate a non-negligible contribution from the P-waves in the outgoing proton-proton subsystem [79], which can be produced for instance via  $^1S_0 \rightarrow ^3P_0s$  or  $^1D_2 \rightarrow ^3P_2s$  transitions. This hypothesis encounters, however, difficulties in describing the excess energy dependence of the total cross section. The amount of the P-wave admixture derived from the proton-proton invariant mass distribution leads to a good description of the excitation function at higher excess energies while at the same time it spoils significantly the agreement with the data at low values of  $Q$ , as depicted by the dashed-dotted line in figure 4.6. However, these difficulties in reproducing the observed energy dependence might be due to the particular model used in reference [79], and thus higher partial wave contributions cannot be excluded a priori.

In contrast to the P-wave contribution the three-body treatment [122, 123] of the  $pp\eta$  system (dashed-double-dotted line) leads to even larger



enhancement of the cross section near threshold than that based on the Ansatz of the factorization of the proton-proton and proton- $\eta$  interactions. It must be kept in mind, however, that too strong FSI effect predicted by the three-body model must be partially assigned to the neglect of the Coulomb repulsion in this preliminary calculations [122,123]. The above considerations illustrate that the simple phenomenological approach shown by the dotted line could fortuitously lead to the proper result, due to a mutual cancellation of the effects caused by the approximations assumed in the calculations and the neglect of higher partial waves. They show also unambiguously that for the complete understanding of the low energy  $pp\eta$  dynamics, in addition to the already discussed excitation function of the total cross section, a knowledge of the differential observables is necessary. These will help to disentangle effects caused by the proton- $\eta$  interaction and the contributions from higher partial waves. This issue will be discussed further in section 4.5, where we present distributions determined experimentally for two sets of orthogonal variables fully describing the  $pp\eta$  system, which was produced at an excess energy of  $Q = 15.5$  MeV via the  $pp \rightarrow pp\eta$  reaction using the COSY-11 [8,61] facility at COSY [62].

### 4.3 Phenomenology of the proton-proton initial and final state interaction

*Thus, it is suggested that among created beings there must be some basic agent which will move things and bring them together [90].*

Aristotle

When reducing the proton-proton FSI effect to a multiplicative factor, one finds that it depends on the assumed nucleon-nucleon potential and on the produced meson mass [132].

This issue was recently vigorously investigated e.g. by authors of references [71,100,101,132,133] and we shall briefly report this here as well. Up to now we factorized the transition matrix element into a primary production of particles and its on-shell rescattering in the exit channel (eqs. (4.1)(4.2)(4.8)). Though it is a crude approximation, neglecting the off-shell effects of the production process completely, it astoundingly leads to a good description of the energy dependence of the total cross section, as already demonstrated in figures 4.5b and 4.6. The off-shell effects, as pointed out by Kleefeld [101], could have been safely neglected

in case of the electromagnetic transitions in atoms or  $\beta$  decays, where the excitation energy of the involved nucleons is by many orders of magnitude smaller than their masses and the initial and final states go hardly off-shell [101]. However, in the case of the  $NN \rightarrow NN \text{ Meson}$  process the large excitation energy of the colliding nucleons is comparable with the nucleon masses and the primary interaction may create the particles significantly far from their physical masses, so that a priori the off-shell effects cannot be disregarded.

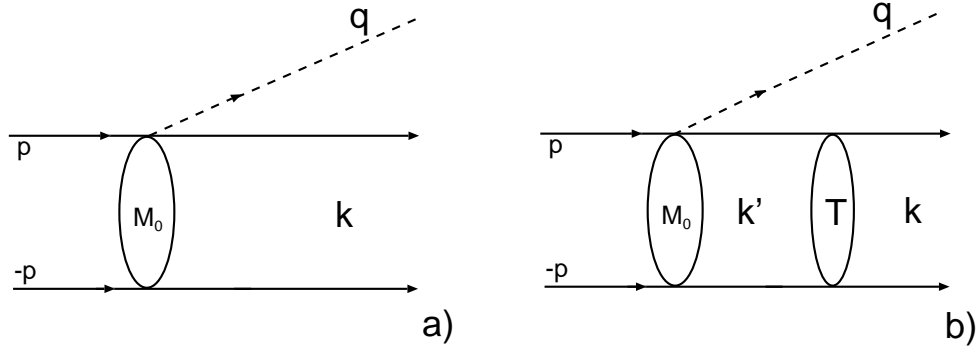


**Figure 4.7:** Diagrammatic representation of the DWBA expressed by equation (4.11). (a) The primary production term. (b) The loop diagram including the nucleon-nucleon FSI.  $T(k', k)$  stands for the half-off-shell  $T$  matrix with  $k$  and  $k'$  denoting the on- and off-shell centre-of-mass momentum in the nucleon-nucleon system, respectively.  $q$  indicates the momentum of the created meson in the reaction centre-of-mass system and  $p$  the momentum of the colliding nucleons.

Generally, the decomposition of the total production amplitude into the primary production and the subsequent nucleon-nucleon interaction visualized in figure 4.7 is expressed by the formula:

$$M = M_0^{on} + M_0^{off} G T_{NN}, \quad (4.11)$$

where the second term of the equation represents the integration over the intermediate ( $k'$ ) momenta of the off-shell production amplitude and the half-off-shell nucleon-nucleon  $T$  matrix [132]. Assuming that the primary production occurs in such a way that one nucleon emits the meson which then re-scatters on the other nucleon and appears as a real particle the authors of reference [132] found that the enhancement of the cross section due to the nucleon-nucleon interaction depends strongly on the mass of the created meson. This is because with the increasing mass of the produced meson the distance probed by the nucleon-nucleon interaction decreases (see table 4.1) and hence the relevant range of the off-shell momenta becomes larger. The effect for the  $pp \rightarrow pp \text{ Meson}$  reactions is

presented in figure 4.8a, where one can see that, when utilizing the Bonn potential model for the nucleon-nucleon  $T$  matrix, the enhancement in case of the  $\pi^0$  production is by about a factor of four larger than for the  $\eta$  or  $\eta'$  mesons. A similar conclusion, but with the absolute values larger by about 40 %, was drawn for the Paris  $NN$  potential [132].

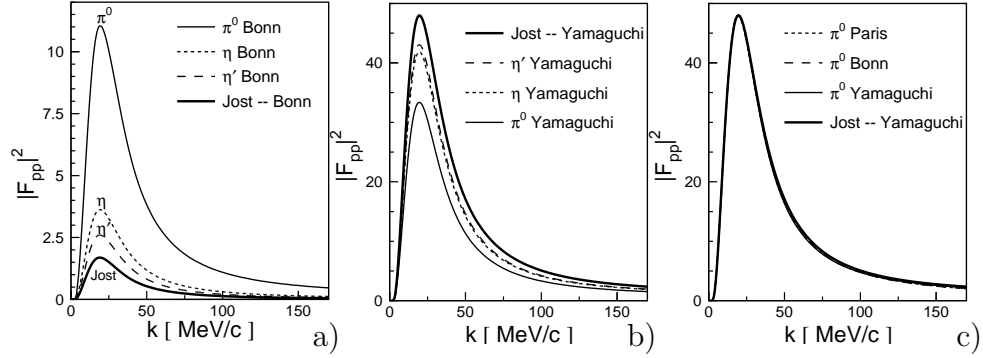


**Figure 4.8:** The FSI factor for Bonn [134] a) and Yamaguchi [135] b) potentials. The solid, dotted and dashed lines correspond to  $\pi^0$ ,  $\eta$ , and  $\eta'$  meson production, respectively. Thick solid lines indicate the inverse of the squared Jost function ( $|F_{pp}(k)|^2 = |J(-k)|^{-2}$ ). c) The FSI factors for  $\pi^0$  production of Paris (dotted curve) [136], Bonn (dashed curve), and Yamaguchi (solid curve) potentials normalized to be equal at maximum to the inverse of the squared Jost function of the Yamaguchi potential (thick solid line). The shapes stemming from different potentials are almost indistinguishable. Note that the thick solid line corresponds to the dashed line in figure 4.5a. The figures have been adapted from reference [132].

On the contrary, when applying the Yamaguchi potential into calculations the enhancement grows with the increasing mass of the meson, as shown in figure 4.8b. The thick solid curves in figures 4.8a and 4.8b show the results of the frequently applied approximation of the nucleon-nucleon FSI effects:

$$\begin{aligned}
 M &= M_0^{on} + M_0^{off} G T_{NN} \approx M_0^{on} \cdot (1 + G T_{NN}) = \\
 &= M_0^{on} J^{-1}(-k) \equiv M_0^{on} F_{NN}(k),
 \end{aligned} \tag{4.12}$$

where the overall transition matrix element  $M$  is factorized to the primary on-shell production and the  $NN$  FSI expressed as the inverse of the Jost function  $J^{-1}(-k)$  [113]. As can be seen in figures 4.8a and 4.8b, the variation of the absolute values – of such obtained enhancement factors – with the applied potential is significant.

Since the physical value of the total cross section cannot depend on the

off-shell features of the potential used in calculations, which are in principle not measurable [137], the differences in the magnitude of the  $|F_{pp}|$  factor must reflect itself in a corresponding dependence of the primary production amplitude on the potential used. Therefore, it is of vital importance to realize that the values of the threshold amplitudes  $|M_0|$  are significant only in the context of the potential they were extracted from. Figure 4.8c demonstrates, however, that the shapes of the enhancement factors, with the meson exchange mechanism assumed for the primary production, are pretty much the same, independently of the applied  $NN$  potential and correspond to the form of the Jost function inferred from the Yamaguchi potential. This indicates that the energy dependence of the  $NN$  FSI factors is predominantly determined by the on-shell  $NN$   $T$  matrix.

In references [71,100,101] the formula for the transition matrix element with explicit dependence on the considered off-shell features for the initial and final state interaction is derived:

$$M = \left\{ 1 + \frac{[\eta(k)e^{2i\delta(k)} - 1] \cdot [1 + P_f(p,k)]}{2} \right\} M_0 \left\{ 1 + \frac{[\eta(p)e^{2i\delta(p)} - 1] \cdot [1 + P_i(p,k)]}{2} \right\}, \quad (4.13)$$

where subscripts  $i$  and  $f$  indicate the initial and final state, respectively. The functions  $P(p,k)$  exhibit all the off-shell effects of the  $NN$  interaction and the primary production current [100] and  $\delta$  and  $\eta$  denote the phase-shift and inelasticity, correspondingly. At threshold, the inelasticity in the exit channel is equal to unity ( $\eta(k) = 1$ ) due to the small relative momentum of the outgoing nucleons. The last term of the formula expresses the influence of the initial state interaction on the production process. Due to the large relative momenta of the colliding protons needed to create a meson it is characterized by a weak energy dependence in the excess energy range of a few tens of MeV. For example in figure 4.1b one can see that the phase-shift variation of the  $^3P_0$  partial wave (having predominant contribution to the threshold production of pseudoscalar mesons) in the vicinity of the threshold for mesons heavier than  $\pi^0$  is indeed very weak. Taking additionally into account that the initial state off-shell function  $P_i(p,k)$  is small (as it is the case at least for meson exchange models [71]) one reduces the influence of the  $NN$  initial state interaction to the reduction factor  $F_{ISI}$  which can be estimated from the phase-shifts and inelasticities only:

$$F_{ISI} = \frac{1}{4} \left| \eta(p) e^{2i\delta(p)} + 1 \right|^2. \quad (4.14)$$

At the threshold for  $\pi$  meson production this is close to unity since at this energy the inelasticity is still nearly 1 and the  $^3P_0$  phase-shift is close to zero (see figure 4.1b). However, at the  $\eta$  threshold, where the phase-shift approaches its minimum, the proton-proton ISI diminishes the total cross section already by a factor of 0.2 [71]. A similar result was obtained using a meson exchange model for  $\eta$  production in the  $pp \rightarrow pp\eta$  reaction and calculating the proton-proton distortion from the coupled-channel  $\pi NN$  model [72]. The authors of reference [72] concluded that the initial proton-proton distortion reduces the total cross section by about a factor of  $\approx 0.26$ , which keeps constant at least in the studied range of 100 MeV in kinetic beam energy. Hence, the closed formula (4.14) disregarding the off-shell effects ( $P_i(p, k)$ ) permits to estimate the cross section reduction due to the initial state distortion with an accuracy of about 25 %. The shape of the  $^3P_0$  phase-shift shown in figure 4.1b indicates that the effect is at most pronounced close to the  $\eta$  production threshold, yet for the  $\eta'$  meson the formula (4.14) leads to a factor  $F_{ISI} = 0.33$  [138]. The primary production amplitude as well as the off-shell effects of the nucleon-nucleon FSI ( $P_f(p, k)$ ) are also weakly energy dependent [100], since they account for the short range creation mechanism, which shall be considered in chapter 5.

#### 4.4 Qualitative comparison between $pp\eta$ , $pp\eta'$ , and $pp\pi^0$ interactions

*But what we must aim at is not so much to ascertain resemblances and differences, as to discover similarities hidden under apparent discrepancies [74].*

Henri Poincaré

The accordance of the experimental data with the simple factorization represented by solid lines in figures 4.5b and 4.6 fully confirms the suppositions considered in the previous sections which imply that the energy dependence of the total cross section is in the first order determined by the on-shell scattering of the outgoing particles. However, since the distortion caused by the nucleons is by some orders of magnitude larger than that resulting from the meson-nucleon interaction, even small fractional inaccuracies in the description of nucleon-nucleon effects may obscure the inference of the meson-nucleon interaction. The differences between the square of the on-shell proton-proton scattering amplitude and the Jost function prescription are presented in figure 4.5a. To minimize the

ambiguities that may result from these discrepancies at least for the quantitative estimation of the effects of the unknown meson-nucleon interaction one can compare the spectra from the production of the meson under investigation to the spectra determined for the production of a meson whose interaction with nucleons is well established. For instance, to estimate the strength of the  $\eta pp$  and  $\eta' pp$  FSI one can compare the appropriate observables to those of the  $\pi^0 pp$  system.

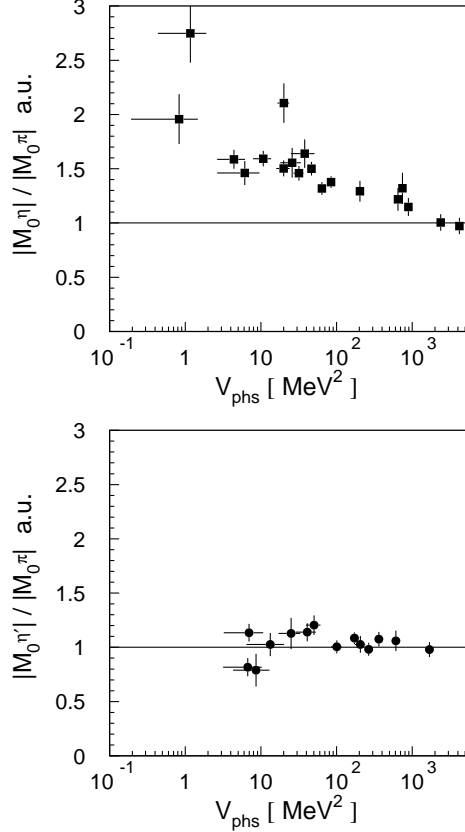


**Figure 4.9:** The ratios of  $|M_0^\eta|/|M_0^{\pi^0}|$  (upper panel) and  $|M_0^{\eta'}|/|M_0^{\pi^0}|$  (lower panel) extracted from the data by means of equation (4.10), assuming a  $pp$ -FSI enhancement factor as depicted by the dotted line in figure 4.5a and neglecting the proton-meson interaction [2].

Upper and lower panels of figure 4.9 show the dependence of  $|M_0|$  on the phase space volume for  $\eta$  and  $\eta'$  production normalized to  $|M_0^{\pi^0}|$ . The values of  $|M_0|$  were extracted from the experimental data by means of equation (4.10) disregarding the proton-meson interaction ( $|M_{p\eta(\eta') \rightarrow p\eta(\eta')}|$  was set to 1). If the influence of the neglected interactions were the same in the cases of the  $\eta(\eta')$  and  $\pi^0$  production the points would be consistent with the solid line. This is the case for the  $pp \rightarrow pp\eta'$  reaction visualizing the weakness of the proton- $\eta'$  interaction independently of the prescription used for the proton-proton FSI [2]. In case of the  $\eta'$  meson its low-energy interaction with the nucleons was expected to be

very weak since there exists no baryonic resonance which would decay into  $N\eta'$  [43]. Figure 4.9a shows – independently of the model used for the correction of the proton-proton FSI – the strong effects of the  $\eta pp$  FSI at low  $V_{ps}$ .

## 4.5 Dalitz plot occupation for the $pp\eta$ system

*... a knowledge of the effects is what leads to an investigation and discovery of causes [139].*

Galileo Galilei

The strength of the interaction between particles depends on their relative momenta or equivalently on the invariant masses of the two-particle subsystems. Therefore it should show up as a modification of the phase space abundance in the kinematical regions where the outgoing particles possess small relative velocities. Only two invariant masses of the three subsystems are independent (see eq. 3.18) and therefore the entire accessible information about the final state interaction of the three-particle system can be presented in the form of the Dalitz plot. Figure 4.10a shows distribution of the events as determined experimentally for the  $pp\eta$  system at an excess energy of  $Q = 15.5$  MeV. This distribution originating from kinematically complete measurements comprises the whole experimentally available information about the interactions of the  $pp\eta$ -system. In this figure one easily recognizes the growth of the population density at the region where the protons have small relative momenta which can be assigned to the strong attractive S-wave interaction between the two protons. This is qualitatively in agreement with the expectation presented in figure 4.10b, which shows the result of Monte-Carlo calculations where the homogeneously populated phase space was weighted by the square of the on-shell  $^1S_0$  proton-proton scattering amplitude. However, already in this two dimensional representation it is visible that the experimentally determined distribution remains rather homogeneous outside the region of the small proton-proton invariant masses, whereas the simulated abundance decreases gradually with growing  $s_{pp}$  (as indicated by the arrow). Figure 4.10c shows the simulated phase space density distribution disregarding the proton-proton interaction but accounting for the interaction between the  $\eta$ -meson and the proton. At this excess energy, corresponding to the small relative momentum range ( $k_{p\eta}^{max} \approx 105$  MeV/c) the variations of the proton- $\eta$  scattering amplitude are quite moderate (see figure 4.15b in the next section).

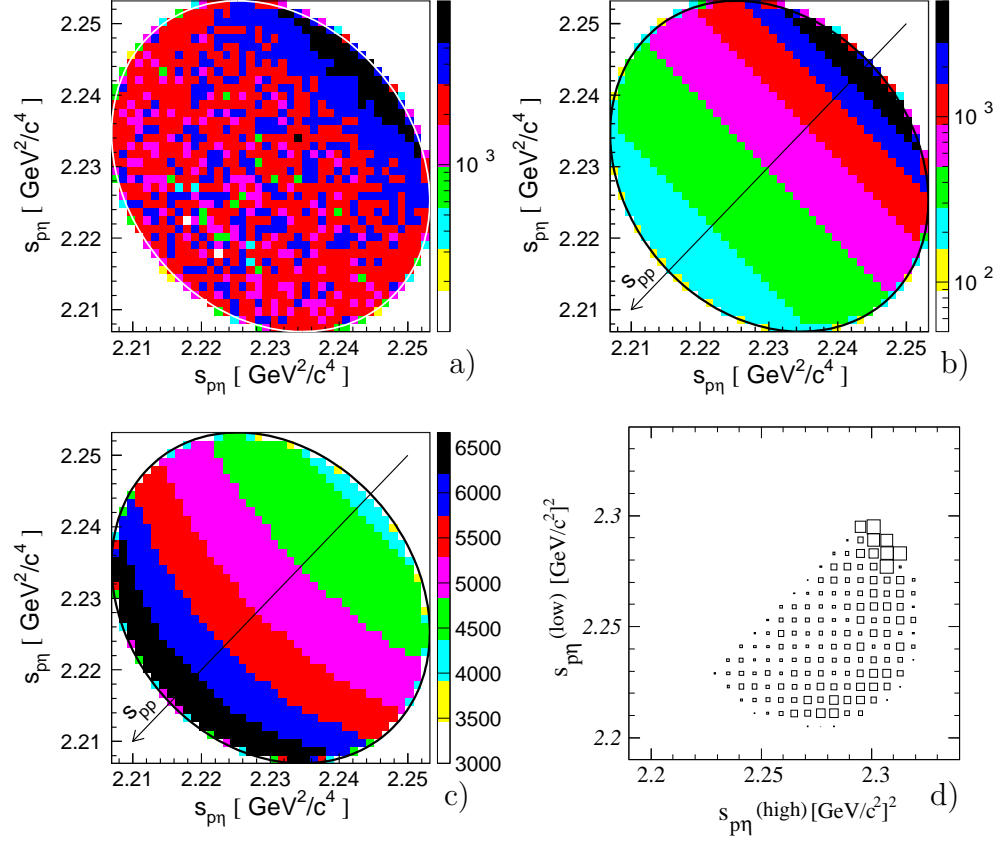


**Figure 4.10:** Dalitz plots. Lines surrounding the plots show the kinematical limits.

(a) Experimental result determined for the  $pp \rightarrow pp\eta$  reaction at  $Q = 15.5$  MeV. Data were corrected for the detection acceptance and efficiency.

(b) Monte-Carlo simulations for the  $pp \rightarrow pp\eta$  reaction at  $Q = 15.5$  MeV: Phase-space density distribution modified by the  $^1S_0$  proton - proton final state interaction.

(c) Simulated phase space density distribution modified by the proton- $\eta$  interaction with a scattering length of  $a_{p\eta} = 0.7 \text{ fm} + i 0.3 \text{ fm}$ . Details of the calculations together with the discussion of the nucleon-nucleon and nucleon-meson final state interaction can be found in reference [4]. The scale in the figure is linear in contrast to the above panels.

(d) Dalitz plot distribution of the  $pp \rightarrow pp\eta$  reaction at an excess energy of  $Q = 37.6$  MeV, corrected for the detection acceptance. Out of the two invariant masses corresponding to two  $p - \eta$  pairs the one being larger is plotted along the x-axis. The figure is taken from reference [50]. A similar spectrum for the  $pp\pi^0$  system [114] reveals the influence of the proton-proton interaction, yet again, as for the total cross section energy dependence (fig. 4.5b), the proton- $\pi^0$  interaction is too weak to affect the density distribution of the Dalitz plot observably.

Due to the low strength of this interaction the expected deviations from a uniform distribution is smaller – from that caused by the proton-proton force – by about two orders of magnitude, yet an enhancement of



the density in the range of low invariant masses of proton- $\eta$  subsystems is clearly visible. Note that the scale in the lower panel of figure 4.10 is linear whereas in the upper panel it is logarithmic. Due to weak variations of the proton- $\eta$  scattering amplitude the enhancement originating from the  $\eta$ -meson interaction with one proton is not separated from the  $\eta$ -meson interaction with the second proton. Therefore an overlapping of broad structures occurs. It is observed that the occupation density grows slowly with increasing  $s_{pp}$ , opposite to the effects caused by the S-wave proton-proton interaction, but similar to the modifications expected for the NN P-wave [87]. From the above example it is obvious that only from experiments with high statistics, signals of the meson-nucleon interaction can be observed on top of the overwhelming nucleon-nucleon final state interaction. The increase of the distribution density at regions of small invariant masses of the proton-proton and proton- $\eta$  subsystems is also visible in figure 4.10d showing experimental results determined at  $Q = 37.6$  MeV by the WASA/PROMICE collaboration. At this excess energy these regions are quite well separated. However, since this is close to the energy where the advent of higher partial waves is awaited, the possible contribution from the P-wave proton-proton interaction cannot be a priori excluded. Specifically, the latter leads to the enhancement at large invariant masses of the proton-proton pair [87] and hence affects the phase space region where the modification from the proton- $\eta$  interaction is expected. A deviation of the experimentally observed population of the phase space from the expectation based on the mentioned assumptions is even better visible in figure 4.11. This figure presents the projection of the phase space distribution onto the  $s_{pp}$  axis corresponding to the axis indicated by the arrows in figures 4.10b and 4.10c. The superimposed lines in figure 4.11 correspond to the calculations performed under the assumption that the production amplitude can be factorized into a primary production and final state interaction. The dotted lines result from calculations where only the proton-proton FSI was taken into account, whereas the thick-solid lines represent results where the overall enhancement was factorized into the corresponding pair interactions of the  $pp\eta$  system. This factorisation Ansatz is only valid if the different amplitudes are completely decoupled which is not the case here. Therefore, these calculations should be considered as a rough estimate of the effect introduced by the FSI in the different two body systems. As introduced in section 4.2, the enhancement factor accounting for the proton-proton FSI has been calculated [2, 4] as the square of the on-shell proton-proton scattering amplitude derived according to the modi-

fied Cini-Fubini-Stanghellini formula including the Wong-Noyes Coulomb corrections [108]. The homogeneous phase space distributions (thin solid lines) deviate strongly from the experimentally determined spectra. The curves including the proton-proton and proton- $\eta$  FSI reflect the shape of the data for small invariant masses of the proton-proton system, yet they deviate significantly for large  $s_{pp}$  and small  $s_{p\eta}$  values. An explanation of this discrepancy could be a contribution of P-wave proton-proton interaction [79], or a possibly inadequate assumption that proton- $\eta$  and proton-proton interaction modify the phase space occupations only as incoherent weights [101].

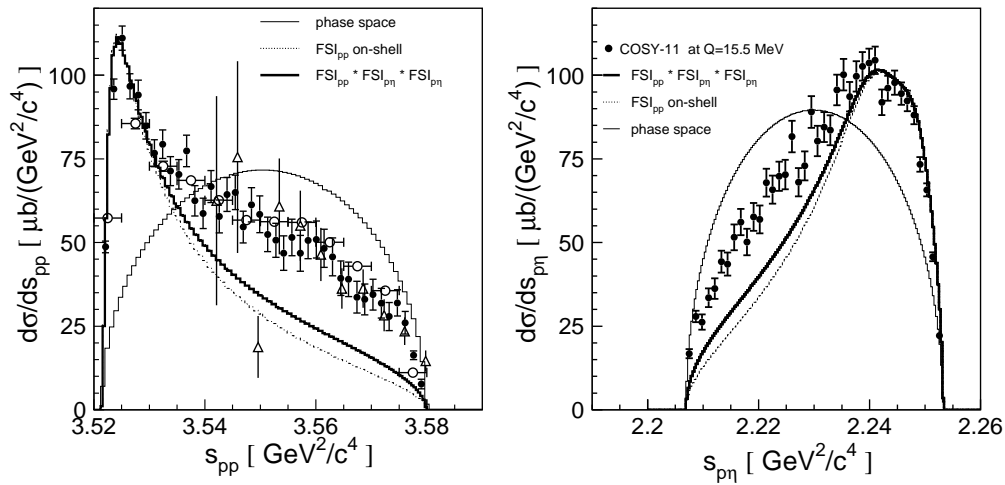


**Figure 4.11:** Distributions of the square of the proton-proton ( $s_{pp}$ ) and proton- $\eta$  ( $s_{p\eta}$ ) invariant masses determined experimentally for the  $pp \rightarrow pp\eta$  reaction at the excess energy of  $Q = 15.5$  MeV by the COSY-11 collaboration (closed circles), at  $Q = 15$  MeV by the TOF collaboration (open circles) [95], and at  $Q = 16$  MeV by PROMICE/WASA (open triangles) [96]. The TOF and PROMICE/WASA data have been normalized to those of COSY-11, since these measurements did not evaluate the luminosities but rather normalized the results to reference [50] (see also comment [140]). The integrals of the phase space weighted by the square of the proton-proton on-shell scattering amplitude  $\text{FSI}_{pp}$  (dotted lines), and by the product of  $\text{FSI}_{pp}$  and the square of the proton- $\eta$  scattering amplitude (thick solid lines), have been normalized arbitrarily at small values of  $s_{pp}$ . The thick solid line was obtained assuming a scattering length of  $a_{p\eta} = 0.7 \text{ fm} + i 0.4 \text{ fm}$ . The expectations under the assumption of the homogeneously populated phase space are shown as thin solid curves.

A slightly better description is achieved when the proton-proton interaction is accounted for by the realistic nucleon-nucleon potential. Figure 4.12a depicts the results obtained using two different models for the production process as well as for the NN interaction [79, 141, 142]. The calculations for the  $^3P_0 \rightarrow ^1S_0$  transition differ slightly, but the differ-

ences between the models are, by far, smaller than the observed signal. Therefore we can safely claim that the discussed effect is rather too large to be caused by the particular assumptions used for the production operator and NN potential.

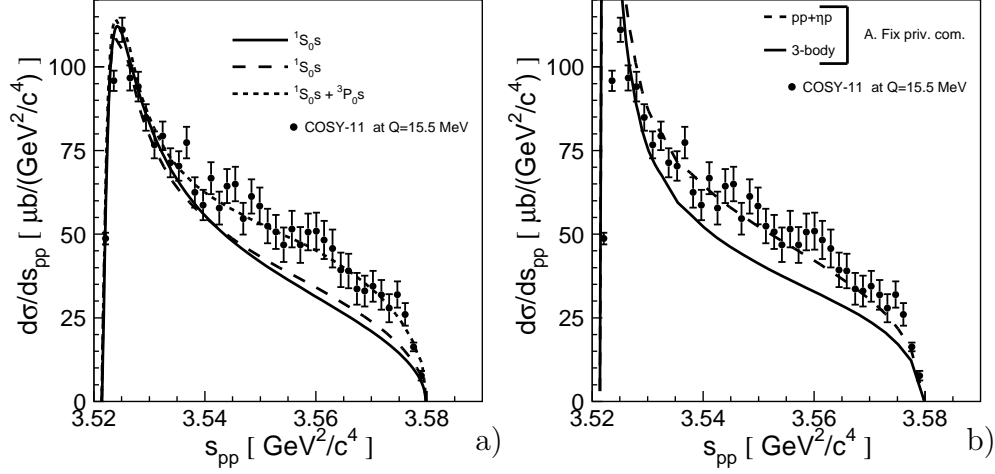


**Figure 4.12:** (a) Distribution of the square of the proton-proton ( $s_{pp}$ ) invariant mass for the  $pp \rightarrow pp\eta$  reaction at an excess energy of  $Q = 15.5$  MeV. Solid and dashed lines correspond to the calculations under the assumption of the  $^3P_0 \rightarrow ^1S_0s$  transition according to the models described in references [141, 142] and [79], respectively. The dotted curve shows the result with the inclusion of the  $^1S_0 \rightarrow ^3P_0s$  contribution as suggested in reference [79]. (b) The same data as above but with curves denoting preliminary three-body calculations [122, 123] of the final  $pp\eta$  system as described in [143]. At present only the dominant transition  $^3P_0 \rightarrow ^1S_0s$  is taken into account and the production mechanism is reduced to the excitation of the  $S_{11}(1535)$  resonance via the exchange of the  $\pi$  and  $\eta$  mesons. The solid line was determined with the rigorous three-body approach [122, 123] where the proton-proton sector is described in terms of the separable Paris potential (PEST3) [144], and for the  $\eta$ -nucleon scattering amplitude an isobar model analogous to the one of reference [145] is used with  $a_{\eta N} = 0.5 \text{ fm} + i \cdot 0.32 \text{ fm}$ . The dashed line is obtained if only pairwise interactions ( $pp + p\eta$ ) are allowed. The effect of proton-proton FSI at small  $s_{pp}$  is overestimated due to neglect of Coulomb repulsion between the protons. The lines are normalized arbitrarily but their relative amplitude is fixed from the model.

As we will see in subsection 6.3.3 in figure 6.23b, the experimental distribution of the  $\eta$  polar angle in the center-of-mass frame is fully isotropic. This is the next evidence – besides the shape of the excitation function and the kinematical arguments discussed in reference [4] – that at this excess energy ( $Q = 15.5$  MeV) the  $\eta$  meson is produced in the center-of-mass frame predominantly with the angular momentum equal to zero. Similarly, the distribution determined for the polar angle of the relative proton-proton momentum with respect to the momentum of the  $\eta$  me-

son as seen in the di-proton rest frame is also consistent with isotropy. Anyhow, even the isotropic distribution in this angle does not imply directly that the relative angular momentum between protons is equal to zero, because of their internal spin equal to  $\frac{1}{2}$ . Therefore, the contribution from the  ${}^3P_0$ -wave produced via the  ${}^1S_0 \rightarrow {}^3P_0s$  transition cannot be excluded. Moreover, as pointed out in reference [79], the isotropic angular distribution, can principally also be achieved by the destructive interference between the transitions  ${}^1S_0 \rightarrow {}^3P_0s$  and  ${}^1D_2 \rightarrow {}^3P_2s$ .

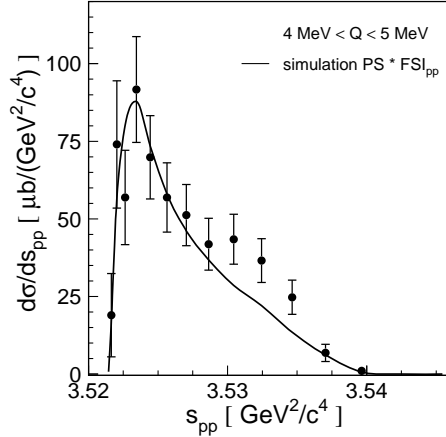


**Figure 4.13:** Distribution of square of the proton-proton invariant mass from the  $pp \rightarrow pp\eta$  reaction measured at COSY-11 for the excess energy range  $4 \text{ MeV} \leq Q \leq 5 \text{ MeV}$  [1, 10, 146]. The superimposed line shows the result of simulations performed under the assumption that the phase space population is determined exclusively by the on-shell interaction between outgoing protons. The “tail” at large  $s_{pp}$  values is due to the smearing of the excess energy, since this former COSY-11 data have not been kinematically fitted. Additionally to the 1 MeV range of  $Q$  a smearing of about 0.3 MeV ( $\sigma$ ) should be taken into account.

Since flat angular distributions do not preclude the occurrence of higher partial-waves an effect of their contribution to the production process was proposed to explain the structure observed in the invariant mass spectra [79]. In fact, as depicted by the dotted line in figure 4.12a, an admixture of the  ${}^1S_0 \rightarrow {}^3P_0s$  transition to the main  ${}^3P_0 \rightarrow {}^1S_0s$  one leads to the excellent agreement with the experimental points. However, at the same time, this conjecture leads to strong discrepancies in the shape of the excitation function as can be deduced from the comparison of the dashed-dotted line and the data in figure 4.6. While it describes the data points in the excess energy range between 40 MeV and 100 MeV it underestimates the total cross section below 20 MeV by a factor of 2. This observation entails that either the contribution of higher partial waves, though conforming with invariant mass spectra and angular distributions, must be excluded or that the simplifications performed e.g. for the description of the final state three-body system were too strong. Interestingly, the enhancement at large  $s_{pp}$  is visible also at much lower excess energy. This can be concluded from figure 4.13 in which the COSY-11 data at  $Q \approx 4.5 \text{ MeV}$  [1, 146] are compared to the simulations based on the assumption that the phase space abundance is

due to the proton-proton FSI only. This observation could imply that the effect is caused by the proton- $\eta$  interaction rather than by higher partial waves, since their contribution at such small energies is quite improbable [4]. However, as shown in the lower part of figure 4.12 the rigorous three-body treatment of the  $pp\eta$  system leads at large values of  $s_{pp}$  to the reduction of the cross section in comparison to the calculation taking into account only first order rescattering ( $pp+p\eta$ ) [122, 123]. Here, both calculations include only the  $^3P_0 \rightarrow ^1S_0 s$  transition. Although the presented curves are still preliminary, we can qualitatively assess that the rigorous three-body approach, in comparison to the present estimations, will on one hand enhance the total cross section near threshold as shown in figure 4.6, while on the other hand it will decrease the differential cross section at large values of  $s_{pp}$ . This is just opposite to the influence of P-waves in the proton-proton system.

From the above presented considerations it is rather obvious that the rigorous three-body treatment of the produced  $pp\eta$  system and the exact determination of the contributions from the higher partial waves may result in a simultaneous explanation of both observations: the near-threshold enhancement of the excitation function of the total cross section, and the strong increase of the invariant mass distribution at large values of  $s_{pp}$ . For the unambiguous determination of the contributions from different partial waves spin dependent observables are required [79]. The first attempt has been already reported in [7], and more comprehensive investigations are in progress [27] (see also section 5.4).

## 4.6 Quasi-bound state

*... which exists either because of some impossible blip on the curve of probability or because the gods enjoy a joke as much as anyone [147].*

Terry Pratchett

*... I am inclined to think that scientific discovery is impossible without faith in ideas which are of a purely speculative kind, and sometimes even quite hazy ... [75].*

Karl Raimund Popper

With the up-to-date experimental accuracy, from all meson- $NN$  systems the  $\eta NN$  one reveals by far the most interesting features. Recently, the dynamics of the  $\eta NN$  system has become a subject of theoretical in-

vestigations in view of the possible existence of quasi-bound or resonant states [148]. A direct measure of the formation – or non-formation – of an  $\eta$ -nuclear quasi-bound state is the real part of the  $\eta$ -nucleon scattering length [150]. The determined values of  $\text{Re}(a_{\eta N})$  range between 0.20 fm [37] and 1.05 fm [39] depending on the analysis method and the reaction studied [38], and at present an univocal answer whether the attractive interaction between the  $\eta$  meson and nucleons is strong enough to form a quasi-bound state is not possible.

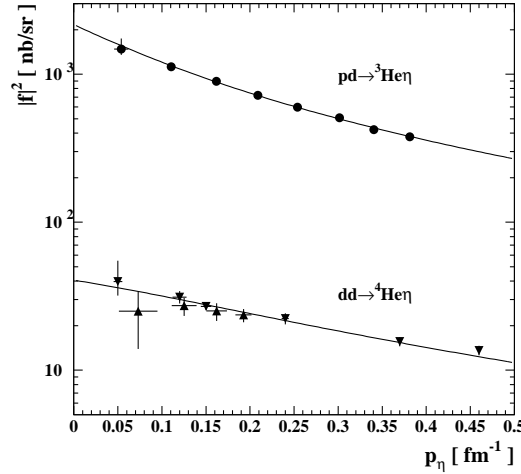


**Figure 4.14:** Averaged squared production amplitudes of the reactions  $pd \rightarrow {}^3\text{He}\eta$  and  $dd \rightarrow {}^4\text{He}\eta$  as function of the centre-of-mass  $\eta$  momentum. The data are taken from references [151–153]. The amplitude  $f_n$  is related to the unpolarized centre-of-mass cross section by the equation  $\frac{d\sigma}{d\Omega} = \frac{p_\eta^*}{p_d^*} |f_n|^2$ , where  $p_\eta^*$  and  $p_d^*$  denote the centre-of-mass momentum in  $\eta {}^3\text{He}$  and  $pd$  systems, respectively. Superimposed lines correspond to the fit of the s-wave scattering-length formula:  $f(p_n) = \frac{\text{constans}}{1 - ip_\eta a_{\eta X}}$ , where  $a_{\eta X}$  denotes the scattering length of the  $\eta$ - ${}^3\text{He}$  or  $\eta$ - ${}^4\text{He}$  potential.

The shape of the energy dependence of the  $pd \rightarrow {}^3\text{He}\eta$  production amplitude (see figure 4.14) implies that either the real or imaginary part of the  $\eta$ - ${}^3\text{He}$  scattering length has to be very large [176], which may be associated with a bound  $\eta$ - ${}^3\text{He}$  system. Similarly encouraging are results of reference [154], where it is argued that a three-body  $\eta NN$  resonant state, which may be formed close to the  $\eta d$  threshold, may evolve into a quasi-bound state for  $\text{Re}(a_{\eta N}) \geq 0.733$  fm. Also the close-to-threshold enhancement of the total cross section of the  $pp \rightarrow pp\eta$  reaction was interpreted as being either a Borromean (quasi-bound) or a resonant  $\eta pp$  state [155] provided that  $\text{Re}(a_{\eta N}) \geq 0.7$  fm. Contrary, recent calculations performed within a three-body formalism [148] indicate that a formation of a three-body  $\eta NN$  resonance state is not possible, independently of the  $\eta N$  scattering parameters. Moreover, the authors of reference [156] exclude the possibility of the existence of an  $\eta NN$  quasi-bound state. Results of both calculations [148, 156], although performed within a three-body formalism, were based on the assumption of a separability of the two-body  $\eta N$  and  $NN$  interactions. However, in the three-body system characterized by the pairwise attractive interactions,

the particles can be pulled together so that their two-body potentials overlap, which may cause the appearance of qualitatively new features in the  $\eta NN$  system [148]. Particularly interesting is the  $\eta d$  final state where the pair of nucleons alone is bound by the strong interaction.

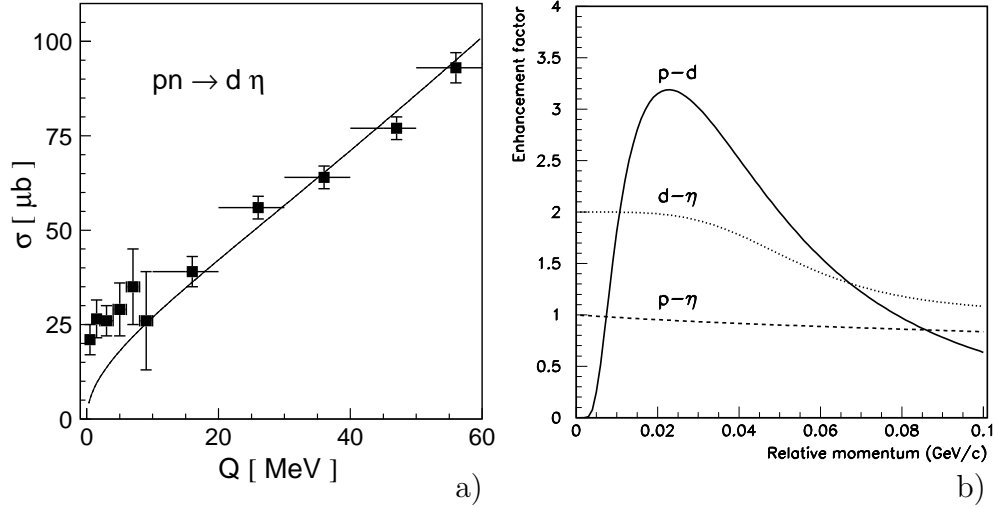


**Figure 4.15:** (a) Total cross section of the quasi-free  $pn \rightarrow d\eta$  reaction as a function of the excess energy [121, 157]. The curve – fitted in amplitude – indicates the energy dependence proportional to the function  $\sqrt{Q} \cdot (1 + Q/83.5)$  which accounts for the s- and p-wave contribution. The ratio of the s- and p-waves magnitudes was taken the same as determined for the  $np \rightarrow d\pi^0$  reaction [158–160]. It was assumed that the p-wave to s-wave ratio is the same for the  $pn \rightarrow d\eta$  and  $pn \rightarrow d\pi^0$  reactions at a corresponding value of  $\eta_M$ . (b) Arbitrarily normalized enhancement factors for  $pd$ -,  $d\eta$ -, and  $p\eta$ -FSI. The  $\eta$ -proton factor is calculated according to equation (4.9), with  $a_{p\eta} = 0.717 \text{ fm} + i 0.263 \text{ fm}$  [161] and  $b_{p\eta} = -1.50 \text{ fm} - i 0.24 \text{ fm}$  [36]. The enhancement factor for  $\eta$ -deuteron has been extracted from the data of panel (a) parametrizing the ratio of the cross section to the phase space volume by the expression [162]:  $F_{d\eta} = 1 + 0.5/(0.5 + (Q/5)^2)$ . The proton-deuteron FSI factor is calculated according to ref. [163].

Figure 4.15a shows the total cross section for the  $pn \rightarrow d\eta$  reaction measured close to the production threshold. For excess energies below 10 MeV the data are enhanced over the energy dependence determined for the  $pn \rightarrow d\pi^0$  reaction indicated by the solid curve. This is in qualitative agreement with the calculations of Ueda [164] for the three-body  $\eta NN$ - $\pi NN$  coupled system, which predict the existence of an  $\eta NN$  quasi-bound state with a width of 20 MeV. Ueda pointed out that the binding of the  $\eta NN$  system is due to the  $S_{11}$   $\eta N$  and  ${}^3S_1$   $NN(d)$  interaction which is characterized by no centrifugal repulsion. Such repulsion makes the  $\pi NN$  system, in spite of the strong  $P_{33}$   $\pi N$  attraction, hard to be bound [165]. Whether the observed cusp at the  $pn \rightarrow d\eta$  threshold is

large enough to confirm the existence of the  $\eta NN$  bound state has been recently vigorously discussed [166, 167].

The enhancement factor for the deuteron- $\eta$  interaction inferred from the data in figure 4.15a varies much stronger in comparison to the proton- $\eta$  one, as demonstrated in figure 4.15b. This suggests that the effects of this interaction should be even more pronounced in the differential distributions of the cross section for the  $pd \rightarrow pd\eta$  reaction as those observed in case of the  $pp \rightarrow pp\eta$  process, especially because the “screening” from the proton-deuteron interaction is by more than an order of magnitude smaller compared to the proton-proton interaction as can be deduced from the comparison of the solid lines in figures 4.15b and 4.5a. Experimental investigations on that issue [162, 168, 169] as well as searches for  $\eta$ -mesic nuclei [170] by measuring proton-deuteron induced reactions in the vicinity of the  $\eta$  production threshold are under way. Theoretically, the existence of mesic nuclei or quasi-bound meson-nucleus systems is not excluded, however, up to now a compelling experimental proof for the formation of such a state is still missing. The probability to create such states depends crucially on the sign and the strength of the meson-nucleus interaction. Since the  $\pi$ -nucleon and  $K^+$ -nucleon interaction have been found to be repulsive, it is unlikely that they will form quasi-bound states. Contrary, there is evidence for an attractive  $K^-$ -nucleon interaction [171], however, corresponding experiments would suffer from the low cross sections for the creation of  $K^-$  mesons [49]. Furthermore, the Coulomb interaction is expected to screen corresponding physical observables and might lead to the formation of mesonic atoms bound by the electromagnetic interactions. In contradistinction to  $K^-$ , the  $\eta$  meson is uncharged and the observation of an attractive  $\eta$ -nucleon interaction led to speculations concerning the existence of  $\eta$ -nuclear quasi-bound states. In the absence of  $\eta$ -meson beams such states bound by the strong interaction would offer a new possibility to study the  $\eta$ -nucleon interaction since the meson would be trapped for a relatively large time in the nuclear medium. In a very first prediction of such states termed  $\eta$ -mesic nuclei Haider and Liu [172, 173] in the framework of an optical model have estimated that it can be formed already for nuclei with atomic numbers of  $A \geq 12$ . Further on, the topic was vigorously discussed [149, 174–178], the limit was lowered considerably, and presently one considers seriously the existence of  $\eta$ -nucleus bound states even for  $d, t, {}^3\text{He}$ , or  ${}^4\text{He}$  nuclei [149, 176].

Experimental evidences for bound states have been found in the near-threshold production of  $\eta$  mesons in the reaction channel  $pd \rightarrow {}^3\text{He}\eta$ .



The unexpected large production amplitude as well as its rapid decrease with increasing energy (figure 4.14) is attributed to a strong s-wave final state interaction associated with a large  $\eta$ - ${}^3\text{He}$  scattering length ( $a_{\eta-{}^3\text{He}} \sim (-2.31 + i 2.57) \text{ fm}$ ) [176].

Assuming that  ${}^3\text{He}$  and  $\eta$  can form a quasi-bound state, it is interesting to compare  $pd \rightarrow {}^3\text{He}\eta$  and  $dd \rightarrow {}^4\text{He}\eta$  production data, where for the latter, according to the higher mass number, the formation of a bound state should be even more probable. A comparison of corresponding near-threshold data is presented in figure 4.14. Interestingly, the slope of the  $f_\eta(p_\eta)$  function of the  $dd \rightarrow {}^4\text{He}\eta$  reaction is smaller than the one of the reaction  $pd \rightarrow {}^3\text{He}\eta$ . This observation suggests, though contra-intuition, that the existence of the  $\eta$ -mesic nucleus is more probable in the case of  ${}^3\text{He}$  than  ${}^4\text{He}$ .

#### 4.7 Search for a signal from $\eta'$ -proton interaction in the invariant mass distributions

*I am sure that everyone, even among those who follow the profession, will admit that everything we know is almost nothing compared with what remains to be discovered... [281].*

René Descartes

A phenomenological analysis – presented in section 4.2 – of the determined excitation function for the  $pp \rightarrow pp\eta'$  reaction (lower part of figure 4.6) revealed no signal which could have been assigned to the proton- $\eta'$  interaction. Later on, in section 4.4, a comparison of the energy dependence of the production amplitudes for the  $pp \rightarrow pp\eta'$ ,  $pp \rightarrow pp\eta$  and  $pp \rightarrow pp\pi^0$  enabled to conclude, in a model-free way, that the proton- $\eta'$  interaction is indeed much weaker than the proton- $\eta$  one, and a trial to determine quantitatively the scattering length of the proton- $\eta'$  potential resulted only in a very modest estimation of an upper limit of its real part ( $|\text{Re } a_{p\eta'}| < 0.8 \text{ fm}$ ) [3]. Seeking for a visible manifestation of the proton- $\eta'$  interaction we have performed a high statistics measurement of  $pp \rightarrow pp\eta'$  reaction in order to determine a distribution of events over the phase space [26]. We expect that the invariant mass spectra for two particle subsystems of the  $pp\eta'$  final state can give the first ever experimental evidence for this still completely unknown interaction. The data are presently analyzed [179]. The missing mass spectrum determined on-line from 10% of the data written on tapes is shown in figure 4.16.

From a clear signal visible at the mass of the  $\eta'$  meson, one can estimate that the overall number of registered  $pp \rightarrow pp\eta'$  events amounts to about 13000. The measurement has been carried out at a beam momentum corresponding to the excess energy of  $Q = 15.5$  MeV for the  $pp \rightarrow pp\eta'$  reaction. Such value of  $Q$  was chosen to enable a direct comparison with the invariant mass spectra obtained for the  $pp \rightarrow pp\eta$  reaction (see figure 4.11), without a need for a correction of kinematical factors.

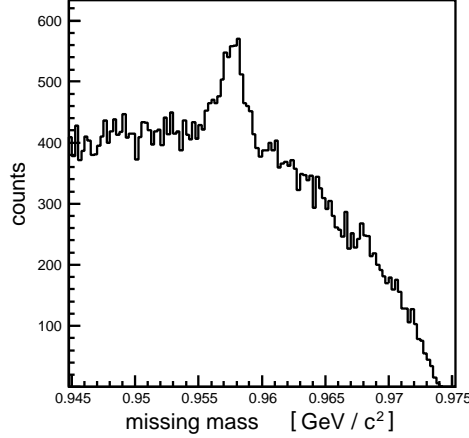


**Figure 4.16:** On-line missing-mass distribution of the  $pp \rightarrow ppX$  reaction measured by means of the COSY-11 detection system in October 2003 [179] at the beam momentum of 3.257 GeV/c, which in the case of the  $pp \rightarrow pp\eta'$  reaction is equivalent to the excess energy of  $Q = 15.5$  MeV.

At present due to the need of the subtraction of the unavoidable multi-pion background, the available statistics allows only for the background-free determination of one-dimensional invariant mass distributions. Yet it would be also desired to determine an occupation density over the Dalitz-plot since this two-dimensional distribution comprises full empirically accessible information of the mutual interaction within a three particle system. However, the present experimental conditions render it impossible, unless the binning was made so large that the possible effect would be smeared out completely. In spite of all, we still endeavour to measure this two-dimensional spectrum for both  $pp\eta$  and  $pp\eta'$  systems free from the background. A detection of protons and gamma quanta from the decay of the meson would allow us to reach this aim. Therefore, when the WASA [180] detector will be installed at the cooler synchrotron COSY [62] we plan to seize the opportunity of performing pertinent investigations [181].

## 5. Dynamics of the near threshold production of $\eta$ and $\eta'$ mesons in collisions of nucleons

*Everything outside of the dynamics is just a verbal description of the table of data, and even then the data table probably yields more information than the verbal description can [182].*

Werner Karl Heisenberg

### 5.1 Comparison of the production yields

*All kinds of reasoning consist in nothing but a **comparison**, and a discovery of those relations, either constant or inconstant, which two or more objects bear to each other [183].*

David Hume

Considerations presented in chapter 4 led to the conclusion, that close to the kinematical threshold, the energy dependence of the total cross section is in first approximation determined via the interaction among the outgoing particles and that the entire production dynamics manifests itself in a single constant, which determines the absolute scale of the total cross section. We demonstrated also that the interaction among created particles increases the production probability drastically, though in the naive time ordered approach the final state interaction takes place after the production. Therefore, the observed increase of the total cross sections close to the kinematical threshold, for the  $pp \rightarrow pp\eta$  and  $pp \rightarrow pp\eta'$  reactions (see figure 4.6), can be considered as a pure quantum mechanical effect, which clearly demonstrates that the production of particles and their mutual interaction must be treated coherently for the proper appraisal of the absolute production cross section. Thus, for the sake of completeness, we will devote one chapter to a brief description of the mechanisms responsible for the production of  $\eta$  and  $\eta'$  mesons in the collisions of nucleons.

As a first step towards the understanding of the creation mechanism underlying the production let us compare the total cross sections for these mesons with their flavour-neutral pseudoscalar partner – the meson  $\pi^0$ .

Since the masses of these mesons are significantly different<sup>1</sup> the influence of the kinematical flux factor  $F$  on the total cross section and the suppression due to the initial state interaction  $F_{ISI}$  depend substantially on the created meson. Therefore, for the comparison of the primary dynamics we will correct for these factors and instead of comparing the total cross section we will introduce – according to reference [2] – a dimensionless quantity  $\sigma \cdot F/F_{ISI}$ , which depends only on the primary production amplitude  $M_0$  and on the final state interaction among the produced particles.

Close-to-threshold the initial state interaction, which reduces the total cross section, is dominated by proton-proton scattering in the  $^3P_0$  state which may be estimated in terms of phase-shifts and inelasticities by employing equation (4.14). The  $F_{ISI}$  factor is close to unity for pion production and amounts to  $\sim 0.2$  [71] and  $\sim 0.33$  [138] for the  $\eta$ , and  $\eta'$  meson, respectively, at threshold.

A comparative study of the production of mesons with significantly different masses encounters the difficulty of finding a proper variable at which the observed yield can be compared. Seeking such quantity let us recall the meaning of the total cross section which is defined as the integral over the available phase space volume of transition probabilities – reflecting the dynamics of the process – from the initial to the final state as written explicitly in equation 3.1. Thus, if the dynamics of the production process of two different mesons were exactly the same then the above introduced yield would also be strictly the same for both mesons, provided it was extracted at the same value of the volume of the phase space  $V_{ps}$  (eq. 3.20). This inference would, however, not be valid if the production yields were compared at the  $\eta_M$  or  $Q$  variables. Therefore, the volume of the available phase space for the produced particles is the most suited quantity for the regarded comparison [2]. This could also be the best choice for the investigation of isospin breaking where the cross sections for the production of particles with different masses need to be compared (e.g.  $\pi^+d \rightarrow pp\eta$  and  $\pi^-d \rightarrow nn\eta$  [185]). Figure 5.1 shows the yield of  $\pi^0$ ,  $\eta$ , and  $\eta'$  mesons in the proton-proton interaction as a function of the available phase space volume.

---

<sup>1</sup> The  $\pi^0$ ,  $\eta$ , and  $\eta'$  masses amount to  $134.98 \text{ MeV}/c^2$ ,  $547.30 \text{ MeV}/c^2$ , and  $957.78 \text{ MeV}/c^2$ , respectively [43].

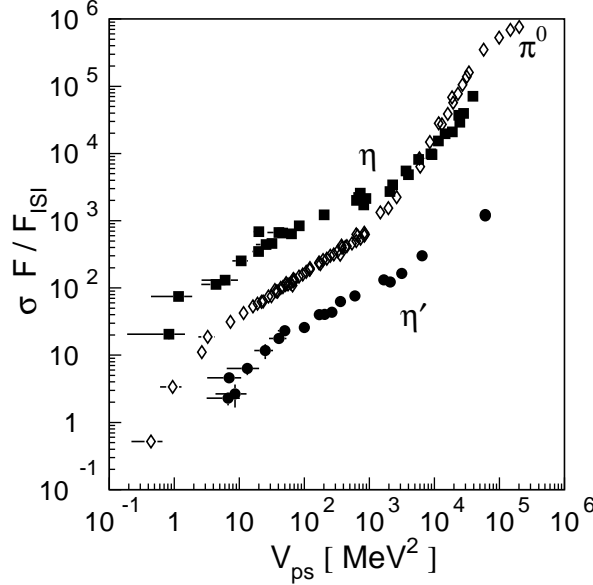


**Figure 5.1:** Total cross section ( $\sigma$ ) multiplied by the flux factor  $F$  and divided by the initial state interaction reduction factor  $F_{ISI}$  versus the available phase space volume for the reactions  $pp \rightarrow pp\eta$  (squares [10, 18, 50–53, 121]),  $pp \rightarrow pp\pi^0$  (diamonds [114–117, 184]), and  $pp \rightarrow pp\eta'$  (circles [3, 5, 11, 53, 97]).

The onset of higher partial waves is seen for  $\pi^0$  and  $\eta$  mesons in the  $V_{ps}$  range between  $10^3$  and  $10^4 \text{ MeV}^2$ , whereas the whole range covered by the  $\eta'$  data seems to be consistent with the pure Ss production. One can also recognize that the data for the Ss final state are grouped on parallel lines indicating a dependence according to the power law  $\sigma \cdot F/F_{ISI} \approx \alpha \cdot V_{ps}^{0.61}$  [186] and that over the relevant range of  $V_{ps}$  the dynamics for  $\eta'$  meson production is about six times weaker than for the  $\pi^0$  meson, which again is a further factor of six weaker than that of the  $\eta$  meson. This is an interesting observation, since the quark wave functions of  $\eta$  and  $\eta'$  comprise a similar amount of strangeness ( $\approx 70\%$  [237]) and hence, in the nucleon-nucleon collision one would expect both these mesons to be produced much less copiously than the meson  $\pi^0$  being predominantly built out of *up* and *down* quarks. On the hadronic level, however, one can qualitatively argue that the  $\eta$  meson – contrary to  $\pi^0$  and  $\eta'$  – owes its rich creation to the existence of the baryonic resonance  $N^*(1535)$  whose branching ratio into the  $N\eta$  system amounts to 30–55% [43]. There is no such established resonance, which may decay into an s-wave  $\eta'N$  system [43], and the  $\pi^0$  meson production with the formation of the intermediate  $\Delta(1232)$  state is strongly suppressed close-to-threshold, because of conservation laws.

## 5.2 Mesonic degrees of freedom

*For what is determinate cannot have  
innumerable explanations [187].*

Nicholas Copernicus

One of the most crucial issue in the investigations of the dynamics of the close-to-threshold meson production is the determination of the relevant degrees of freedom for the description of the nucleon-nucleon interaction, especially in case when the nucleons are very close together<sup>2</sup>. The transition region from the hadronic to constituent quark degrees of freedom does not have a well defined boundary and at present both approaches are evaluated in order to test their relevance in the description of close-to-threshold meson production in the collision of nucleons. Simple geometrical considerations presented in figure 5.2 indicate that at distances smaller than 2 fm the internucleon potential should begin to be free of meson exchange effects and may be dominated by the residual colour forces [189].

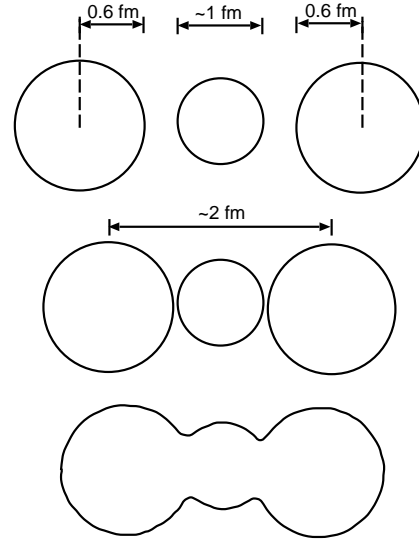


**Figure 5.2:** A cartoon illustrating in naive geometrical terms that for  $r < 2r_N + 2r_M$  meson exchange is unlikely to be appropriate for the description of the internucleon potential. Figure and caption are taken from reference [189].

In section 4.2 it was shown, that the close-to-threshold production of mesons occurs when the colliding nucleons approach distances of about 0.5 fm in case of  $\pi^0$  and of about 0.18 fm in case of  $\phi$  production (see table 4.1). This distance is about one order of magnitude smaller than 2 fm and it is rather difficult to imagine – in coordinate space – an exchange

<sup>2</sup> These investigations are listed as one of the key issues in hadronic physics [188].

of mesons between nucleons as mechanism of the creation process. Thus, the meson exchange for the threshold meson production can be understood as an effective description of the process occurring on the deeper level. Such small collision parameters imply that the interacting nucleons – objects of about 1 fm – overlap and their internal degrees of freedom may be of importance. On the other hand, as demonstrated by Hanhart [81], if there is a meson exchange current possible at leading order it should dominate the creation process. This can be derived from the strong dependence of the production operator on the distance between the colliding nucleons.

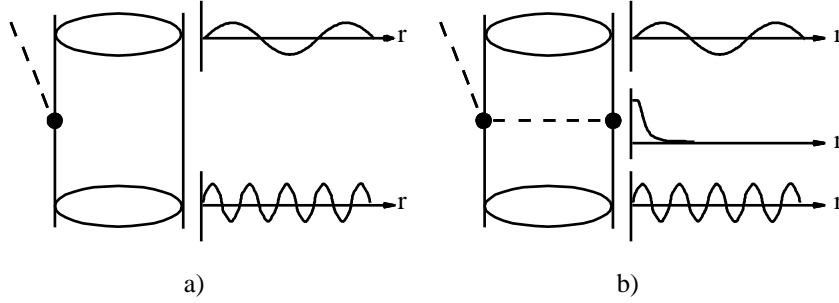


**Figure 5.3:** Illustration of the momentum mismatch. The picture shows why one should a priori expect meson exchange currents to be very important close to the threshold. The figure and title are adapted from reference [81]. By courtesy of C. Hanhart.

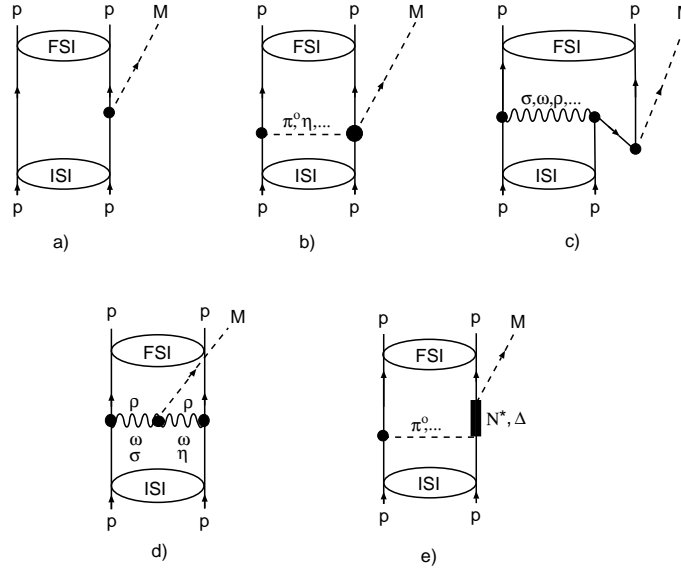


**Figure 5.4:** Diagrams for the  $pp \rightarrow pp \text{ Meson}$  reaction near threshold: (a) *Meson-bremsstrahlung* (nucleonic current) (b) “rescattering” term (nucleonic current) (c) production via heavy-meson-exchange (d) emission from virtual meson (mesonic current) (e) excitation of an intermediate resonance (nucleon resonance current).

This particular feature of the meson exchange current will prevent the cancellation of the transition matrix element being a convolution of the rapidly and mildly oscillating initial and final state wave functions, as it is illustrated in figure 5.3. Consequently, during the last decade, the effective theory based on meson exchanges, which accounts for the size of the participating particles by introduction of the momentum transfer dependent form factors, has been extensively employed for the description of the creation process. Figure 5.4 represents the mechanisms in question. In the next sections we will report on the stage of understanding of the  $\eta$  and  $\eta'$  mesons creation on the hadronic level, and thereafter we shall briefly present first attempts to explain the meson threshold production in the domain of quarks and gluons.

### 5.3 Baryonic resonance – a doorway state for the production of the meson $\eta$

*...although these excitations of the soul are often joined with the passions that are like them, they may also frequently be found with others, and may even originate from those that are in opposition to them [190].*

René Descartes

It is at present rather well established [67, 72, 124, 191–196] that the  $\eta$  meson is produced predominantly via the excitation of the  $S_{11}$  baryonic resonance  $N^*(1535)$  which subsequently decays into  $\eta$  and nucleon, and whose creation is induced through the exchange of  $\pi$ ,  $\eta$ ,  $\rho$ ,  $\sigma$ , and  $\omega$  mesons, as shown in figure 5.4e. Although all the quoted groups reproduce the magnitude of the total cross section, their models differ significantly as far as the relative contributions from the  $\pi$ ,  $\eta$ , and  $\rho$  exchange mechanisms are concerned. The discrepancies are due to the not well known strength of *Meson-N-S<sub>11</sub>* couplings and the  $\eta N$  scattering potential. For example, while the dominance of the  $\rho$  meson exchange is anticipated by authors of references [67, 124, 191–193], it is rather the exchange of the  $\eta$  meson which dominates the production if one takes into account the effects of the off-shell  $\eta N$  scattering [198], or uses the multi-channel multi-resonance model [72]. In any case, the hitherto performed studies aiming to describe the total cross section show that the close-to-threshold production of  $\eta$  mesons in nucleon-nucleon collisions



is dominated by the intermediate virtual  $S_{11}$  nucleon isobar whose width overlaps with the threshold.

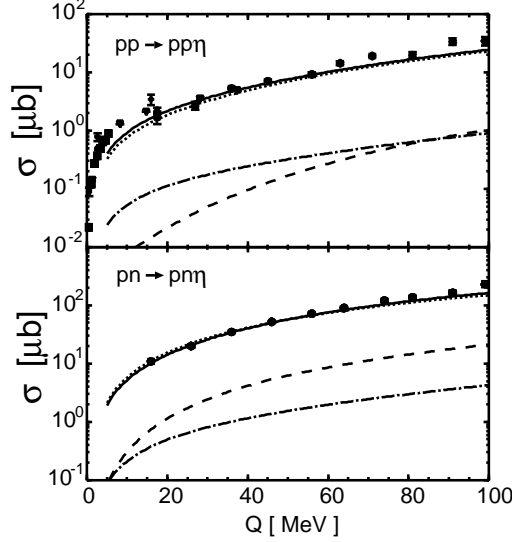


**Figure 5.5:** Total cross sections for the  $pp \rightarrow pp\eta$  (upper panel) and  $pn \rightarrow pn\eta$  (lower panel) reactions as a function of excess energy. The dashed curves correspond to the nucleonic current contribution and the dash-dotted curves to the mesonic current consisting of  $\eta\rho\rho$ ,  $\eta\omega\omega$ , and  $\eta a_0\pi$  contributions. The resonance current presented by the dotted line consists of the predominant  $S_{11}(1535)$  and of the  $P_{11}(1440)$  and  $D_{13}(1520)$  resonances excited via exchange of  $\pi$ ,  $\eta$ ,  $\rho$ , and  $\omega$  mesons. The solid curves are the total contribution. The deviation from the data at low  $Q$  in the upper panel reflects the  $\eta p$  FSI which was not included in the calculations. The data are from refs. [10,50–53,197]. The figure is adapted from [100].

In order to disentangle the various scenarios of the  $S_{11}$  excitation a confrontation of the predictions with other observables is needed. The interference between considered amplitudes causes a different behaviour – depending on the assumed scenario – e.g. of the  $\eta$  meson angular distributions. These differences, however, are too weak in the close-to-threshold region to judge between different models. Also the ratio of the  $\eta$  meson production via the reactions  $pp \rightarrow pp\eta$  and  $pn \rightarrow pn\eta$  can be equally well described by either assuming the  $\rho$  meson exchange dominance [193] or by taking pseudoscalar and vector mesons for exciting the  $S_{11}$  resonance [195]. In the latter case, shown in figure 5.5, the excitation of the resonance via the  $\rho$  meson exchange was found to be negligible. Yet, promisingly, the predictions of the analyzing power depend crucially on the assumed mechanism [193, 195]. This fact has already triggered experimental investigations which aim to determine the spin observables. First results of tentative measurements and perspectives of these studies will be presented in section 5.4.

## 5.4 Spin degrees of freedom – a tool to study details of the $pp \rightarrow pp\eta$ reaction dynamics

*I thought ..., that scientific theories were not the digest of observation, but that they were inventions-conjectures boldly put forward for trial, to be eliminated if they clashed with observation; with observations which were rarely accidental but as a rule **undertaken with definite intention of testing a theory by obtaining, if possible, a decisive refutation** [183].*

David Hume

In spite of the precise measurements of the total cross section for the creation of  $\eta$  meson in proton-proton [10,18,50–53,121] as well as proton-neutron [197] collisions there are still many ambiguities in the description of the mechanism underlying the production process. Calculations performed under different - often mutually exclusive - assumptions led to an equally satisfying description of the data. As we had already described in section 5.3, it is generally anticipated [67,72,191,192,194,196,198–200] that the  $\eta$  meson is produced predominantly via the excitation of the  $S_{11}$  baryonic resonance  $N^*(1535)$ , whose creation is induced through the exchange of the virtual  $\pi$ ,  $\eta$ ,  $\rho$ ,  $\sigma$ , and  $\omega$  mesons, however, at present it has still not been established what the relative contributions originating from a particular meson are. Measurements of the total cross section in different isospin channels add some more limitations to the models, yet still the  $\eta$  meson production in the  $pp \rightarrow pp\eta$  and  $pn \rightarrow pn\eta$  reactions can be equally well described by e.g. assuming the  $\rho$  meson exchange dominance [193] or by taking contributions from the pseudoscalar meson exchanges [195]. Therefore, for a full understanding of the production dynamics the determination of more selective observables is mandatory. A natural choice seems to be an extension of the research to encompass the spin degrees of freedom. Figure 5.6 shows that predictions of the analyzing power  $A_y$  are strongly sensitive to the type of the exchanged particle. A discrepancy between considered models is so pronounced that even a measurement of the beam analysing power with a precision of  $\pm 0.05$  **could exclude at least one of the above mentioned possibilities** with a statistical significance better than three standard deviations. A tentative measurement of that quantity was conducted [7] and points in figure 5.6b indicate the obtained result. Unfortunately, the

present statistics is insufficient to allow discrimination between the alternatives considered, and for a conclusive inference a better accuracy of the data is required. After successful measurement of  $A_y$  for the  $\vec{p}p \rightarrow pp\eta$

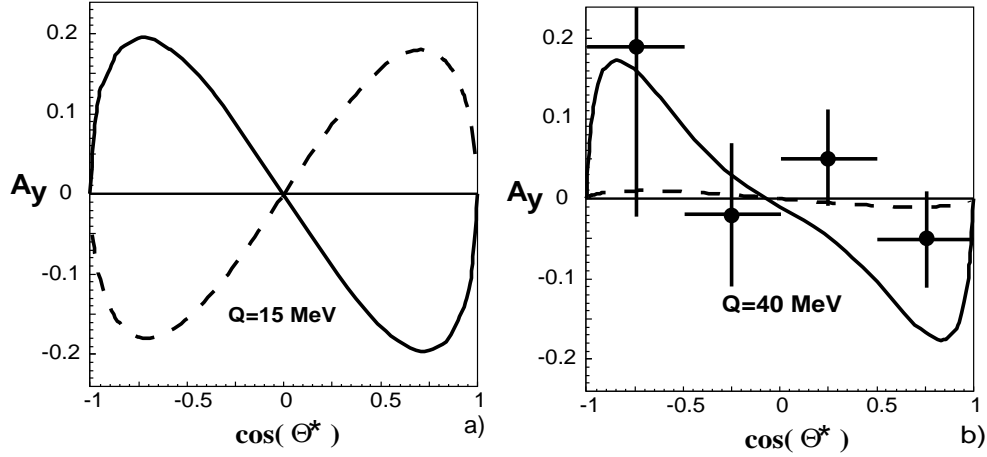


**Figure 5.6:** Predictions for the angular dependence of the analysing power of the reaction  $\vec{p}p \rightarrow pp\eta$  at  $Q = 15$  (a) and at  $Q = 37$  MeV (b) compared to the data taken at  $Q = 40$  MeV [7]. Solid lines present results of the model [195] characterized by the dominance of the exchange of the pseudoscalar mesons in the production process. Dashed lines show expectation obtained under the assumption that the production mechanism is predominated by the exchange of the  $\rho$  meson [193].

reaction at  $Q = 40$  MeV, we continued the study at  $Q = 37$  MeV and at  $Q = 10$  MeV [27, 201, 202]. The measurement at  $Q = 37$  MeV was performed with proton beam polarisation amounting to approximately 70 %, a value significantly larger than in the first measurement. Moreover, the luminosity integrated over the measurement period was larger by about a factor of 1.5. These two factors together, improve the accuracy of the measurement more than twice, in the sense, that the errors corresponding to those in figure 5.6b are expected to be two times smaller. The second measurement was performed at  $Q = 10$  MeV since at this excess energy the maximum of the discrepancy between the predictions of the regarded models [193, 195] is expected. The data on the angular distributions of the analysing power would also enable to determine the relative magnitudes – or at least to set upper limits – for the contribution from the higher than s-wave partial waves to the production dynamics. This can be done with an accuracy by far better than the one resulting from the measurements of the distributions of the spin averaged cross sections. This is because the polarisation observables are sensitive to

the interference terms between various partial amplitudes, which may become measurable even if one of the interfering terms alone appears to be insignificant in case of the spin averaged cross sections. The analysis would be based on the formalism developed for the measurement of the  $\pi^0$  meson production with a polarized proton beam and target [78], which we have already used for the analysis of our first measurement with a polarized proton beam [7, 203, 204]. This procedure permits the derivation of all available information contained in the distributions of the cross sections and the analysing power. Information about the partial wave decomposition is of crucial importance for the interpretation of the production dynamics but also for the study of the mutual interaction of the produced  $\eta$ -proton-proton system. The strength of the proton- $\eta$  interaction cannot be derived univocally from the differential cross section distributions without the knowledge of the contribution of various partial waves.

Measurements with the polarized beam and target would allow determination of these shares. As demonstrated in references [78, 91] the close-to-threshold contributions of the  $Ps$  and  $Pp$  partial waves can be determined in the model-free way from the measurements of the spin dependent total cross sections only. For example the strength of the  $Ps$  final state can be expressed as [78]:

$$\sigma(Ps) = \frac{1}{4} \left( \sigma_{tot} + \Delta\sigma_T + \frac{1}{2}\Delta\sigma_L \right), \quad (5.1)$$

where  $\sigma_{tot}$  denotes the total unpolarized cross section and  $\Delta\sigma_T$  and  $\Delta\sigma_L$  stand for differences between the total cross sections measured with anti-parallel and parallel beam and target polarizations. Subscripts  $T$  and  $L$  associate the measurements with the transverse and longitudinal polarizations, respectively.

At present none of the experimental facilities enable to investigate the  $\vec{p}\vec{p} \rightarrow pp\eta$  reaction. However, an installation of the WASA detector at COSY will offer possibility to accomplish such studies. Corresponding measurements have been already proposed [205], and the predictions of the spin correlation functions are given e.g. in references [79, 206].

## 5.5 Possible mechanisms responsible for the creation of the $\eta'$ meson

*But in fact, even if all writers were honest and plain; even if they never passed off matters of doubt upon us as if they were truths, but set forth everything in good faith; nevertheless, since there is hardly anything that one of them says but someone else asserts the contrary, we should be continually uncertain which side to believe. It would be no good to count heads, and then follow the opinion that has most authorities for it; for if the question that arises is a difficult one, it is more credible that the truth of the matter may have been discovered by few men than by many [207].*

René Descartes

In case of the  $\eta'$  meson the investigations of the mechanisms underlying the production process are even less advanced than these of  $\eta$  and  $\pi$ . This is partly due to the fact that there is no well established baryonic resonance decaying into  $\eta'N$  channel, which could constitute a doorway state for the  $\eta'$  production, and hence there is no mechanism whose strength could be regarded as dominant allowing for the neglect of other possibilities at least in the first order. There is also not much known about the  $\eta'NN$  and other relevant coupling constants, making impossible inferences about the relative strength of different mechanisms on the level achieved in the understanding of the  $\pi$  meson creation [81, 208]. It is also partly because the experimental database is much poorer than this for  $\eta$  and  $\pi$  mesons. This holds not only for the data on the  $\eta'$  production in the collisions of nucleons, but also for the data at relevant energies on nucleon-nucleon elastic scattering. The latter are needed for the estimation of the reduction of the production cross section due to the interaction between nucleons in the initial state. It must be stated, however, that in the recent years the database – relevant for the production of the  $\eta'$  meson – for the proton-proton reactions [3, 53, 97, 209] improved significantly, yet measurements with a corresponding accuracy for the proton-neutron channel are still missing.

### 5.5.1 Meson exchange models

**Salviati.** *But if, of many computations, not even two came out in agreement, what would you think of that? (...)*

**Simplicio.** *If that is how matters stand, it is truly a serious defect [139].*

Galileo Galilei

For the  $\eta$  meson case a contribution from the mesonic current where the meson is created in the fusion of virtual e.g.  $\rho$  or  $\omega$  mesons emitted from both colliding nucleons is by a factor of thirty weaker in comparison to the overwhelming strength of the resonance current (figure 5.5). In contrast, the mesonic current suffices to explain the magnitude of the close-to-threshold  $\eta'$  meson production in the proton-proton interaction, which is just by about a factor of thirty smaller compared to the  $\eta$  meson. Among the mesonic currents regarded by authors of reference [138] the  $\rho\rho\eta'$  gives the dominant contribution, by a factor of five larger than the  $\sigma\eta\eta'$ - and  $\omega\omega\eta'$ -exchange. However, the understanding of the  $\eta'$  production on the hadronic level is far from being satisfactory. The magnitude of the total cross section was also well reproduced in the frame of a one-boson-exchange model (nucleonic current) where the virtual boson ( $B = \pi, \eta, \sigma, \rho, \omega, a_0$ ) created on one of the colliding protons converts to the  $\eta'$  on the other one [69]. Taking into account the off-shell effects of the  $Bp \rightarrow \eta'p$  amplitude it was found that the short range  $\sigma$  and  $\rho$  meson exchanges dominate the creation process, whereas the  $\pi$  exchange plays a minor role. On the contrary, other authors [210] reproduced the magnitude of the total cross section with  $\pi$  exchange only and concluded that the  $\eta$ ,  $\rho$ , and  $\omega$  exchange currents either play no role or cancel each other. However, in both of the above quoted calculations [69, 210] the initial state interaction between protons, which reduces the rate by a factor of about 3, was not taken into account and hence the obtained results would in any case reproduce only 30 % of the entire magnitude of the cross section and could be at least qualitatively reconciled with the mentioned result of reference [138], where the nucleonic current was found to be small. Moreover, the choice of another prescription for the form factors could reduce the one-pion-exchange contribution substantially [138]. However, the picture that the  $\eta'$  meson is predominantly created through the mesonic current, remains at present unclear as well. This is because the magnitude of the total cross section could have also been described assuming that the production of  $\eta'$  is resonant [138]. As possible intermediary resonances the recently reported [211]  $S_{11}(1897)$  and  $P_{11}(1986)$  have

been considered. These resonances were deduced from  $\eta'$  photoproduction data, under the assumption that the close-to-threshold enhancement observed for the  $\gamma p \rightarrow \eta' p$  reaction can be utterly assigned to resonance production. Further, as well strong, assumptions have been made in the derivation of the  $g_{NN^*\eta'}$  and  $g_{NN^*\pi}$  coupling constants [138].

Hence, it is rather fair to state that in the case of the close-to-threshold  $\pi^0$  and  $\eta$  meson production in nucleon-nucleon collisions the dynamics is roughly understood on the hadronic level, but the mechanisms leading to the  $\eta'$  creation are still relatively unknown.

Until now it has not been possible to satisfactorily estimate the relative contributions of the nucleonic, mesonic, and resonance current to the production process. In fact, model uncertainties allow that each one separately could describe the absolute values of the  $pp \rightarrow pp\eta'$  total cross section. This rather pessimistic conclusion calls for further experimental and theoretical research. The understanding of the production dynamics of the  $\eta'$  meson on both hadronic and the quark-gluon level is particularly important since its wave function comprises a significant gluonic component [212], distinguishing it from other mesons and hence the comprehension of the mechanism leading to its creation in collisions of hadrons may help to determine its quark-gluon structure. That, in turn will be helpful when investigating possible glueball candidates [212]. Hereafter we will briefly report of the gluonic mechanisms which may – along with the meson exchange processes discussed above – contribute to the  $\eta'$  production.

### 5.5.2 Approaches on the quark-gluon level

*We must clearly acquire knowledge of factors that are primary. For we claim to know a thing only when we believe that we have discovered what primarily accounts for its being [90].*

Aristotle

As afore mentioned, the close-to-threshold production of  $\eta$  and  $\eta'$  mesons in the nucleon-nucleon interaction requires a large momentum transfer between the nucleons and hence can occur only at distances of about 0.3 fm (see table 4.1). This suggests that the quark-gluon degrees of freedom may indeed play a significant role in the production dynamics of these mesons. A possibly large glue content of the  $\eta'$  and the dominant flavour-singlet combination of its quark wave function may

cause that the dynamics of its production process in nucleon-nucleon collisions is significantly different from that responsible for the production of other mesons. In particular, the  $\eta'$  meson can be efficiently created via a “contact interaction” from the glue which is excited in the interaction region of the colliding nucleons [44]. A gluon-induced contact interaction contributing to the close-to-threshold  $pp \rightarrow pp\eta'$  reaction derived in the frame of the U(1)-anomaly extended chiral Lagrangian is discussed in references [44, 213, 214]. The strength of this contact term is related to the amount of spin carried by polarized gluons in a polarized proton [214, 215], thus making the study of the close-to-threshold  $\eta'$  meson production even more interesting.

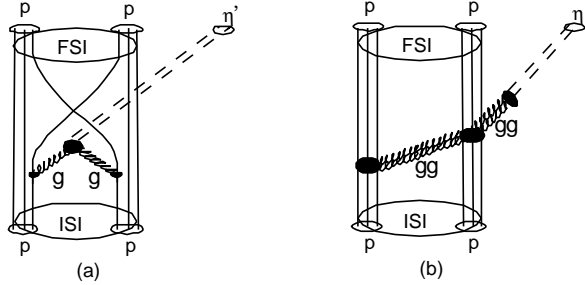


**Figure 5.7:** Diagrams depicting possible quark-gluon dynamics of the reaction  $pp \rightarrow pp\eta'$ . (a) production via a fusion of gluons [216] with rearrangement of quarks. (b) production via a rescattering of a “low energy pomeron”.

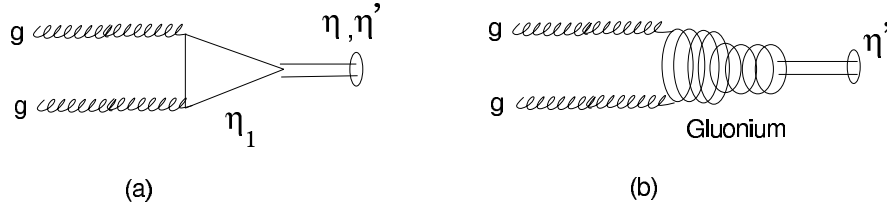


**Figure 5.8:** Coupling of  $\eta$  and  $\eta'$  to two gluons through (a) quark and antiquark triangle loop and (b) gluonic admixture.  $\eta_1$  denotes the flavour-singlet quark-antiquark state. This indicates that gluons may convert into the  $\eta$  or  $\eta'$  meson via a triangle quark loop only by coupling through their flavour singlet part. The figure is taken from reference [217].

Figure 5.7 depicts possible short-range mechanisms which may lead to the creation of the  $\eta'$  meson via a fusion of gluons emitted from the exchanged quarks of the colliding protons [216] or via an exchange of a colour-singlet object made up from glue, which then re-scatters and



converts into  $\eta'$  [218]. The hadronization of gluons to the  $\eta'$  meson may proceed directly via its gluonic component or through its overwhelming flavour-singlet admixture  $\eta_1$  (see fig. 5.8). Contrary to the significant meson exchange mechanisms and the fusion of gluons of figure 5.7 graph a), the creation through the colour-singlet object proposed by S.D. Bass (graph 5.7b) is isospin independent, and hence should lead to the same production yield of the  $\eta'$  meson in both reactions ( $pp \rightarrow pp\eta'$  and  $pn \rightarrow pn\eta'$ ) because gluons do not distinguish between flavours. This property should allow to test the relevance of a short range gluonic term [219] by the experimental determination of the cross section ratio  $R_{\eta'} = \sigma(pn \rightarrow pn\eta')/\sigma(pp \rightarrow pp\eta')$ , which in that case should be close to unity after correcting for the final and initial state interaction between participating baryons. The other extreme scenario – assuming the dominance of the isovector meson exchange mechanism – should result in the value of  $R_{\eta'}$  close to 6.5 as had already been established in the case of the  $\eta$  meson [197]. Perspectives of the experimental investigations aiming to determine  $R_{\eta'}$  and the discussion to what extent these studies may help to establish contributions from quarks and gluons in the  $\eta'$  meson will be presented in section 5.6. In addition to the investigation presented above [44, 213], the interesting features of the close-to-threshold meson production, in particular the large cross section for the  $\eta$  meson in proton-proton interactions exceeding the one of the pion, or even more surprisingly large cross section of the  $\eta$  production in proton-neutron collisions, encouraged also other authors to seek the underlying – OZI rule violating – creation mechanisms in the frame of microscopic models of QCD [220–222]. The hitherto regarded processes are presented in figure 5.9. As indicated in the pictures the structure of participating baryons has been modeled as quark-diquark objects with harmonic confinement [223]. In the upper graphs the large momentum transfer is shared by the exchanged gluons with a subsequent interchange of quarks to provide a colourless object in the final state. The lower graphs depict the two examples of instanton induced interactions with a 6-quark-antiquark (fig. 5.9d) and two-gluon vertex (fig. 5.9e). Adjusting the normalization to the cross section of the  $pp \rightarrow pp\pi^0$  reaction at a single energy point the model [220] accounts roughly for close-to-threshold cross sections of other pseudoscalar and vector mesons in proton-proton collisions.

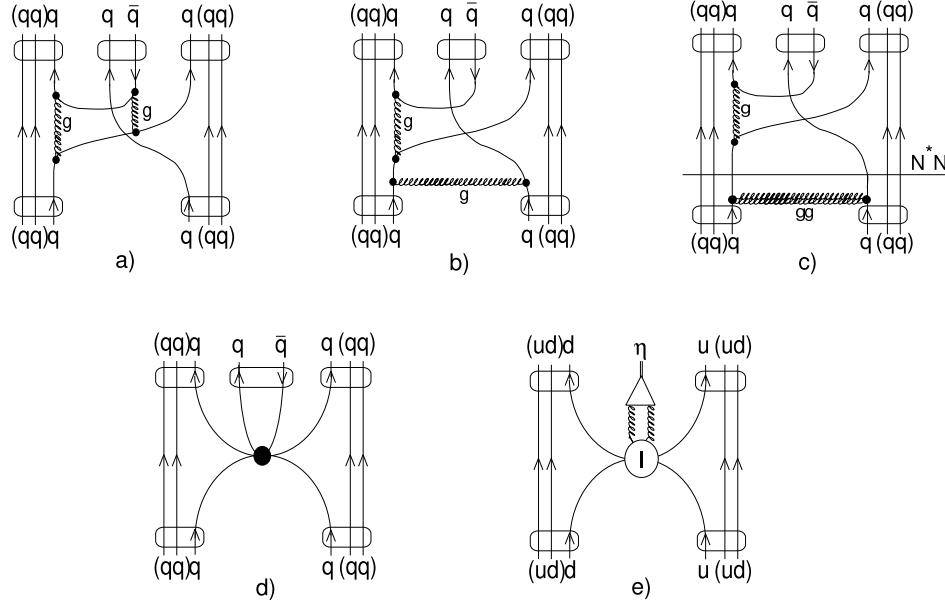


**Figure 5.9:** Diagrams for the  $qq \rightarrow qq(q\bar{q})$  production operator: (a), (b) Two-gluon exchange and rescattering mechanism (c) Correlated, colourless two-gluon exchange. The dashed line indicates the excitation of an intermediate  $NN^*$  system. (d) Instanton induced 6-quark interaction. Figures (a-d) according to [220]. (e) The instanton contribution to the  $\eta$  meson production in the proton-neutron interaction. Figure copied from [221].

Though this approach is characterized by a significantly smaller number of parameters than in the meson exchange models, their uncertainties allow for the description of the data equally well, either by the gluon exchange or by the instanton induced interactions, at least in case of the  $\pi^0$ ,  $\eta'$ ,  $\omega$ , and  $\phi$  mesons. Yet for the resonance dominated  $\eta$  and  $K^+$  meson production in proton-proton collisions it was found that the instanton induced interaction presented by graph 5.9d is not sufficient. Similarly, the authors of reference [221] argue that the instanton induced interaction with a quark-gluon vertex (graph 5.9e) should be of no importance for the  $\eta$  production in proton-proton collisions. This arises from the properties of the vertex which lead to the  $\eta$  production only in case of an interaction between quarks of different flavours ( $ud \rightarrow u\bar{d}gg$ ) and in the quark-diquark model of baryons the proton consists of  $ud$ -diquark and  $u$ -quark and correspondingly the neutron is modeled as  $ud$ -diquark and  $d$ -quark. Although negligible in case of proton-proton interactions, this mechanism may contribute significantly to the total cross section of the  $pn \rightarrow pn\eta$  reaction and indeed as shown in reference [221] it reproduces the data. However, the magnitude of the cross section is very sensitive to the size of the instanton in the QCD vacuum and – similar to the

uncertainty of coupling constants in case of the hadronic approach – at present it makes precise predictions impossible. Thus, despite the partial successes, at the present stage of developments both approaches – on the quark-gluon and on the hadronic level – do not provide an unambiguous answer to the dynamics of the close-to-threshold meson production in the nucleon-nucleon interaction.

## 5.6 Exploration of isospin degrees of freedom

*When a person is placed between two choices, the person bends himself or herself toward the choice he or she desires [224].*

Hildegard von Bingen

Treating proton and neutron as different states of nucleon distinguished only by the isospin projection,  $+\frac{1}{2}$  for the proton and  $-\frac{1}{2}$  for the neutron, we may classify the  $NN \rightarrow NNX$  reactions according to the total isospin of the nucleons pair in the initial and final state. A total isospin of two nucleons equals 1 for proton-proton and neutron-neutron pairs, and may acquire the value of 1 or 0 for the neutron-proton system.

Since  $\eta$  and  $\eta'$  mesons are isoscalars, there are only two pertinent transitions for the  $NN \rightarrow NNX$  reaction, provided that it occurs via the isospin conserving interaction. These are  $\sigma_{00}$  and  $\sigma_{11}$ , where the first and second subscript – labeling the total cross section – describe the total isospin of the nucleon pair in the initial and final state, correspondingly.

It is thus enough to measure two reaction channels for an unambiguous determination of isospin 0 and 1 cross sections. In particular for the total cross section the following relations are satisfied:

$$\sigma_{pp \rightarrow pp\eta'} = \sigma_{11}, \quad (5.2)$$

and

$$\sigma_{pn \rightarrow pn\eta'} = \frac{1}{2}(\sigma_{00} + \sigma_{11}). \quad (5.3)$$

In the case of the proton-neutron reaction the total cross sections add incoherently since the different isospin of the  $NN$  pairs implies that either total spin or angular momentum of these pairs must differ. This is because the  $NN$  system is bound to satisfy the Pauli Principle. Therefore, different isospin states do not interfere as far as the total cross section is concerned [81].

It is needless to mention, that experimental determination of cross sections for different isospin configurations allows for deeper insight into the production mechanism. In sections 6.4 and 6.6 we will present how one can conduct the study of the meson production in the proton-neutron and neutron-neutron reactions and in the next section we will give an example of inferences which may be drawn from the comparison of the total cross sections for the  $pp \rightarrow pp\eta'$  and  $pn \rightarrow pn\eta'$  reactions.

### 5.6.1 Glue content of the $\eta'$ meson

*... even God does not know his own nature [225].*

Bryan Magee

*Experience no doubt teaches us that this or that object is constituted in such and such a manner, but not that it could not possibly exist otherwise [32].*

Immanuel Kant

The most remarkable feature – in the frame of the quark model – distinguishing the  $\eta'$  meson from all other pseudoscalar and vector ground state mesons, is the fact, that the  $\eta'$  is predominantly a flavour-singlet combination of quark-antiquark pairs and therefore can mix with purely gluonic states. A comprehensive discussions on the issue of how one can experimentally determine the differences in the quark-gluon structure between  $\eta'$  and other mesons can be found in the proceedings of the International Workshop on the Structure of the  $\eta'$  Meson held in Las Cruces [226]. Unfortunately, except for the gedanken experiments, no experimentally feasible test allowing for the model-independent conclusions was suggested.

Due to the short life-time of this meson it is impossible to use it as a beam or target. This fact entails that the study must be performed by measurements of the reactions where the  $\eta'$  meson is created in the collisions or decays of more stable particles, and preferentially the studied observables should depend – in a predictive manner – on properties of the  $\eta'$  meson.

In this section we will argue that a comparison of the close-to-threshold total cross sections for the  $\eta'$  meson production in both the  $pp \rightarrow pp\eta'$  and  $pn \rightarrow pn\eta'$  reactions should provide insight into the flavour-singlet (perhaps also into gluonium) content of the  $\eta'$  meson and the relevance of quark-gluon or hadronic degrees of freedom in the creation process. It

is of great credit to S. D. Bass for this idea to be shared with us [218]. However, prior to the formulation of the main conjectures we will recall the most important facts of the production mechanism necessary for the understanding of the further conclusions.

Close-to-threshold production of  $\eta$  and  $\eta'$  mesons in the nucleon-nucleon interaction requires a large momentum transfer between the nucleons and occurs at distances in the order of  $\sim 0.3$  fm. This implies that the quark-gluon degrees of freedom may play a significant role in the production dynamics of these mesons. Therefore, additionally to the mechanisms associated with meson exchanges it is possible that the  $\eta'$  meson is created from excited glue in the interaction region of the colliding nucleons [44, 214], which couple to the  $\eta'$  meson directly via its gluonic component or through its SU(3)-flavour-singlet admixture. The production through the colour-singlet object as suggested in reference [44] is isospin independent and should lead to the same production yield of the  $\eta'$  meson in the  $pn \rightarrow pn \text{ gluons} \rightarrow pn\eta'$  and  $pp \rightarrow pp \text{ gluons} \rightarrow pp\eta'$  reactions after correcting for the final and initial state interaction between the nucleons.

Investigations of the  $\eta$ -meson production in collisions of nucleons allowed to conclude that, close to the kinematical threshold, the creation of  $\eta$  meson from isospin  $I = 0$  exceeds the production with  $I = 1$  by about a factor of 12. This was derived from the measured ratio of the total cross sections for the reactions  $pn \rightarrow pn\eta$  and  $pp \rightarrow pp\eta$  ( $R_\eta = \frac{\sigma(pn \rightarrow pn\eta)}{\sigma(pp \rightarrow pp\eta)}$ ), which was determined to be  $R_\eta \approx 6.5$  in the excess energy range between 16 MeV and 109 MeV [197]. The large difference of the total cross section between the isospin channels suggests the dominance of isovector meson ( $\pi$  and  $\rho$ ) exchange in the creation of  $\eta$  in nucleon-nucleon collisions [197, 227]. Since the quark structure of  $\eta$  and  $\eta'$  mesons is very similar we can – by analogy to the  $\eta$  meson production – expect that in the case of dominant isovector meson exchange the ratio  $R_{\eta'}$  should also be about 6.5. If, however, the  $\eta'$  meson was produced via its flavour-blind gluonic component from the colour-singlet glue excited in the interaction region, the ratio  $R_{\eta'}$  should approach unity after corrections for the interactions between the participating baryons.

Figure 5.10 demonstrates qualitatively the fact that the production of mesons in the proton-neutron collisions may be more probable than in the proton-proton interaction if it is driven by the isovector meson exchanges only. This is because in the case of the proton-neutron collisions there are always more possibilities to realize an exchange or fusion of the isovector mesons than in the case of the reaction of protons. More precisely, for the

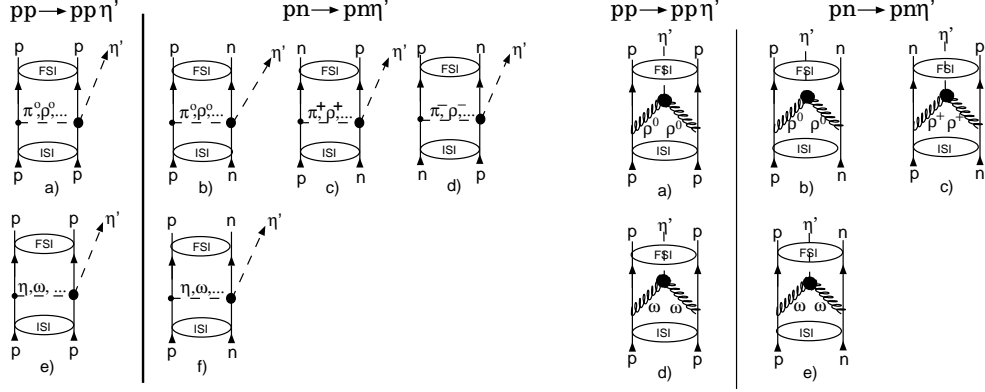


**Figure 5.10:** (left) Example of diagrams with the isovector (upper row) and isoscalar (lower row) meson exchange leading to the creation of the meson  $\eta'$  in the proton-proton and proton-neutron collisions. (right) Fusion of the virtual  $\omega$  (isoscalar) and  $\rho$  (isovector) mesons emitted from the colliding nucleons.

one meson exchange diagrams, when considering  $\pi$ ,  $\eta$ ,  $\rho$ , and  $\omega$  mesons and neglecting initial and final state interaction, the matrix element has the following structure [227]:

$$|M(pn \rightarrow pn\eta)|^2 = \frac{1}{2} [|T_\pi + T_\eta - T_\rho - T_\omega|^2 + |3T_\pi - T_\eta + 3T_\rho - T_\omega|^2];$$

$$|M(pp \rightarrow pp\eta)|^2 = |T_\pi + T_\eta - T_\rho - T_\omega|^2 \quad (5.4)$$

where the amplitudes are labeled by the names of the exchanged mesons. In general, when regarding the isospin structure of the exchange current, as shown in reference [81], if the production operator accounts for the isoscalar meson exchange then  $\sigma_{00} = \sigma_{11}$ , and in case of isovector exchange  $\sigma_{00} = 9\sigma_{11}$ . This is also clear from the particular case represented by equations 5.4, when combined with formulae 5.2 and 5.3. Exploiting these equations we can estimate that, if the production of  $\eta'$  meson via the  $pp \rightarrow pp\eta'$  was governed only by the exchange of the isovector mesons the ratio  $R_{\eta'}$  would be equal to five, and in the case of isoscalar mesons it would be equal to unity.

A very important result of the theoretical investigation, relevant for further consideration, is that regardless of whether it is a mesonic, nucleonic, or resonance current the contribution from the exchange of isovector mesons ( $\rho$  or  $\pi$ ) is much larger from that of isoscalar ones ( $\omega$  or  $\eta$ ) [138, 141, 227]. This unequivocally entails that if the ratio  $R_{\eta'}$  – corrected for FSI and ISI distortions – will be found to be close to unity we

will have a clear indication that the  $\eta'$  is produced directly by gluons. Gluons, as we discussed in chapter 5, may hadronize to  $\eta'$  either via its  $SU(3)_F$  flavour-singlet component or via its gluonic content. In order to disentangle these two effects a substantial theoretical input is required. The benefit of the invested effort will be the determination of the quark-gluon structure of the  $\eta'$  meson. If, however, the measured ratio  $R_{\eta'}$  will not be equal to one, a quantitative determination of the contribution from gluonic mechanism to the production process will require a better understanding of the meson exchange currents. Then if the contribution of meson exchange currents is once understood we will also be able to infer the one from gluons. The dynamics of the meson production in both hadro- and photo-production is at present vigorously studied. The recent results are reported e.g. in references [4, 81, 228, 229].

The close-to-threshold excitation function for the  $pp \rightarrow pp\eta'$  reaction has been already determined [3, 11, 53, 97] whereas the total cross section for the  $\eta'$  meson production in the proton-neutron interaction remains unknown. As a first step towards the determination of the value of  $R_{\eta'}$  the feasibility of the measurement of the  $pn \rightarrow pn\eta'$  reaction by means of the COSY-11 facility was studied using a Monte-Carlo method [20, 230]. As a second step, a test experiment of the  $pn \rightarrow pn\eta$  reaction – suspected to have by at least a factor of thirty larger cross section than the one for the  $pn \rightarrow pn\eta'$  reaction – was performed. In this test measurement, using a beam of stochastically cooled protons and a deuteron cluster target, we have proven the ability of the COSY-11 facility to study the quasi-free creation of mesons via the  $pn \rightarrow pnX$  reaction. Appraisals of simulations [20, 230] and preliminary results of the tentative measurements of the quasi-free  $pn \rightarrow pn\eta$  reaction performed using the newly extended COSY-11 facility [21, 25, 28] will be presented in section 6.5.

## 5.7 Transition probability as a function of particles' “virtuality”

*Es gibt keine freie Masse, genauso wie es kein leeres Vakuum gibt [231].*

Kurt Kilian

First of all the title of this section requires apology and the explanation what is meant under the notion of virtuality. Usually we consider and measure the reactions of free particles for which the difference between the squared energy and momentum is equal to the square of its mass. This is not the case for the nucleons bound inside the nuclei, whose

masses may differ from the mass of the free particles. In particular, in case of the deuteron, the entire difference (summed for both nucleons) amounts to at least a value equivalent to the binding energy. The inner motion of nucleons inside a nucleus makes this difference even larger. Thus principally the virtual nucleons inside a deuteron may not be identical with their free equivalent. By virtuality we would like to name the difference between the mass of the real particle and the mass calculated as a difference between squared energy and squared momentum of its virtual counterpart. When using a deuteron as a source of neutrons for the measurement of e.g. proton-neutron reactions this difference is usually regarded as an obstacle making difficult a direct comparison of free and quasi-free scattering. Here we would like to suggest how to take advantage of this fact. Namely we intend to make a systematic study of the dependence of the cross sections for a meson production in nucleon-nucleon collisions as a function of their virtuality, which in the first order, if a deuteron is used as a target, can be deduced from the momentum of the nucleon which does not take part in the reaction.

There is a difference between the free and bound nucleon since they have different masses. Hence it is natural to expect that they will also differ in other aspects. Recently a chance appeared to realise such studies at the WASA facility [180], which is planned to be installed at COSY in the near future, and the corresponding letter of intent has been already prepared [181].

## 5.8 Natural width of mesons – does it depend on the momentum transfer?

*Throughout the history of spectroscopy, improved resolution has led to discoveries of finer and finer structures [232].*

Bogdan Castle Maglich

Although only loosely connected to the subject of this monograph, we would like to comment on a very recent and highly interesting hypothesis announced by Maglich at the HADRON'03 conference in Aschaffenburg [232]. Based on the experience gained from measurements of the  $a_1$  and  $a_2$  mesons via the  $\pi^- p \rightarrow pX^-$  reactions, he postulated that the width of mesons may be a function of the momentum transfer  $|t|$ , and in particular that the mesons width grows with decreasing value of  $|t|$ . According to his idea the intrinsic widths of all meson states are narrow



and can be observed only at high momentum transfers  $|t| > 0.2$ . Since the production cross sections are inversely proportional to  $|t|$ , the experimental data samples are dominated by events corresponding to low values of the momentum transfer, and therefore the observed widths of mesons appear to be broad [232]<sup>3</sup>.

Nothing can be a priori excluded, however we would like to indicate that the broadening of the width of mesons may only be an apparent effect caused by the error propagation through the formula exploited for the missing mass calculation. Such effects have been observed at the missing mass spectra from measurements of the  $\eta$  meson at the COSY-11 [1] and TOF [95] facilities.

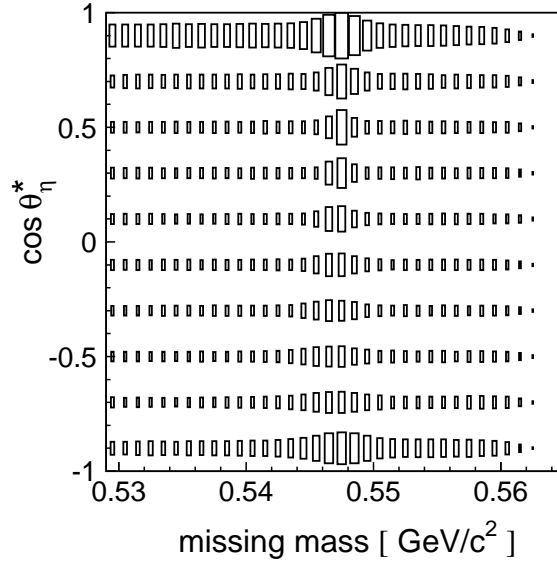


**Figure 5.11:** Distribution of the polar scattering angle of the X system created via the  $pp \rightarrow ppX$  reaction measured at  $Q = 15.5$  MeV above the threshold for the production of the  $\eta$  meson [18].

Figure 5.11 presents the dependence of the missing mass distribution as a function of the polar angle of the emission of the produced system X. At a mass value corresponding to the mass of the  $\eta$  meson one observes a strip of enhanced population-density over a smooth multi-pion background (figure 6.11 from section 6.3 constitutes the projection of this plot onto a mass axis). Here it is incontestably evident that the width of the signal originating from the reaction  $pp \rightarrow pp\eta$  is not constant but rather varies with the polar angle  $\Theta_\eta^*$ . Specifically, the signal from  $\eta$  meson is

<sup>3</sup>An alternate explanation proposed after completion of this treatise can be found in reference [233].

much sharper for  $\cos\Theta_\eta = 0.3$  than for  $\cos\Theta_\eta^* = -0.95$ . The difference cannot be assigned to the variation of the width of the  $\eta$  meson, since this is three orders of magnitude smaller ( $\Gamma_\eta = 1.18 \pm 0.11$  KeV). The effect is also seen by comparison of left and right panel in figure 6.22.

In general the ground-state pseudoscalar mesons are too narrow to study a possible variation of their width via the missing mass method at any of the up-to-date missing mass spectrometers. For this purpose vector mesons would be much better suited, and in particular mesons  $\omega$  and  $\phi$  possessing width of 8.4 MeV and 4.3 MeV, respectively. In figure 1.2 we demonstrated that the COSY-11 detection setup combined with the stochastically cooled proton beam [234] of COSY results in a mass resolution of about 0.7 MeV (FWHM). In the case of  $\phi$  or  $\omega$  mesons, such a precision would enable to observe effects in the order of 10% without necessity of any sophisticated analysis. Unfortunately the limited acceptance of COSY-11 setup allows for the reliable (model independent) evaluation of the data only in the vicinity of the kinematical threshold, which in case of the broad<sup>4</sup> mesons makes the derivation of their spectral function rather complicated due the strong variation of the phase space over a resonance range [6]. A comparable resolution but with by far higher acceptance shall be obtainable at the WASA detector. Its installation at cooler synchrotron COSY will allow for investigations of all ground state pseudoscalar and vector flavour-neutral mesons and we consider to perform such a study for the  $\omega$  meson.

In case the bold hypothesis rised by Maglich [232] were wrong it can be easily falsified by the high statistics measurements of the  $\omega$  mesons at the upcoming facility WASA@COSY. If confirmed it would be a sensation.

---

<sup>4</sup> For a comprehensive discussion of a notion of the threshold and the definition of the total cross section in case of broad resonances the reader is referred to reference [6].

## 6. Experiment

*Science is the attempt to discover, by means of observation, and reasoning based upon it, first, particular facts about the world, and then laws connecting facts with one another and (in fortunate cases) making it possible to predict future occurrences [235].*

Bertrand Russell

Major part of the experimental results, constituting the basis for the inferences considered in this work, has been obtained using the COSY-11 facility. This chapter will be devoted to the description of this detection system placing emphasis on its use for the determination of the total cross section in the case of the  $pp \rightarrow pp\eta'$  reaction and derivation of the differential cross sections for the reaction  $pp \rightarrow pp\eta$ . The description will be focused on the data analysis including the methods for the off-line monitoring of the beam and target parameters, model independent multi-dimensional acceptance corrections, the procedure of kinematical fitting and the subtraction of the background, especially in case of the derivation of the differential cross sections.

For details of the functioning of the employed detectors, the description methods of their calibration, as well as for the elucidation of the hardware event selection and the data acquisition the reader is referred to references [236, 237].

### 6.1 Measurement of the total cross section on the example of the $pp \rightarrow pp\eta'$ reaction

*I hold that most observations are more or less indirect, and that it is doubtful whether the distinction between directly observable incidents and whatever is only indirectly observable leads us anywhere [238].*

Karl Raimund Popper

The COSY-11 facility enables exclusive measurements of the meson production occurring via interaction of nucleons in the range of the kinematical threshold. The collisions of protons are realized using the cooler

synchrotron COSY-Jülich [62, 239] and the  $H_2$  cluster target [240, 241] installed in front of one of the regular COSY dipole magnets, as shown schematically in figure 6.1. The target being a beam of  $H_2$  molecules grouped inside clusters of up to  $10^5$  atoms, crosses perpendicularly the beam of  $\sim 2 \cdot 10^{10}$  protons circulating in the ring.

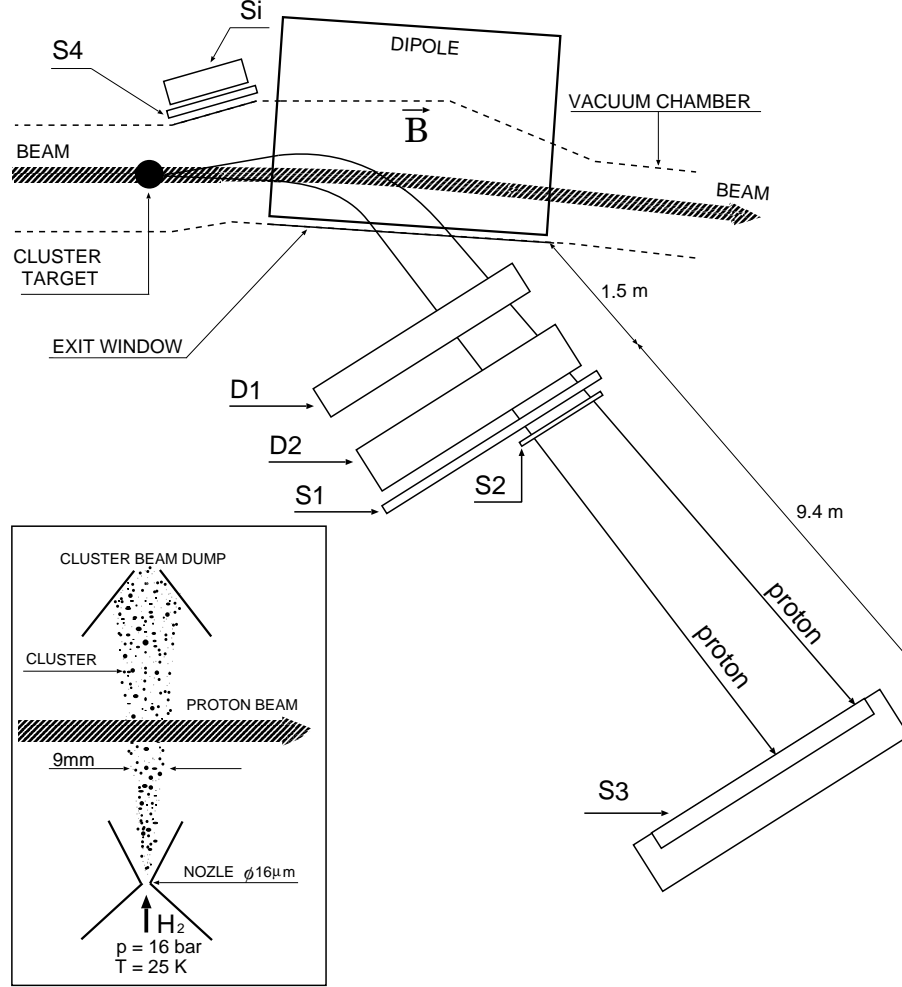


**Figure 6.1:** Schematic view of the part of the COSY-11 detection setup [61]. The cluster target [240] is located in front of the accelerator dipole magnet. Positively charged particles which leave the scattering chamber through the thin exit foil are detected in two drift chamber stacks D1, D2 [242] and in the scintillator hodoscopes S1, S2 [243], and S3 [244, 245]. Scintillation detector S4 and the position sensitive silicon pad detector Si [246] are used in coincidence with the S1 counter for the registration of the elastically scattered protons. Elastic scattering is used for an absolute normalisation of the cross sections of the investigated reactions and for monitoring both the geometrical spread of the proton beam and the position at which the beam crosses the target [8]. In the left-lower corner a schematic view of the interaction region is depicted. The figure has been adapted from reference [237].

The beam of accelerated protons is cooled stochastically during the measurement cycle [234]. Longitudinal and vertical cooling enables to keep the circulating beam practically without energy losses and without a spread of its dimensions even during a 60 minutes cycle, when passing more than  $10^6$  times per second through the  $10^{14}$  atoms/cm<sup>2</sup> thick target.

If at the intersection point of the cluster beam with the COSY proton beam the collision of protons results in the production of a meson, then the ejected protons - having smaller momenta than the beam protons - are separated from the circulating beam by the magnetic field. Further they leave the vacuum chamber through a thin exit foil and are registered by the detection system consisting of drift chambers and scintillation counters [10,61]. The hardware trigger, based on signals from scintillation detectors, was adjusted to register all events with at least two positively charged particles. Tracing back trajectories from drift chambers through the dipol magnetic field to the target point allowed for the determination of the particles momenta. Having momentum and velocity, the latter measured using scintillation detectors, it is possible to identify the mass of the particle. Figure 6.2a shows the squared mass of two simultaneously detected particles.

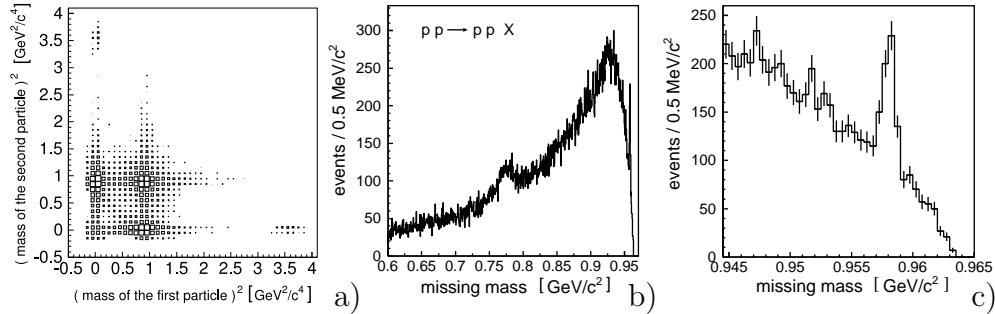


**Figure 6.2:** (a) Squared masses of two positively charged particles measured in coincidence. Pronounced peaks are to be recognized when two protons, proton and pion, two pions, or pion and deuteron were registered. Note that the number of events is shown in logarithmic scale. (b)(c) Mass spectrum of the unobserved particle or system of particles in the  $pp \rightarrow ppX$  reaction determined at  $Q = 5.83$  MeV above the  $\eta'$  production threshold.

A clear separation is seen into groups of events with two protons, two pions, proton and pion, and also deuteron and pion. This spectrum enables to select events with two registered protons. The knowledge of the momenta of both protons before and after the reaction allows to calculate the mass of an unobserved particle or system of particles created in the reaction. The four-momentum conservation applied to the  $pp \rightarrow ppX$  reaction leads to the following expression:

$$m_x^2 = E_x^2 - \vec{P}_x^2 = (E_{beam} + E_{target} - E_1^p - E_2^p)^2 - |\vec{P}_{beam} + \vec{P}_{target} - \vec{P}_1^p - \vec{P}_2^p|^2,$$

where the used notation is self-explanatory<sup>1</sup>. Figure 6.2b depicts the missing mass spectrum obtained for the  $pp \rightarrow ppX$  reaction at an excess-energy of  $Q = 5.8$  MeV above the  $\eta'$  meson production threshold. Most of the entries in this spectrum originate from the multi-pion production [11, 237], forming a continuous background to the well distinguishable peaks accounting for the creation of  $\omega$  and  $\eta'$  mesons, which can be seen at mass values of  $782 \text{ MeV}/c^2$  and  $958 \text{ MeV}/c^2$ , respectively. The signal of the  $pp \rightarrow pp\eta'$  reaction is better to be seen in the figure 6.2c, where the missing mass distribution only in the vicinity of the kinematical limit is presented. Figure 6.3a shows the missing mass spectrum for the measurement at  $Q = 7.57$  MeV (above kinematical threshold of the  $pp \rightarrow pp\eta'$  reaction) together with the multi-pion background (dotted line) as combined from the measurements at different excess-energies. Subtraction of the background leads to the spectrum with a clear signal at the mass of the  $\eta'$  meson as shown by the solid line in figure 6.3b. The dashed histogram in this figure corresponds to the Monte-Carlo simulations where the beam and target conditions were deduced from the measurements of elastically scattered protons in the manner described in the next section. The magnitude of the simulated distribution was fitted to the data, but the consistency of the widths is a measure of understanding of the detection system and the target-beam conditions. Histograms from a measurement at  $Q = 1.53$  MeV shown in figures 6.3c,d demonstrate the achieved missing-mass resolution at the COSY-11 detection system, when using a stochastically cooled proton beam. The width of the missing mass distribution (figure 6.3d), which is now close to the natural width of the  $\eta'$  meson ( $\Gamma_{\eta'} = 0.202 \text{ MeV}$  [43]), is again well reproduced by the Monte-Carlo simulations. The broadening of the width of the  $\eta'$  signal with increasing excess-energy (compare figures 6.3b and 6.3d) is a kinematical effect discussed in more detail in reference [10]. The decreasing of the signal-to-background ratio with growing excess-energy is due to the broadening of the  $\eta'$  peak and the increasing background when moving away from the kinematical limit (see e.g. figure 6.2c or 6.3c). At the same time, the shape of the background, determined by the convolution of the detector acceptance and the distribution of the two- and three-pion production [237], remains unchanged within the studied range of the beam momentum. The signal-to-background ratio changes from 1.8 at  $Q = 1.53$  MeV to 0.17 at  $Q = 23.64$  MeV. The geometrical acceptance, being defined by the gap of a dipole yoke and the scintillation detector most distant from the target [10, 61], decreases from 50 % to

---

<sup>1</sup> The missing mass technique was first applied by authors of reference [247].

4 % within this excess-energy range. However, in the horizontal plane it is still 100 % and thus covers the whole phase space. This issue will be considered in details in subsection 6.3.2.

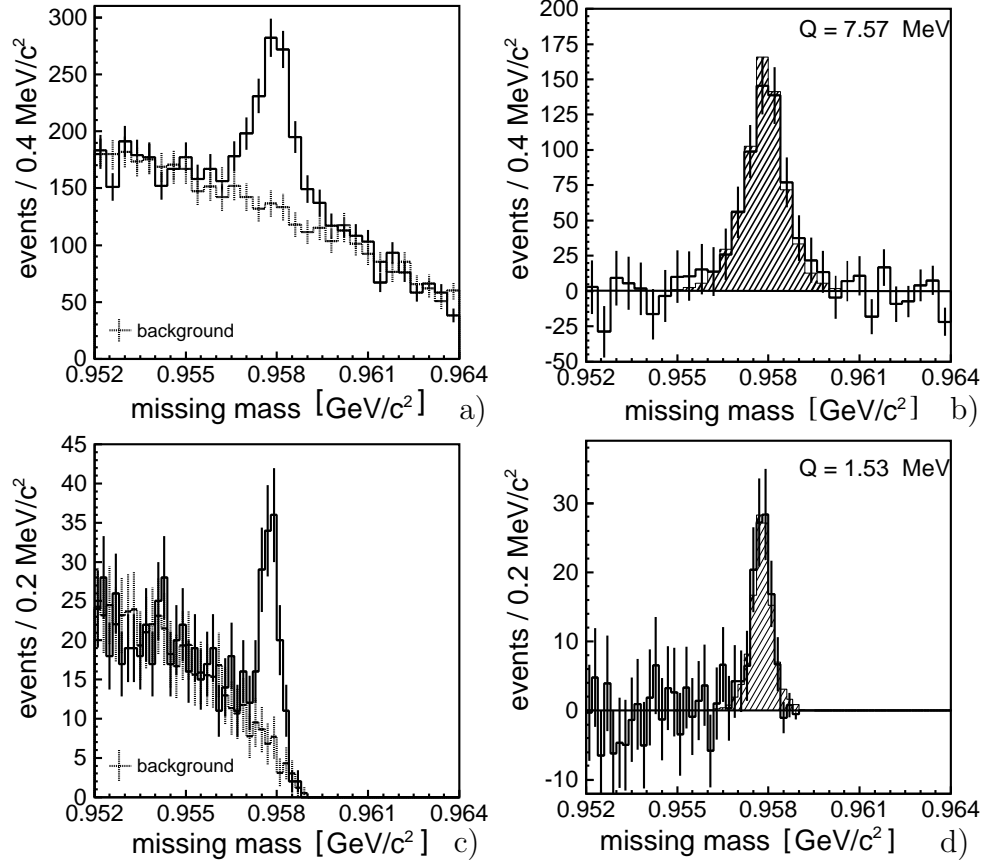


**Figure 6.3:** Missing mass distribution with respect to the proton-proton system: (a),(b) measurements at  $Q = 7.57$  MeV above the threshold of the  $pp \rightarrow pp\eta'$  reaction and (c),(d) at  $Q = 1.53$  MeV. Background shown as dotted lines is combined from the measurements at different energies shifted to the appropriate kinematical limits and normalized to the solid-line histogram. Dashed histograms are obtained by means of the Monte-Carlo simulations.

The absolute value of the excess-energy was determined from the position of the  $\eta'$  peak in the missing mass spectrum, which should correspond to the actual mass of the meson  $\eta'$ . The systematic error of the excess-energy established by this method equals to 0.44 MeV and constitutes of 0.14 MeV due to the uncertainty of the  $\eta'$  meson mass [43] and of 0.3 MeV due to the inaccuracy of the detection system geometry [248], whereby the largest effect originates in the inexactness of relative settings of target, dipole, and drift chambers.

## 6.2 Monitoring of beam and target parameters

*Since we can never know anything for sure, it is simply not worth searching for certainty; but it is well worth searching for truth; and we do this chiefly by searching for mistakes, so that we can correct them [249].*

Karl Raimund Popper

An exact extraction of absolute cross sections from the measured data demands a reliable estimation of the acceptance of the detection system. This in turn crucially depends on the accuracy of the determination of the position and dimensions of both the beam and the target. In this section we will describe a method for estimating the dimensions of the proton beam, based on the momentum distribution of elastically scattered protons, which can be measured simultaneously with the investigated reaction.

As already pointed out, the production of short-lived uncharged mesons ( $\eta$ ,  $\omega$ ,  $\eta'$ , or  $\phi$ ) is investigated at the COSY-11 facility (see figures 6.1 and 6.4b) by means of the missing mass technique via the  $pp \rightarrow ppX$  reaction, with the four-momenta of protons being fully determined experimentally. The accuracy of the extracted missing mass value, which decides whether the signal from the given meson is visible over a background, depends on the precision of the momentum reconstruction of the registered protons, which in turn depends on the detector resolution and both the momentum- and the geometrical spread of the accelerator proton beam interacting with the internal cluster target beam. The momentum reconstruction is performed by tracing back trajectories from drift chambers through the dipole magnetic field to the target, which is ideally assumed to be an infinitely thin vertical line. In reality, however, the reactions take place in that region of finite dimensions where beam and target overlap, as depicted in figure 6.4a. Consequently, assuming in the analysis an infinitesimal target implies a smearing out of the momentum vectors and hence of the resolution of the missing mass signal. The part of the COSY-11 detection setup used for the registration of elastically scattered protons is shown in figure 6.4b. Trajectories of protons scattered in the forward direction are measured by means of two drift chambers (D1 and D2) and a scintillator hodoscope (S1), whereas the recoil protons are registered in coincidence with the forward ones using a silicon pad detector arrangement (Si) and a scintillation detector (S4).



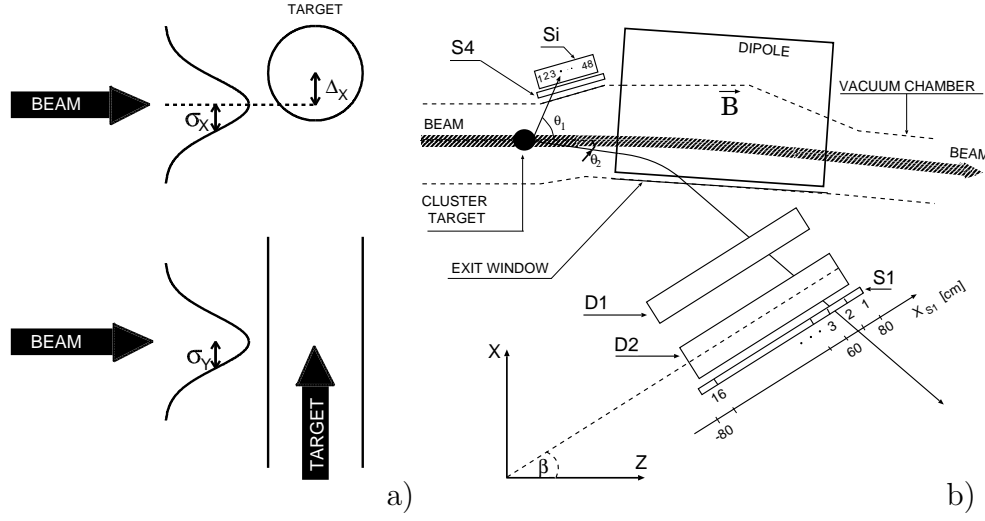


**Figure 6.4:** (a) Schematic description of the relative beam and target setting. Seen from above (upper part), and from aside (lower part),  $\sigma_x$  and  $\sigma_y$  denote the horizontal and vertical standard deviation of the assumed Gaussian distribution of the proton beam density, respectively. The distance between the centres of the proton and the target beam is described as  $\Delta_x$ .

(b) Schematic view of the COSY-11 detection setup. Only detectors used for the measurement of elastically scattered protons are shown. Numbers, at the silicon pad detector (Si), and below the scintillator hodoscope (S1), indicate the order of segments. D1 and D2 denote drift chambers. The  $X_{S1}$  axis is defined such that the first segment of the S1 ends at 80 cm and the sixteenth ends at -80 cm. The proton beam, depicted by a shaded line, circulates in the ring and crosses each time the  $H_2$  cluster target installed in front of one of the bending dipole magnets of the COSY accelerator.

The two-body kinematics gives an unambiguous relation between the scattering angles  $\Theta_1$  and  $\Theta_2$  of the recoiled and forward flying protons. Therefore, as seen in figure 6.5a, events of elastically scattered protons can be identified from the correlation line formed between the position in the silicon pad detector Si, and the scintillator hodoscope S1, the latter measured by the two drift chamber stacks. For those protons which are elastically scattered in forward direction and are deflected in the magnetic field of the dipole the momentum vector at the target point can be determined. According to two-body kinematics, momentum components parallel and perpendicular to the beam axis form an ellipse, from which a section is shown as a solid line in figure 6.5b, superimposed on data selected according to the correlation criterion from figure 6.5a for elastically scattered events.

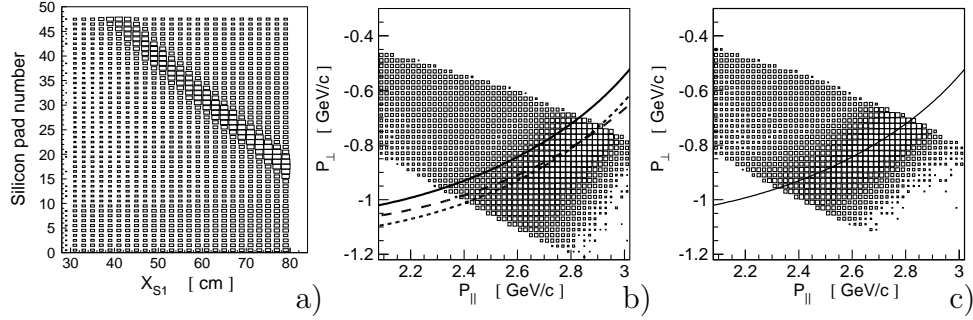


**Figure 6.5:** (a) Identification of elastically scattered protons from the correlation of hits in the silicon detector Si and the S1 scintillator hodoscope. Note that the number of entries per bin is given in a logarithmic scale, ranging from 1 (smallest box) to 19000 (largest box). (b) Perpendicular versus parallel (with respect to the beam direction) momentum components of particles registered at a beam momentum of 3.227 GeV/c. The number of entries per bin is shown logarithmically. The solid line corresponds to the momentum ellipse expected for elastically scattered protons at a beam momentum of 3.227 GeV/c, the dashed line refers to a beam momentum of 3.350 GeV/c, and the dotted line shows the momentum ellipse obtained for a proton beam inclined by 40 mrad. (c) The same data as shown in b) but analyzed with the target point shifted by -0.2 cm perpendicularly to the beam direction (along the X-axis in figure 6.4b). The solid line shows the momentum ellipse at a beam momentum of 3.227 GeV/c.

In figure 6.5b, similarly as in figure 6.5a, it is obvious that data of elastically scattered events arise clearly over a certain low level background. However, what is important here is that the mean of the elastically scattered data is significantly shifted from the expected line, indicating that the reconstructed momenta are on average larger than expected. This discrepancy cannot be explained by an alternative assumption of either the proton beam momentum or the proton beam angle because of the following reason: Trying to reach an acceptable agreement between data and expectation the beam momentum must be changed by more than 120 MeV/c (dashed line in figure 6.5b), which is 40 times more than the conservatively estimated error of the absolute beam momentum ( $\pm 3$  MeV/c) [62, 248, 250]. Similarly, the effect could have been corrected by changing the beam angle by 40 mrad (see dotted line in figure 6.5b), which also exceeds the admissible deviation of the beam angle ( $\pm 1$  mrad [62]) by at least a factor of 40.

However, the observed discrepancy can be explained by shifting the assumed reaction point relative to the nominal value by  $-0.2$  cm perpendicular to the beam axis towards the center of the COSY-ring along the X-axis defined in figure 6.4b. The experimentally extracted momentum components obtained under this assumption, shown in figure 6.5c,

agree with the expectation depicted by the solid line, and the data are now spread symmetrically around the ellipse. This spread is essentially due to the finite extensions of the cluster target and the proton beam overlap, which corresponds to about  $\pm 0.2$  cm as can easily be inferred from the value of the target shift required. Other contributions as the spread of the beam momentum and still some multiple scattering events appear to be negligible and therefore we consider further the influence of the effective target dimensions and the spread of the COSY beam.

Assuming both the target beam to be described by a cylindrical pipe, with a diameter of 9 mm, homogeneously filled with protons [240, 251], and the COSY proton beam density distribution to be described by Gaussian functions with standard deviations  $\sigma_X$  and  $\sigma_Y$  for the horizontal and vertical directions, respectively [62, 252], we performed Monte-Carlo calculations varying the distance between the target and the beam centres ( $\Delta_X$ ), and the horizontal proton beam extension ( $\sigma_X$ ) (see figure 6.4a).

In order to account for the angular distribution of the elastically scattered protons, to each generated event an appropriate weight  $w$  was assigned according to the differential distributions of the cross sections measured by the EDDA collaboration [253]. The generated events were analyzed in the same way as the experimental data. A comparison of the data from figure 6.5b (data analyzed by using the nominal interaction point) with the corresponding simulated histograms allows to determine both  $\sigma_X$  and  $\Delta_X$ . For finding an estimate of the parameters  $\sigma_X$  and  $\Delta_X$  we construct the  $\chi^2$  statistic according to the *method of least squares*:

$$\chi^2 = \sum_i \frac{(\alpha N_i^s + b_i - N_i^e)^2}{\alpha^2 \sum_{i^{th} bin} w^2 + N_i^e + b_i}, \quad (6.1)$$

where  $N_i^e$  and  $N_i^s = \sum_{i^{th} bin} w$  denote the content of the  $i^{th}$  bin of the  $P_\perp$ -versus- $P_\parallel$  spectrum determined from experiment (figure 6.5b) and simulations, respectively. The background events  $b_i$  in the  $i^{th}$  bin amount to less than one per cent of the data [237] and were estimated by linear interpolations between the inner and outer part of a broad distribution surrounding the expected ellipse originating from elastically scattered protons. The free parameter  $\alpha$  allows to adjust the overall scale of the fitted Monte-Carlo histograms. Thus, varying the  $\alpha$  parameter the  $\chi_{min}^2$  for each pair of  $\sigma_X$  and  $\Delta_X$  was established as a minimum of the  $\chi^2(\alpha)$  distribution.

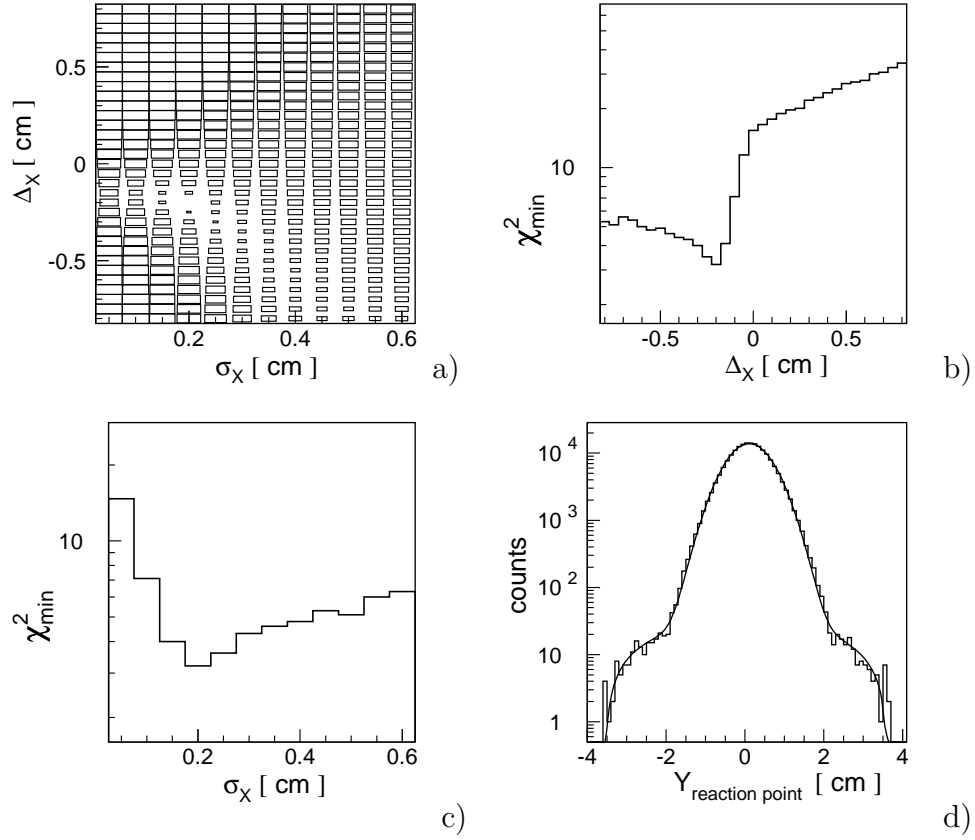


**Figure 6.6:** (a)  $\chi^2_{min}$  as a function of  $\sigma_X$  and  $\Delta_X$ . The number of entries is shown in a logarithmic scale. (b)  $\chi^2_{min}$  as a function of  $\Delta_X$ . (c)  $\chi^2_{min}$  as a function of  $\sigma_X$ . The minimum value of  $\chi^2_{min}$  is larger than two. However, it decreases when only a part of the 60 minutes long COSY cycle is taken into account (see subsection 6.2.1). This is due to the fact that the beam changes during the cycle and its shape, when integrated over the whole cycle time, does not suit perfectly to the shape assumed in Monte-Carlo simulations. (d) Distribution of the vertical component of the reaction points determined by tracing back trajectories from the drift chambers through the dipole magnetic field to the centre of the target (in the horizontal plane). “Tails” are due to secondary scattering on the vacuum chamber and were parametrized by a polynomial of second order. The solid line shows the simultaneous fit of the Gaussian distribution and the polynomial of second order.

Figure 6.6a shows the logarithm of the obtained  $\chi^2_{min}$  as a function of the values of  $\sigma_X$  and  $\Delta_X$  used in the Monte-Carlo calculations: A valley identifying a minimum range is clearly recognizable, which gives the unique possibility to determine the varied parameters  $\sigma_X$  and  $\Delta_X$ . The overall minimum of the  $\chi^2_{min}(\sigma_X, \Delta_X)$ -distribution, at  $\sigma_X = 0.2$  cm and  $\Delta_X = -0.2$  cm, is obviously and better seen in figures 6.6b and 6.6c,

which show the projections of the valley line onto the respective axis. The same results were obtained when employing the Poisson likelihood  $\chi^2$  derived from the maximum likelihood method [254, 255]

$$\chi^2 = 2 \cdot \sum_i [\alpha N_i^s + b_i - N_i^e + N_i^e \ln(\frac{N_i^e}{\alpha N_i^s + b_i})], \quad (6.2)$$

The vertical beam extension of  $\sigma_Y = 0.51$  cm was established directly from the distribution of the vertical component of the particle trajectories at the centre of the target. This is possible, since for the momentum reconstruction only the origin of the track in the horizontal plane is used, while the vertical component remains a free parameter. As shown in figure 6.6d, the reconstructed distribution of the vertical component of the reaction points indeed can well be described by a Gaussian distribution with the  $\sigma = 0.53$  cm. The width of this distribution is primarily due to the vertical spread of the proton beam. The spread caused by multiple scattering and drift chambers resolution was determined to be about 0.13 cm (standard deviation) [237]. Therefore,  $\sigma_Y = \sqrt{0.53^2 - 0.13^2} \approx 0.51$  cm.

The effect of a possible drift chamber misalignment, i. e. an inexactness of the angle  $\beta$  in figure 6.4b, was estimated to cause a shift in the momentum plane corresponding to a value of 0.15 cm for  $\Delta_X$ . This gives a rather large systematic bias to the estimation of the absolute value of  $\Delta_X$ , but it does not influence the implications concerning the parameter  $\sigma_X$ , and still allows for the determination of relative beam shifts  $\Delta_X$  during the measurement cycle.

The absolute value of  $\Delta_X$  can be found if one additionally takes into account the width of the mass spectrum of the studied meson. Clearly, using in the analysis a wrong value of  $\Delta_X$  broadens a missing mass distribution. Therefore, the real value of  $\Delta_X$  can be determined as the one at which the width of the mass spectrum of the investigated meson is the least.

### 6.2.1 Influence of the stochastic cooling on the proton beam quality

*The cooling of a single particle circulating in a ring is particularly simple [256].*

Simon van der Meer

Meson production cross sections in the proton-proton collisions increase rapidly with the beam momentum, and change by more than one or-

der of magnitude when the excess energy grows from 1 MeV to 10 MeV [2, 3, 10]. Due to the rapid change of the total cross section, studies of the close-to-threshold meson production require a precise beam with both small momentum and geometrical spread, and an accurate determination of the momenta of the reaction products. The use of a stochastically cooled beam [62, 234, 256, 257] and of internal cluster target facilities allows to realize these conditions. Very low target densities ( $\approx 10^{14}$  atoms  $\text{cm}^{-2}$ ) [240] minimize changes in the ejectiles' momentum vectors due to secondary scattering in the target, and simultaneously allow the beam to circulate through the target without significant intensity losses and changes of the momentum. An improvement of the experimental conditions caused by the stochastic cooling can be deduced already from a time dependence of the trigger frequency presented in figure 6.7.

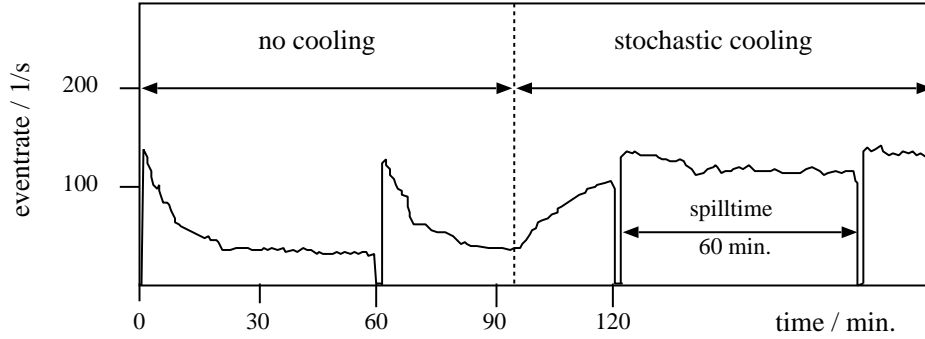


**Figure 6.7:** Rate of coincidences between the detectors S1 and S4 shown in figure 6.4b. In the middle of the second spill the cooling system was switched on.

This figure presents the rate of the coincidence between the scintillator detectors S4 and S1. The observed event rate is proportional to the number of reactions occurring in the region of the beam and target overlap. A steep decrease in the beginning of the first and second shown cycles is caused by the outward movement of the uncooled beam from the target center. Switching on the longitudinal and horizontal stochastic cooling, during the second cycle, clearly increases the luminosity and in the subsequent spills prevents the beam from spreading and shifting out of the target location. Consequently, a constant counting rate is obtained during the cycles with a cooled beam. In the following the beam monitoring technique introduced in the previous section will be applied to inspect in more details an influence of the stochastic cooling on the proton beam quality.

The horizontal stochastic cooling [62] is intended to squeeze the proton beam in the horizontal direction until the beam reaches the equilibrium between the cooling and the heating due to the target.

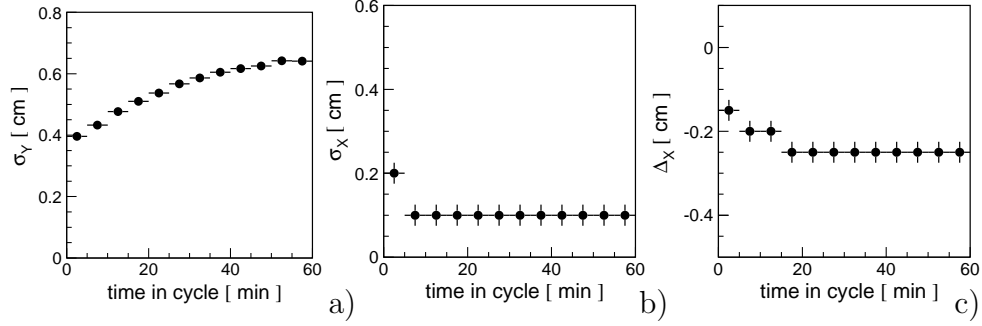


**Figure 6.8:** The vertical a) and horizontal b) beam width (one standard deviation) determined for each five minutes partition of the COSY cycle.

Please note that the beam width  $\sigma_x$  determined for each five minutes period is smaller than the  $\sigma_x$  averaged over the whole cycle (compare figure 6.6c). This is due to the beam shift relative to the target during the experimental cycle as shown in the panel c).

c) Relative settings of the COSY proton beam and the target centre versus the time of the measurement cycle.

The vertical error bars in pictures b) and c) denote the size of the step used in the Monte-Carlo simulations ( $\pm 0.025$  cm ; the bin width of figures 6.6b and 6.6c).

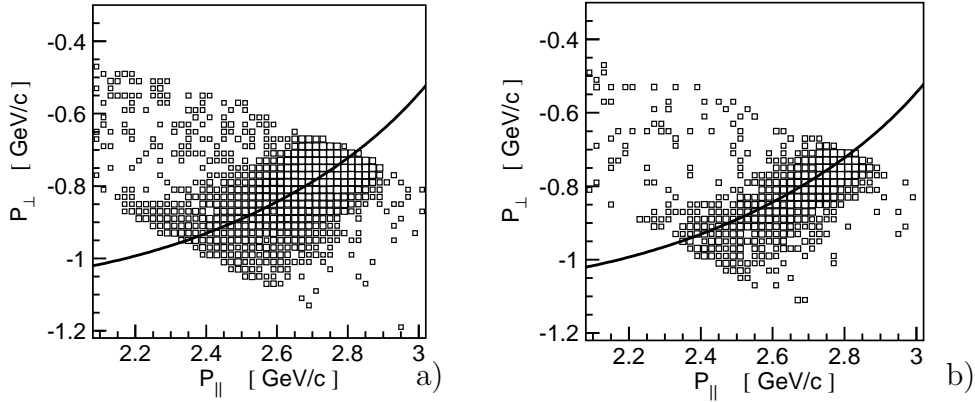


**Figure 6.9:** Perpendicular versus parallel momentum components with respect to the beam direction of particles registered at a beam momentum of 3.227 GeV/c, as measured during the first (a), and the last minute (b) of the 60 minutes long COSY cycle. The data at the first minute were analyzed with  $\Delta_x = -0.15$  cm, and the data of the 60's minute with  $\Delta_x = -0.25$  cm, see figure 6.8c. The number of entries per bin is shown logarithmically. The solid line corresponds to the momentum ellipse expected for protons scattered elastically at a beam momentum of 3.227 GeV/c.

In case of an uncooled beam its size would increase during the cycle as can be seen in figure 6.8a, which shows the spreading of the beam in the vertical plane during the 60 minutes cycle. This was expected since during the discussed experiment the stochastic cooling in the vertical plane was not used. The influence of the applied cooling in the horizontal plane is clearly visible in figure 6.8b. During the first five minutes of the cycle the horizontal size of the beam of about  $2 \cdot 10^{10}$  protons was reduced by a factor of 2 reaching the equilibrium conditions, and remaining constant for the rest of the COSY cycle. Figure 6.9 depicts the accuracy of the momentum reconstruction, reflected in the spreading of the data, which is mainly due to the finite horizontal size of the beam and target overlap. The left and right panel correspond to the first and the last minute of the measurement cycle, respectively. The data were analyzed correcting for the relative target and beam shifts  $\Delta_X$ . The movement of the beam relative to the target, during the cycle, is quantified in figure 6.8c. The shift of the beam denotes also changes of the average beam momentum, due to the nonzero dispersion at the target place. After some minutes the beam remains unchanged, this can be understood as reaching the equilibrium between the energy losses when crossing  $1.6 \cdot 10^6$  times per second through the  $H_2$  cluster target, and the power of the longitudinal stochastic cooling which cannot only diminish the spread of the beam momentum but also shifts it as a whole.

### 6.3 Detailed data analysis on the example of the $pp \rightarrow pp\eta$ reaction

*Precision and exactness are not intellectual values in themselves, and we should never try to be more precise or exact than is demanded by the problem in hand [249].*

Karl Raimund Popper

Significant part of the differential distributions of the cross sections used in this work was derived from a high statistics measurement of the  $pp \rightarrow pp\eta$  reaction at a nominal beam momentum of 2.027 GeV/c. The experiment performed at the COSY-11 facility was based on the four-momentum registration of both outgoing protons, whereas the  $\eta$  meson was identified via the missing mass technique. The method allows for the extraction of the kinematically complete information of the produced  $pp\eta$  system, provided that the reaction was identified. This is not feasible on the event-by-event basis due to the unavoidable physical background



originating from multi-pion production. However, with a large number of identified events the background subtraction can be performed separately for each interesting phase space interval. In practice, the size of the studied phase space partitions must be optimized between the statistical significance of the signal-to-background ratio and the experimental resolution.

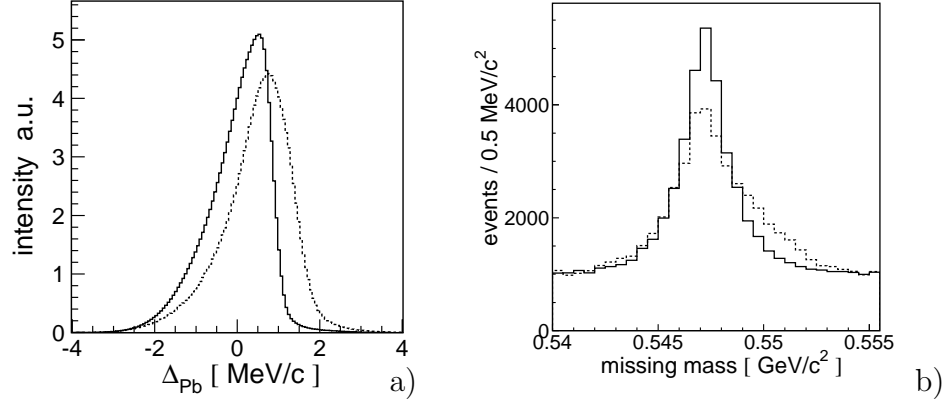


**Figure 6.10:** (a) The dashed curve denotes the proton beam momentum distribution integrated over the whole measurement period. On the horizontal scale, the value of zero is set at a nominal beam momentum equal to 2.027 GeV/c. The solid line shows the beam momentum distribution after the correction for the mean value which was determined in 10 second intervals. (b) Missing mass distribution for the  $pp \rightarrow ppX$  reaction determined by means of the COSY-11 detection system at a beam momentum of 2.027 GeV/c. The solid histogram presents the data corrected for effects of the time dependent relative shifts between the beam and the target using the method described in section 6.2. The dashed histogram shows the result before the correction.

The accuracy of the missing mass reconstruction depends on two parameters: the spread of the beam momentum as well as the precision of the measured momenta of the outgoing protons. The latter is predominantly due to the geometrical spread of the beam. Since for the reconstruction of the momenta we assume that the reaction takes place in the middle of the target we cannot correct on an event-by-event basis for the momentary spread of the beam. However, we can rectify the smearing due to the shifts of the centre of the beam relative to the target as well as the average changes of the absolute beam momentum during the experiment. Therefore, after the selection of events with two registered protons, as a first step of the more refined analysis the data were corrected for the mean beam momentum changes (see fig. 6.10a) determined from the measured Schottky frequency spectra and the known

beam optics. In a next step, from the distributions of the elastically scattered protons, the Schottky frequency spectrum, and the missing mass distribution of the  $pp \rightarrow ppX$  reaction, we have estimated that the spread of the beam momentum, and the spread of the reaction points in horizontal and vertical direction amount to  $\sigma(p_{beam}) = 0.63 \pm 0.03$  MeV/c,  $\sigma(x) = 0.22 \pm 0.02$  cm, and  $\sigma(y) = 0.38 \pm 0.04$  cm, respectively. Details of this procedure can be found in section 6.2.

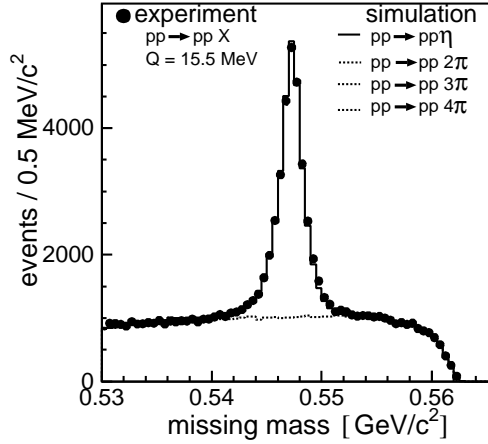


**Figure 6.11:** Missing mass spectrum for the  $pp \rightarrow ppX$  reaction determined in the experiment at a beam momentum of 2.0259 GeV/c. The mass resolution amounts to 1 MeV/c<sup>2</sup>( $\sigma$ ). The superimposed histograms present the simulation for  $1.5 \cdot 10^8$  events of the  $pp \rightarrow pp\eta$  reaction, and  $10^{10}$  events for the reactions  $pp \rightarrow pp2\pi$ ,  $pp \rightarrow pp3\pi$ , and  $pp \rightarrow pp4\pi$ . The simulated histograms were fitted to the data varying only the magnitude. The fit resulted in  $24009 \pm 210$  events for the production of the  $\eta$  meson.

Further on, a comparison of the experimentally determined momentum spectra of the elastically scattered protons with the distributions simulated with different beam and target conditions allows us to establish the position at which the centre of the beam crosses the target with an accuracy of 0.25 mm. Accounting for the movement of the beam relative to the target we improved the missing mass resolution as demonstrated in figure 6.10b.

After this betterment, the peak originating from the  $pp \rightarrow pp\eta$  reaction became more symmetric and the signal-to-background ratio increased significantly. The background was simulated taking into account  $pp \rightarrow ppX$  reactions with  $X = 2\pi$ ,  $3\pi$ , and  $4\pi$ . Since we consider here only the very edge of the phase space distribution where the protons are produced predominantly in the S-wave the shape of the background can be reproduced assuming that the homogeneous phase space distribution is modified only by the interaction between protons. Indeed, as can be observed in figure 6.11 the simulation describes the data very well. The calculated spectrum is hardly distinguishable from the experimental points. The position of the peak on the missing mass spectrum and the known mass of the  $\eta$  meson [43] enabled to determine the actual absolute beam

momentum to be  $p_{beam} = 2.0259 \text{ GeV}/c \pm 0.0013 \text{ GeV}/c$ , which agrees within error limits with the nominal value of  $p_{beam}^{nominal} = 2.027 \text{ GeV}/c$ . The real beam momentum corresponds to an excess energy of the  $pp\eta$  system equal to  $Q = 15.5 \pm 0.4 \text{ MeV}$ .

### 6.3.1 Covariance matrix and kinematical fitting

*Beobachtungen, welche sich auf Grössenbestimmungen aus der Sinnenwelt beziehen, werden immer, so sorgfältig man auch verfahren mag, grösseren oder kleineren Fehlern unterworfen bleiben [258].*

Carl Friedrich Gauss

As already mentioned in the previous section, at the COSY-11 facility the identification of the  $pp \rightarrow pp\eta$  reaction is based on the measurement of the momentum vectors of the outgoing protons and the utilisation of the missing mass technique. Inaccuracy of the momentum determination manifests itself in the population of kinematically forbidden regions of the phase space, preventing a precise comparison of the theoretically derived and experimentally determined differential cross sections.

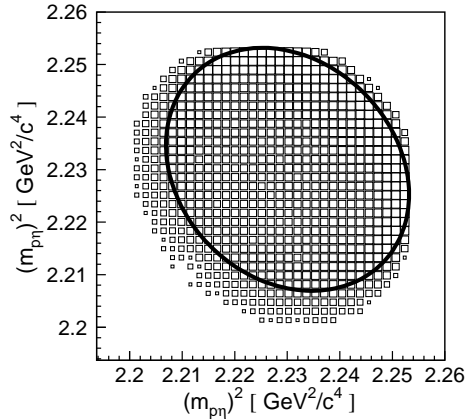


**Figure 6.12:** Dalitz plot distribution of the  $pp \rightarrow pp\eta$  reaction simulated at  $Q = 15.5 \text{ MeV}$ . The number of entries is shown in a logarithmic scale. The solid line gives the kinematically allowed area. The result was obtained taking into account the experimental conditions as described in the text.

Figure 6.12 visualizes this effect and clearly demonstrates that the data scatter significantly outside the kinematically allowed region (solid line), in spite of the fact that the precision of the fractional momentum determination in the laboratory system ( $\sigma(p_{lab})/p_{lab} \approx 7 \cdot 10^{-3}$ ) is quite high. Therefore, when seeking for small effects like for example the influence of the proton- $\eta$  interaction on the population density of the phase space, one needs either to fold the theoretical calculations with the experimental resolution, or to perform a kinematical fitting of the data. Both

procedures require the knowledge of the covariance matrix, and thus its determination constitutes a necessary step in the differential analysis and interpretation of the data.

In order to derive the covariance matrix we need to recognize and quantify all possible sources of errors in the reconstruction of the two proton momenta  $\vec{p}_1$  and  $\vec{p}_2$ . The four dominant effects are: i) finite distributions of the beam momentum and of the reaction points, ii) multiple scattering in the dipole chamber exit foil, air, and detectors, iii) finite resolution of the position determination of the drift chambers, and iv) a possible inadequate assignment of hits to the particle tracks in drift chambers in the case of very close tracks. Some of these, like the multiple scattering, depend on the outgoing protons' momenta, others, like the beam momentum distribution, depend on the specific run conditions and therefore must be determined for each run separately.

In order to estimate the variances and covariances for all possible combinations of the momentum components of two registered protons we have generated  $1.5 \cdot 10^8$   $pp \rightarrow pp\eta$  events and simulated the response of the COSY-11 detection setup taking into account the above listed factors and the known resolutions of the detector components. Next, we analysed the signals by means of the same reconstruction procedure as used in case of the experimental data. Covariances between the  $i^{th}$  and the  $j^{th}$  components of the event vector ( $P = [p_{1x}, p_{1y}, p_{1z}, p_{2x}, p_{2y}, p_{2z}]$ ) were established as the average of the product of the deviations between the reconstructed and generated values. The explicit formula for the sample of  $N$  reconstructed events reads:

$$cov(i, j) = \frac{1}{N} \sum_{k=1}^N (P_{i,gen}^k - P_{i,recon}^k)(P_{j,gen}^k - P_{j,recon}^k),$$

where  $P_{i,gen}^k$  and  $P_{i,recon}^k$  denote the generated and reconstructed values for the  $i^{th}$  component of the vector  $P$  describing the  $k^{th}$  event.

Because of the inherent symmetries of the covariance matrix ( $cov(i, j) = cov(j, i)$ ) and the indistinguishability of the registered protons<sup>2</sup> there are only 12 independent values which determine the 6 x 6 error matrix  $V$  unambiguously.

Since inaccuracies of the momentum determination depend on the particle momentum itself (eg. multiple scattering) and on the relative momentum between protons (eg. trajectories reconstruction from signals in drift chambers), we have determined the covariance matrix as a

---

<sup>2</sup> The symmetry of all observables under the exchange of the two protons ( $\vec{p}_1 \leftrightarrow \vec{p}_2$ ) implies that  $cov(i, j) = cov(i \pm 3, j \pm 3)$ , where the '+' has to be taken for  $i, j = 1, 2, 3$  and the '-' for  $i, j = 4, 5, 6$ . Thus for example  $cov(2, 4) = cov(5, 1)$ .

function of the absolute momentum of both protons:  $cov(i, j, |\vec{p}_1|, |\vec{p}_2|)$ . As an example we present the covariance matrix for the mean values of  $|\vec{p}_1|$  and  $|\vec{p}_2|$  in units of  $\text{MeV}^2/c^2$ , as established in the laboratory system with the  $z$ -coordinate parallel to the beam axis and  $y$ -coordinate corresponding to the vertical direction.

$$V = \begin{array}{ccccc} & p_{1x} & p_{1y} & p_{1z} & p_{2x} & p_{2y} & p_{2z} \\ \begin{bmatrix} 5.6 & 0.0 & -13.7 & 1.7 & 0.1 & -3.0 \\ - & 7.1 & 0.1 & - & -0.2 & -0.2 \\ - & - & 37.0 & - & - & 5.4 \\ - & - & - & - & - & - \\ - & - & - & - & - & - \\ - & - & - & - & - & - \end{bmatrix} & p_{1x} \\ & p_{1y} \\ & p_{1z} \\ & p_{2x} \\ & p_{2y} \\ & p_{2z} \end{array} \quad (6.3)$$

Since the measurements have been performed close to the kinematical threshold the ejectile momentum component parallel to the beam is by far the largest one and its variance ( $var(p_z) = 37 \text{ MeV}^2/c^2$ ) determines in first order the error of the momentum measurement. The second largest contribution stems from an anti-correlation between the  $x$ - and  $z$ - momentum components ( $cov(p_x, p_z) = -13.7 \text{ MeV}^2/c^2$ ), which is due to the bending of the proton trajectory – mainly in the horizontal direction – inside the COSY-11 dipole magnet (see fig. 6.1). There is also a significant correlation between the  $z$  components of different protons which is due to the smearing of the reaction points, namely, if in the analysis the assumed reaction point differs from the actual one, a mistake made in the reconstruction affects both protons similarly.

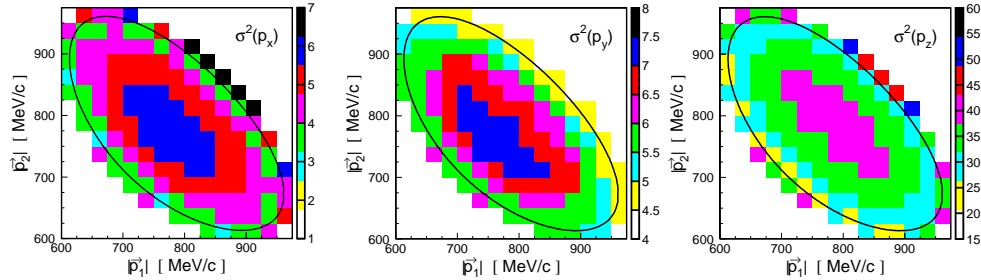


**Figure 6.13:** Variances of the protons's momentum components  $\sigma^2(p_x)$ ,  $\sigma^2(p_z)$ , and  $\sigma^2(p_y)$  shown as a function of the absolute values of the measured momenta.

Figure 6.13 depicts the variation of  $var(p_x)$ ,  $var(p_y)$ , and  $var(p_z)$  over the momentum plane ( $|\vec{p}_1|$ ,  $|\vec{p}_2|$ ). Taking into account components of the covariance matrices  $V(|\vec{p}_1|, |\vec{p}_2|)$  and the distribution of the proton momenta for the  $pp \rightarrow pp\eta$  reaction at  $Q = 15.5 \text{ MeV}$  results in an average

error for the measurement of the proton momentum of about 6 MeV/c. This can be also deduced from the distribution of the difference between the generated and reconstructed absolute momenta of the protons. The corresponding spectrum is plotted as a dashed line in figure 6.14.

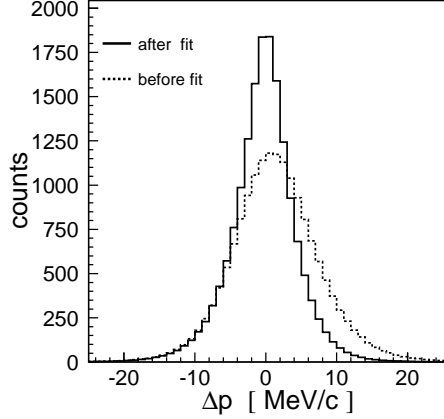


**Figure 6.14:** Spectrum of differences between generated and – after simulation of the detector response – reconstructed absolute momenta of protons, as determined before (dashed line) and after the kinematical fit (solid line). The picture shows results obtained taking into account the experimental conditions as described in the text.

In the experiment we have measured 6 variables and once we assumed that the event corresponds to the  $pp \rightarrow pp\eta$  reaction only 5 of them are independent. Thus we have varied the values of the event components demanding that the missing mass is equal to the mass of the  $\eta$  meson and we have chosen that vector which was the closest to the experimental one in the sense of the Mahalanobis distance. The inverse of the covariance matrix was used as a metric for the distance calculation. The kinematical fit improves the resolution by a factor of about 1.5 as can be concluded from comparing the dashed and solid lines in figure 6.14. The finally resulting error of the momentum determination amounts to 4 MeV/c.

### 6.3.2 Multidimensional acceptance corrections

*Unfehlbar hätte ich umkommen müssen, wenn ich mich nicht mit der Stärke meiner Arme an meinem eigenen Haarzopf samt meinem Pferd, das ich fest zwischen meine Knie schloß, wieder herausgezogen hätte [259].*

Baron Münchhausen

At the excess energy of  $Q = 15.5$  MeV the COSY-11 detection system does not cover the full  $4\pi$  solid angle in the centre-of-mass system of the  $pp \rightarrow pp\eta$  reaction. Therefore, the detailed study of differential cross sections requires corrections for the acceptance. Generally, the acceptance

should be expressed as a function of the full set of mutually orthogonal variables which describe the studied reaction unambiguously. As introduced in section 3.4, to define the relative movement of the particles in the reaction plane we have chosen two squares of the invariant masses:  $s_{pp}$  and  $s_{p\eta}$ , and to define the orientation of this plane in the center-of-mass frame we have taken the three Euler angles: The first two are simply the polar  $\phi_\eta^*$  and azimuthal  $\theta_\eta^*$  angles of the momentum of the  $\eta$  meson and the third angle  $\psi$  describes the rotation of the reaction plane around the axis defined by the momentum vector of the  $\eta$  meson.

In the data evaluation we considerably benefit from the basic geometrical symmetries satisfied by the  $pp \rightarrow pp\eta$  reaction. Due to the axial symmetry of the initial channel of the two unpolarized colliding protons the event distribution over  $\phi_\eta^*$  must be isotropic. Thus, we can safely integrate over  $\phi_\eta^*$ , ignoring that variable in the analysis. Furthermore, taking advantage of the symmetry due to the two identical particles in the initial channel, without losing the generality, we can express the acceptance as a function of  $s_{pp}, s_{p\eta}, |\cos(\theta_\eta^*)|$ , and  $\psi$ . To facilitate the calculations we have divided the range of  $|\cos(\theta_\eta^*)|$  and  $\psi$  into 10 bins and both  $s_{pp}$  and  $s_{p\eta}$  into 40 bins each. In the case of  $s_{pp}$  and  $s_{p\eta}$  the choice was made such that the width of the interval corresponds to the standard deviation of the experimental accuracy. For  $|\cos(\theta_\eta^*)|$  and  $\psi$  we have taken only ten partitions since from the previous experiments we expect only a small variation of the cross section over these variables [83, 95, 96]. In this representation, however, the COSY-11 detection system covers only 50% of the phase space for the  $pp \rightarrow pp\eta$  reaction at  $Q = 15.5$  MeV. To proceed with the analysis we assumed that the distribution over the angle  $\psi$  is isotropic as it was for example experimentally determined for the  $pp \rightarrow pp\omega$ ,  $pp \rightarrow ppp$ , or  $pp \rightarrow pp\phi$  reactions [83, 89]. Please note that this is the only assumption of the reaction dynamics performed in the present evaluation. The validity of this supposition in the case of the  $pp \rightarrow pp\eta$  reaction will be discussed later.

In the calculations we exploit also the symmetry of the cross sections under the exchange of the two identical particles in the final state which reads:  $\sigma(s_{p_1\eta}, \psi) = \sigma(s_{p_2\eta}, \psi + \pi)$ . The resultant acceptance is shown in figure 6.15. One recognizes that only a small part (3%) of the phase space is not covered by the detection system. In further calculations these holes were corrected according to the assumption of a homogeneous phase space distribution. Additionally it was checked that the corrections under other suppositions e.g. regarding also the proton-proton FSI lead to negligible differences.

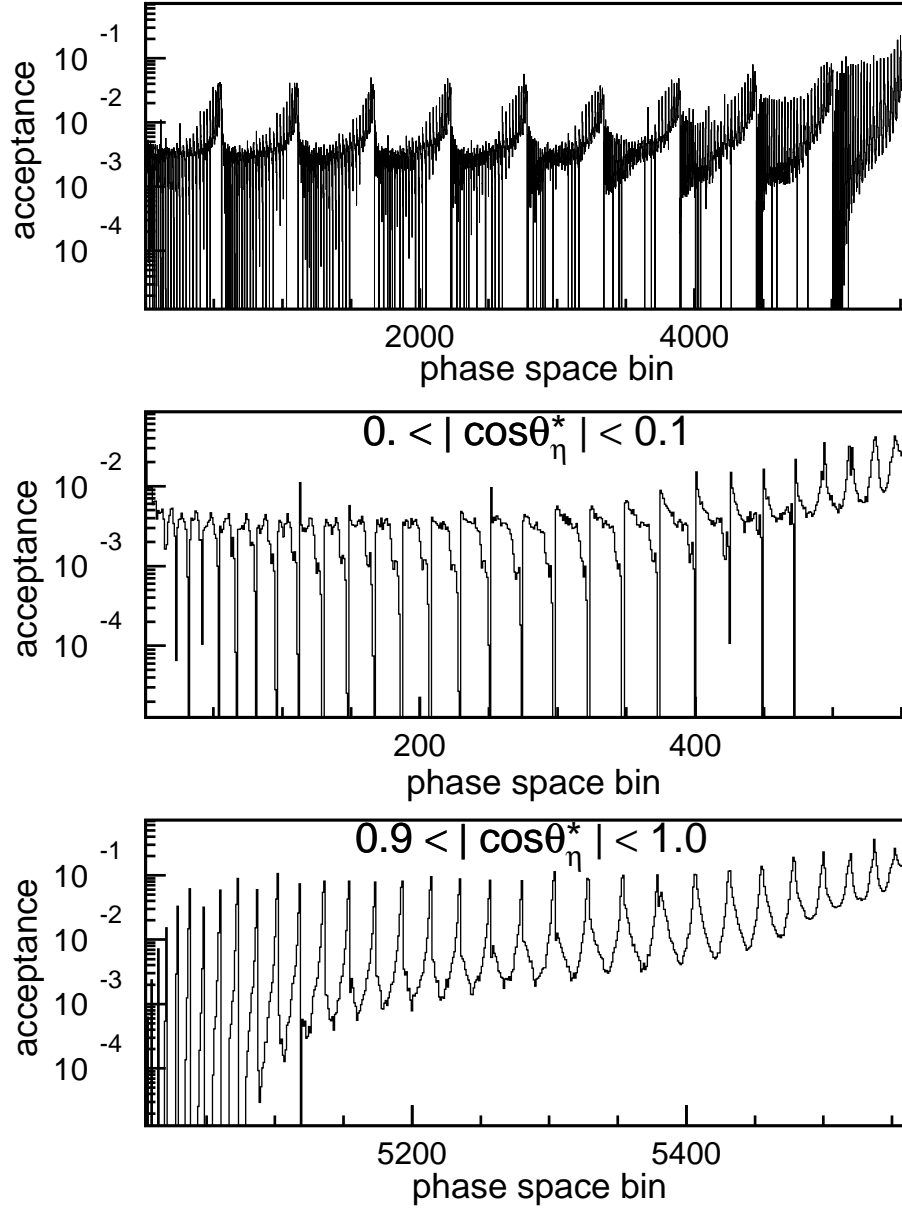


**Figure 6.15:** Acceptance of the COSY-11 detection system for the  $pp \rightarrow pp\eta$  reaction at an excess energy of  $Q = 15.5$  MeV presented as a function of  $s_{pp}, s_{p\eta}$ , and  $|\cos(\theta_{\eta}^*)|$ . The numbers were assigned to the bins in the three dimensional space  $s_{pp} - s_{p\eta} - |\cos(\theta_{\eta}^*)|$  by first incrementing the index of  $s_{pp}$  next of  $s_{p\eta}$  and in the end that of  $|\cos(\theta_{\eta}^*)|$ . Partitioning of  $|\cos(\theta_{\eta}^*)|$  into ten bins is easily recognizable. The two lower pictures show the acceptance for the first and the last bin of  $|\cos(\theta_{\eta}^*)|$ .



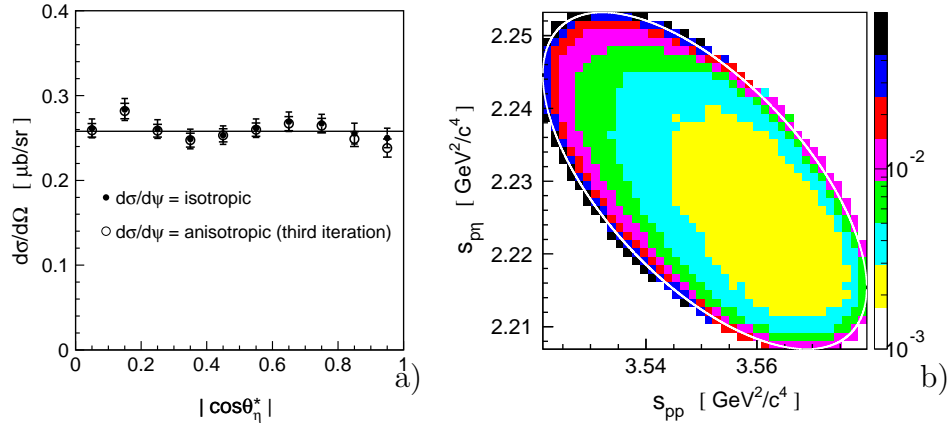


**Figure 6.16:** (a) Distribution of the polar angle of the emission of the  $\eta$  meson in the centre-of-mass system. Experimental data were corrected for the acceptance in the three dimensional space ( $s_{pp}$ ,  $s_{p\eta}$ ,  $|\cos(\theta_\eta^*)|$ ). Full circles show the result with the assumption that the distribution of the  $\psi$  angle is isotropic, and the open circles are extracted under the assumption that  $\frac{d\sigma}{d\psi}$  is as derived from the data (see text). Both results have been normalized to each other in magnitude.

(b) COSY-11 detection acceptance as a function of  $s_{pp}$  and  $s_{p\eta}$ , calculated under the assumption that the differential cross sections  $\frac{d\sigma}{d\cos(\theta_\eta^*)}$  and  $\frac{d\sigma}{d\psi}$  are isotropic.

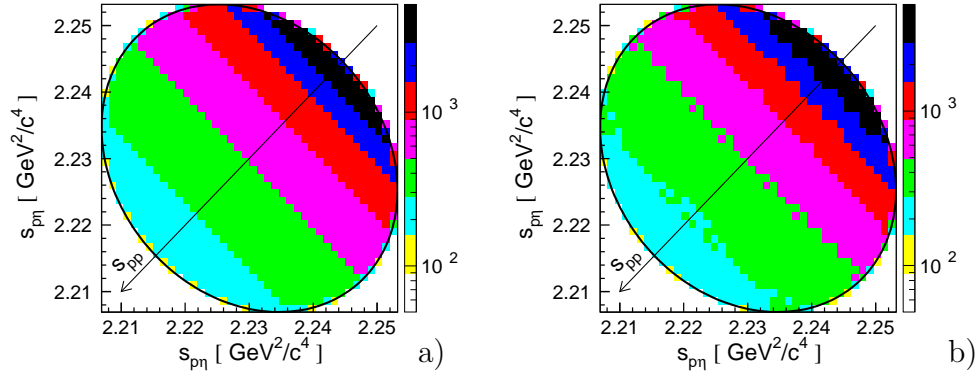


**Figure 6.17:** (a) Dalitz plot distribution simulated for the  $pp \rightarrow pp\eta$  reaction at  $Q = 15.5$  MeV. In the calculations the interaction between protons was taken into account. (b) Dalitz plot distribution reconstructed from the response of the COSY-11 detectors simulated for events from figure (a) taking into account the smearing of beam and target, multiple scattering in the materials, and the detectors' resolution. The evaluation included momentum reconstruction, kinematical fitting, and the acceptance correction exactly in the same way as performed for the experimental data. The lines surrounding the Dalitz plots depict the kinematical limits.

Full points in figure 6.16a present the distribution of the polar angle of the  $\eta$  meson as derived from the data after the acceptance correction.

Within the statistical accuracy it is isotropic. Taking into account this angular distribution of the cross section we can calculate the acceptance as a function of  $s_{pp}$  and  $s_{p\eta}$  only. This is shown in figure 6.16b, where one sees that now the full phase space is covered. This allows us to determine the distributions of  $s_{pp}$  and  $s_{p\eta}$ . The correctness of the performed procedures for the simulation of the detectors response, the event reconstruction programs, the kinematical fitting, and acceptance correction can be confirmed by comparing the distribution generated (figure 6.17a) with the ones which underwent the complete analysis chain described in this section (figure 6.17b).

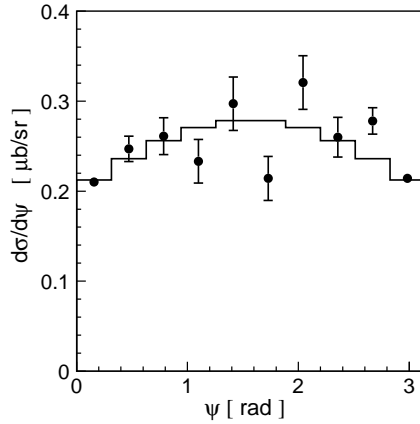


**Figure 6.18:** Distribution of the cross section as a function of the angle  $\psi$  as determined in the first iteration. The superimposed histogram corresponds to the fit of the function  $\frac{d\sigma}{d\psi} = a + b \cdot |\sin(\psi)|$ . The range of the  $\psi$  angle is shown from 0 to  $\pi$  only, since in the analysis we take advantage of the symmetry  $\frac{d\sigma}{d\psi}(\psi) = \frac{d\sigma}{d\psi}(\psi + \pi)$ .

Knowing the distribution of the polar angle of the  $\eta$  meson  $\theta_\eta^*$  and those for the invariant masses  $s_{pp}$  and  $s_{p\eta}$  we can check whether the assumption of the isotropy of the cross section distribution versus the third Euler's angle  $\psi$  is corroborated by the data. For that purpose we calculated the acceptance as a function of  $\psi$  and  $s_{p\eta}$  assuming the shape of the differential cross sections of  $\frac{d\sigma}{ds_{pp}}$  and  $\frac{d\sigma}{d\cos(\theta_\eta^*)}$  as determined experimentally. The obtained  $\frac{d\sigma}{d\psi}$  distribution is shown in figure 6.18 and is not isotropic as assumed at the beginning. A fit of the function of the form  $\frac{d\sigma}{d\psi} = a + b \cdot |\sin(\psi)|$  gives the value of  $b = 0.079 \pm 0.014 \mu\text{b}/\text{sr}$ , indeed significantly different from the isotropic solution. This deviation cannot be assigned to any unknown behaviour of the background since the obtained distribution can be regarded as background free. This is because the number of  $pp \rightarrow pp\eta$  events was elaborated for each invariant mass interval separately. The exemplarily missing mass spectra for the first, fourth, seventh, and tenth interval of  $\psi$  values, corrected for the acceptance, are presented in figure 6.19. From this figure one can infer

that the shape of the background is well reproduced not only for the overall missing mass spectrum as shown previously in figure 6.11 but also locally in each region of the phase space. Since the experimental data are quite well described by the simulations one can rather exclude the possibility of a significant systematic error which could cause the observed anisotropy of the differential cross section  $\frac{d\sigma}{d\psi}$ .

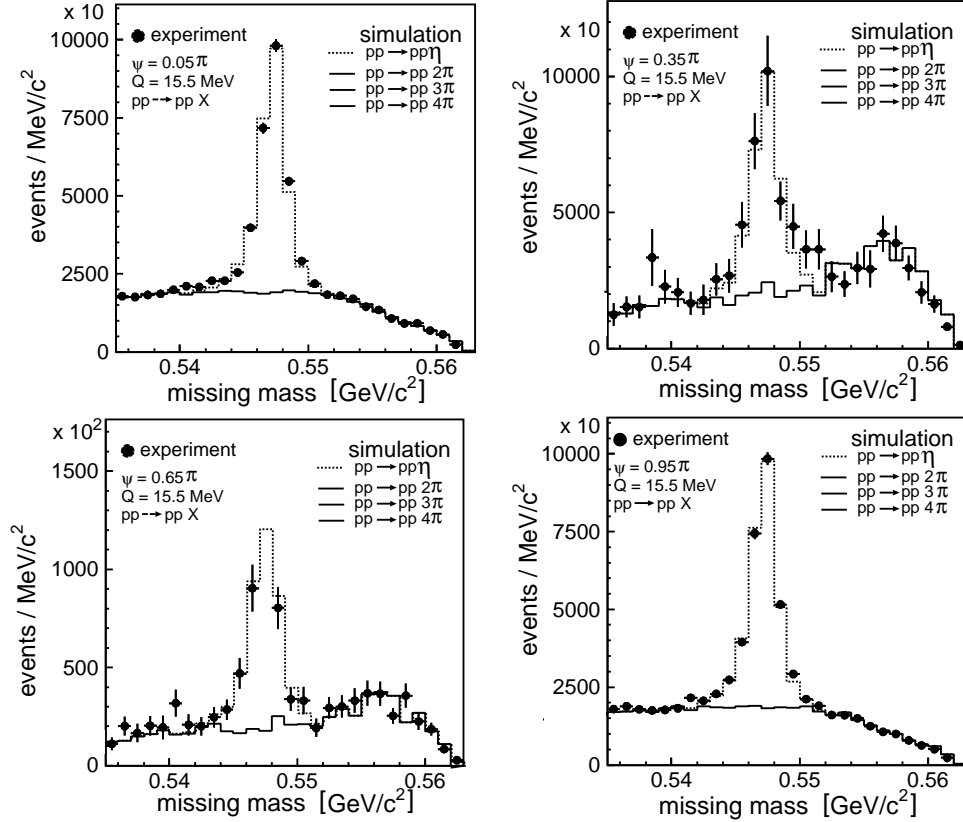


**Figure 6.19:** Missing mass distributions for the first, fourth, seventh, and tenth bin of  $\psi$  with the superimposed lines from the simulation of  $pp \rightarrow pp\eta$  and the multi-pion background  $pp \rightarrow pp(m\pi)$  reactions. Amplitudes of simulated distributions were fitted to the experimental points.

The evaluated distribution is however in disagreement with the working assumption that  $\sigma(\psi)$  is isotropic. Therefore we performed a full acceptance correction procedure from the very beginning assuming that the distribution of  $\frac{d\sigma}{d\psi}$  is as determined from the data. After repeating the procedure three times we observed that the input and resultant distributions are in good agreement. The result after the third iteration is

shown in figure 6.20 by the full circles. It is only slightly different from the one obtained after the first iteration as shown in figure 6.18.

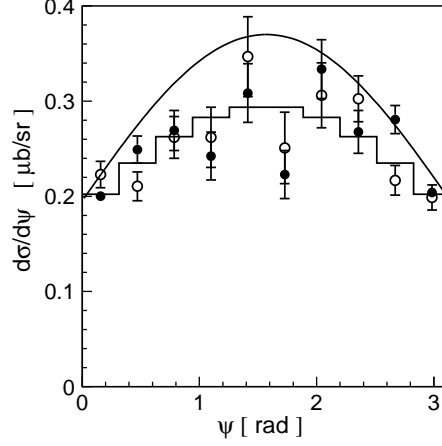


**Figure 6.20:** Distribution of the cross section as a function of the angle  $\psi$ . Full circles stand for the final results of the  $\frac{d\sigma}{d\psi}$  obtained after three iterations. The superimposed histogram (solid line) corresponds to the fit of the function  $\frac{d\sigma}{d\psi} = a + b \cdot |\sin(\psi)|$  which resulted in  $a = 0.186 \pm 0.004 \mu b/sr$  and  $b = 0.110 \pm 0.014 \mu b/sr$ . The dashed line shows the entry distribution used for the second series of iterations as described in the text. Open circles represent the data from the left upper corner of the Dalitz plot (see for example figure 6.16b). At that region of the Dalitz plot due to the non-zero four dimensional acceptance over  $(s_{pp}, s_{p\eta}, |\cos(\theta_\eta^*)|, \psi)$  bins the spectrum (open circles) was corrected without a necessity of any assumptions concerning the reaction cross section.

To raise the confidence of the convergence of the performed iteration we accomplished the full procedure once more, but now assuming that the distribution of  $\frac{d\sigma}{d\psi}$  is much more anisotropic than determined from the data. As an entry distribution we took the dashed line shown in figure 6.20. Again after two iterations we have got the same result as before. To corroborate this observation we have evaluated the distribution over the  $\psi$  angle (see figure 6.20) from the phase space region which has no holes in the acceptance expressed as a four-dimensional function of the variables  $s_{pp}$ ,  $s_{p\eta}$ ,  $|\cos(\theta_\eta^*)|$ , and  $\psi$ , this is for the values of  $s_{pp}$  and  $s_{p\eta}$  corresponding to the upper left corner of figure 6.16b. Again the obtained distribution presented as open circles in figure 6.20 is anisotropic, and moreover agrees with the spectrum determined from all events. It is important to note that the shape of the  $s_{pp}$ ,  $s_{p\eta}$ , and  $\cos(\theta_\eta^*)$  distributions keeps unchanged during the whole iteration procedure. Figure 6.21 shows the distributions of the square of the proton-proton and proton- $\eta$  invariant masses. The spectra after the second and third iterations are shown. One recognizes that the form of the spectra remains unaltered. The same

conclusion can be drawn for the  $\frac{d\sigma}{d|\cos(\theta_\eta^*)|}$  distribution as demonstrated in figure 6.16a.

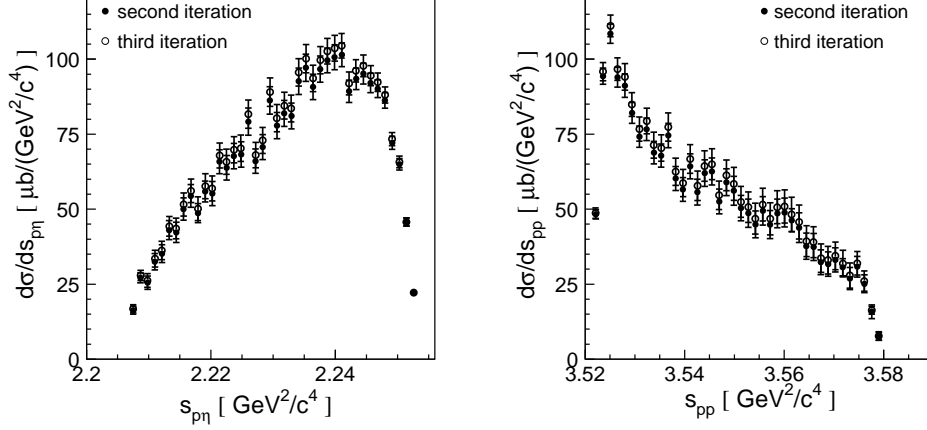


**Figure 6.21:** Distributions of the invariant masses  $s_{pp}$  and  $s_{p\eta}$  determined for the two different assumptions about the cross section dependence of the  $\psi$  angle.

From that comparison one can conclude that the shapes of the determined distributions are – within the statistical accuracy – independent of the shape of the  $\frac{d\sigma}{d\psi}$  cross section and can be treated as derived in a completely model independent manner. Similarly, as in the case of the  $\frac{d\sigma}{d\psi}$  distribution, the differential cross sections in all other variables reported in this article are not deteriorated by the background. This is because the number of  $pp \rightarrow pp\eta$  events was determined for each investigated phase space interval separately.

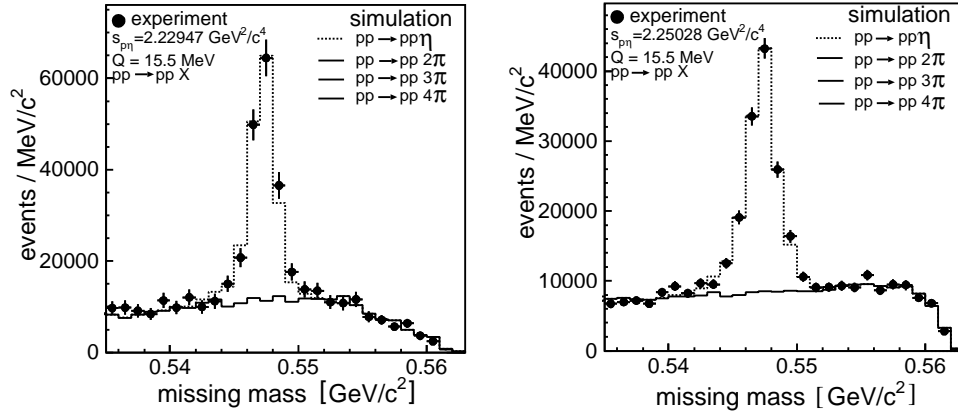


**Figure 6.22:** Missing mass distributions determined for the invariant mass bins as depicted inside the figures. The spectra were corrected for the acceptance. The histograms show the simulations for the multi-pion background  $pp \rightarrow pp(m\pi)$  and the  $pp \rightarrow pp\eta$  reactions fitted to the data with the amplitudes as the only free parameters.

As an example the missing mass spectra for two bins of the proton- $\eta$  invariant mass are presented in figure 6.22. As already noticed for  $\frac{d\sigma}{d\psi}$  the shape of the background is well reproduced locally in each region of the phase space.

### 6.3.3 Angular distributions

*Before we declare our consent we must carefully examine  
the shape of the architecture the rhythm of the drums and pipes  
... [260].* Zbigniew Herbert

In previous subsections we derived the distributions of the cross section in the invariant masses  $s_{pp}$  and  $s_{p\eta}$  (figure 6.21), and in angle  $\psi$  (figure 6.20). For the sake of completeness we will also present the distribution in the  $\cos(\theta_\eta^*)$ ,  $\cos(\theta_N^*)$ , and  $\psi_N$ . This will allow us to have insight into distributions in all nontrivial variables describing the  $pp\eta$  system in the case when the polarization of nucleons is ignored. Here, as introduced in section 3.4 we consider two different sets of orthogonal variables, namely  $(s_{pp}, s_{p\eta}, |\cos(\theta_\eta^*)|, \psi)$  and  $(s_{pp}, s_{p\eta}, |\cos(\theta_N^*)|, \psi_N)$ . If possible the data will be compared to the results of measurements performed at the non-magnetic spectrometer COSY-TOF [95].

In the previous subsection we have shown that even close-to-threshold at  $Q = 15.5$  MeV the production of the  $pp\eta$  system is not fully isotropic. In particular, we found that the cosine of angle  $\psi$  is not uniformly populated. The anisotropy of the cross section reflects itself in an anisotropy of the orientation of the emission plane, and the latter has a simple physical interpretation.

The determined cross section distribution in function of the polar angle  $\theta_N^*$  of the vector normal to that plane is shown in figure 6.23a. The distribution is not isotropic, which is particularly visible for the low values of  $|\cos(\theta_N^*)|$  burdened with small errors. As depicted in figure 3.3 the  $|\cos(\theta_N^*)| = 0$  denotes such configurations of the ejectiles momenta in which the emission plane comprises the beam axis. In that case the acceptance of the COSY-11 detection system is much larger than for the configuration where the emission plane is perpendicular to the beam. Due to this reason the error bars in figure 6.23a increase with growth of  $|\cos(\theta_N^*)|$ . It is worth to stress that the tendency of the  $pp\eta$  system to be produced preferentially if the emission plane is perpendicular to the beam is in line with the preliminary analysis of the experiment performed by the TOF collaboration [261]. Elucidation of that non-trivial behaviour can reveal interesting features of the dynamics of the production process.

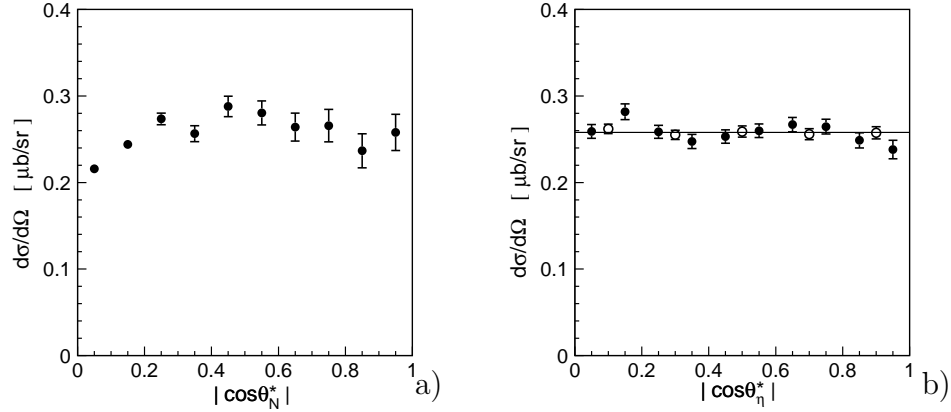


**Figure 6.23:** (a) Differential cross section as a function of the polar angle of the vector normal to the emission plane. (b) Differential cross section of the  $pp \rightarrow pp\eta$  reaction as a function of the  $\eta$  meson centre-of-mass polar angle. Full circles depict experimental results for the  $pp \rightarrow pp\eta$  reaction measured at  $Q = 15.5$  MeV by the COSY-11 collaboration (this article) and the open circles were determined by the TOF collaboration at  $Q = 15$  MeV [95]. The TOF points were normalized in amplitude to our result, since for that data the absolute scale is not evaluated.

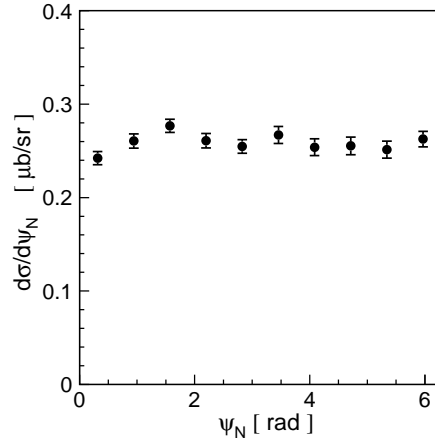


**Figure 6.24:** Differential cross section in  $\psi_N$  for the  $pp \rightarrow pp\eta$  reaction measured at  $Q = 15.5$  MeV. The variable  $\psi_N$  is defined in section 3.4.

The distribution of the polar angle of the  $\eta$  meson emission in the centre-of-mass system is shown in figure 6.23b. Clearly, the COSY-11 data agree very well with the angular dependence determined by the TOF collaboration. As already mentioned, the two identical particles in the initial state of the  $pp \rightarrow pp\eta$  reaction imply that the angular distribution of either ejectile must be symmetric around 90 degree in the centre-of-mass frame. Here we use that reaction characteristic, yet in figure 4.3a (see also reference [18]) we presented the differential cross section of the  $\eta$  meson centre-of-mass polar angle for the full range of  $\cos(\theta_\eta^*)$  and found that this is completely symmetric around  $\cos(\theta_\eta^*) = 0$ .

These observations can be regarded as a check of the correctness of the acceptance calculation. The cross section distribution in the angle  $\psi_N$  – defining the orientation of the  $pp\eta$  system within the emission plane – is shown in figure 6.24.

Up to now we presented invariant mass spectra of the proton-proton and proton- $\eta$  systems and angular distribution for two sets of non-trivial angles which describe the orientation of ejectiles within the emission plane and the alignment of the plane itself, namely  $(\cos(\theta_\eta^*), \psi)$  and  $(\cos(\theta_N^*), \psi_N)$ . However, since one of the important issues discussed in this work is the contribution from higher partial waves we evaluated also an angular distribution of the relative momentum of two protons seen from the proton-proton centre-of-mass subsystem (see figure 6.25a). The distribution of that angle should deliver information about the partial waves of the proton-proton system in the exit channel (see section 3.2).

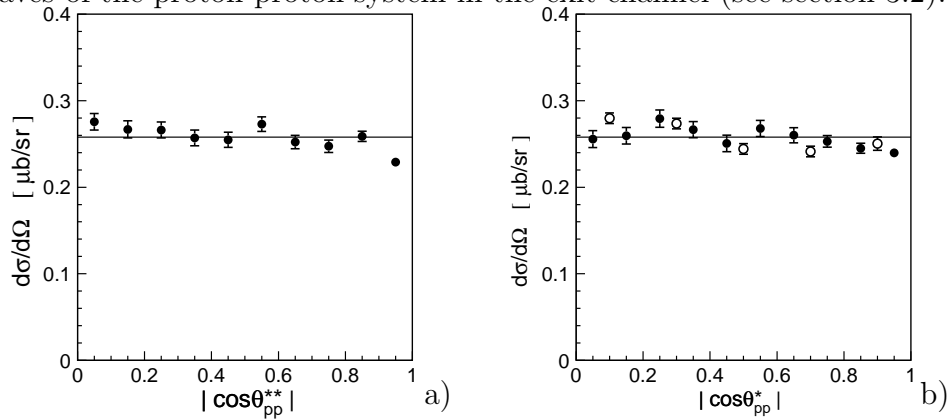


**Figure 6.25:** (a) Differential cross section in  $\theta_{pp}^*$  as determined for the  $pp \rightarrow pp\eta$  reaction at  $Q = 15.5$  MeV.

(b) Distribution of the centre-of-mass polar angle of the relative protons momentum with respect to the beam direction determined for the  $pp \rightarrow pp\eta$  reaction at  $Q = 15.5$  MeV. The COSY-11 result (closed circles) is compared to the data points determined at  $Q = 15$  MeV by the TOF collaboration (open circles) [95].

Figure 6.25b presents the differential cross section as a function of angle  $\theta_{pp}^*$  of the relative proton momentum seen from the overall centre-of-mass frame, as this is often considered in the theoretical works. This figure compares COSY-11 results to the angular distribution extracted by the TOF collaboration. Both experiments agree very well within the statistical accuracy, and both indicate a slight decrease of the cross section with increasing  $|\cos(\theta_{pp}^*)|$ .



## 6.4 Usage of the spectator model for the study of the $\eta$ and $\eta'$ mesons via the proton-neutron interaction

*As regards any subject we propose to investigate, we must inquire not what other people have thought, or what we ourselves conjecture, but what we can clearly and manifestly perceive by intuition or deduce with certainties. For there is no other way of acquiring knowledge [207].*

René Descartes

In order to measure the  $pn \rightarrow pn \text{ Meson}$  reactions by means of the proton beam it is necessary to use a nuclear target, since a pure neutron target does not exist. Naturally, least complications in the interpretation of the experiment will be encountered when using the simplest nuclei. Therefore, here deuterons will be considered as a source of neutrons, and for the evaluation of the data an impulse approximation will be exploited. The main conjecture of this approach is that the bombarding proton interacts exclusively with one nucleon in the target nucleus and that the other nucleons affect the reaction by providing a momentum distribution to the struck constituent only (fig. 6.26). This assumption is justified if the kinetic energy of a projectile is large compared to the binding energy of the hit nucleus. In fact, as noticed by Slobodrian [262], also the scattering of protons on a hydrogen target, where the protons are bound by molecular forces, may serve as an extreme example of the quasi-free reaction. In that case, although the hydrogen atoms rotate or vibrate in the molecule, their velocities and binding forces are totally negligible with respect to the velocity and nuclear forces operating the scattering of the relativistic proton [262].

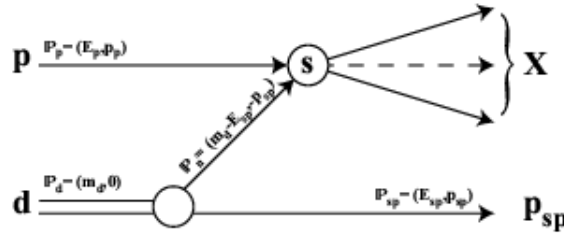


**Figure 6.26:** Spectator model for a particle production reaction via  $pd \rightarrow p_{sp}X$ .

The deuteron is also relatively weakly bound with a binding energy of  $E_B \approx 2.2 \text{ MeV}$ , which is by far smaller – more than two orders of magni-

tude in the case of pion and already more than three orders of magnitude in the case of  $\phi$  meson – than the kinetic energy of the bombarding protons needed for the creation of mesons in the proton-neutron interaction. However, it has to be considered that even the low binding energy of  $E_B \approx 2.2$  MeV results in large Fermi momenta of the nucleons which can not be neglected. The momentum and kinetic energy distributions of the nucleons in the deuteron are shown in figure 6.27. In the considered approximation the internucleon force manifests itself only as the Fermi motion of the nucleons and hence the struck neutron is treated as a free particle in the sense that the matrix element for quasi-free meson production off a bound neutron is identical to that for the free  $pn \rightarrow pn$  Meson reaction. The reaction may be symbolically presented as:

$$p \begin{pmatrix} n \\ p \end{pmatrix} \longrightarrow \begin{matrix} p \text{ } n \text{ Meson} \\ p_{sp} \end{matrix} \quad (6.4)$$

where  $p_{sp}$  denotes the proton from the deuteron regarded as a spectator which does not interact with the bombarding particle, but rather escapes untouched and hits the detectors carrying the Fermi momentum possessed at the moment of the collision.

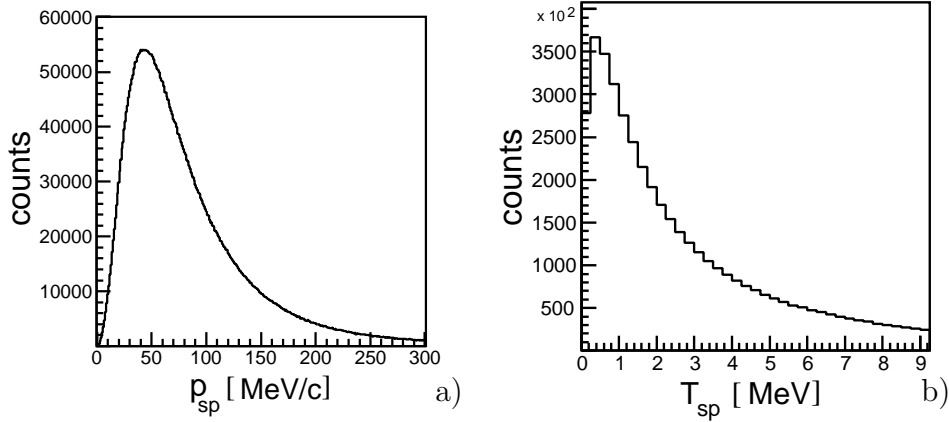


**Figure 6.27:** (a) Momentum and (b) kinetic energy distribution of the nucleons in the deuteron, generated according to an analytical parametrization of the deuteron wave function [263, 264] calculated from the Paris potential [136].

From the measurement of the momentum vector of the spectator proton  $\vec{p}_{sp}$  one can infer the momentum vector of the neutron  $\vec{p}_n = -\vec{p}_{sp}$  and hence calculate the excess energy  $Q$  for each event, provided that the beam momentum is known. As an example, a distribution of the excess energy in the quasi-free  $pn \rightarrow pn\eta'$  reaction is presented in figure 6.28a [20]. Due to the large centre-of-mass velocity ( $\beta \approx 0.75$ ) with

respect to the colliding nucleons, a few MeV wide spectrum of the neutron kinetic energy inside a deuteron (fig. 6.27b) is broadened by more than a factor of thirty.

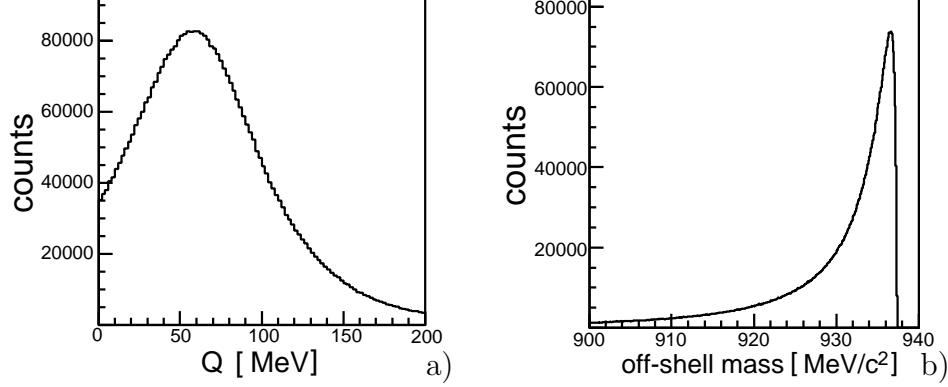


**Figure 6.28:** (a) Distribution of the excess energy  $Q$  for the  $pn\eta'$  system originating from the reaction  $pd \rightarrow p_{sp}pn\eta'$  calculated with a proton beam momentum of 3.350 GeV/c and the neutron momentum smeared out according to the Fermi distribution shown in figure 6.27a. (b) Spectrum of the off-shell mass of the interacting neutron, as calculated under the assumption of the impulse approximation.

Therefore, especially in the case of near-threshold measurements, where the cross section grows rapidly with increasing excess energy (see e.g. fig. 4.6), the total centre-of-mass energy  $\sqrt{s}$  has to be determined on an event-by-event level. For this purpose, the spectator protons are usually registered by means of silicon pad- or  $\mu$ -strip detectors [20, 158, 265] which allow to determine their kinetic energy ( $T_{sp}$ ) and polar emission angle ( $\theta$ ). Thus, it is useful to express the total energy squared  $s$  as function of these variables:

$$s = |\mathbb{P}_p + \mathbb{P}_n|^2 = s_0 - 2 T_{sp} (m_d + E_p) + 2 p_p \sqrt{T_{sp}^2 + 2m_p T_{sp}} \cos(\theta) \quad (6.5)$$

with  $s_0$  denoting the squared centre-of-mass energy, assuming a vanishing Fermi motion. Measuring both the energy and the emission angle of the spectator protons it is possible to study the energy dependence of a meson production cross section from data taken at only one fixed beam momentum.

It must be noted, however, that in the framework of the impulse approximation, illustrated in figure 6.26, the measured spectator proton is a physical particle, yet the reacting neutron is off its mass shell, where the explicit expression for its four-momentum vector  $\mathbb{P}_n$ , in the rest frame of the deuteron, reads:

$$\mathbb{P}_n = (m_d - m_p - T_{sp}, -\vec{p}_{sp}), \quad (6.6)$$

with  $T_{sp}$  and  $\vec{p}_{sp}$  denoting the kinetic energy and the momentum vector of a spectator proton, respectively. The mass spectrum of the interacting neutron ( $m_n^2 = |\mathbb{P}_n|^2$ ) resulting from the distribution of Fermi momentum is shown in figure 6.28b. It can be seen that the maximum of this spectrum differs only by about  $3 \text{ MeV}/c^2$  from the free neutron mass ( $m_n = 939.57 \text{ MeV}/c^2$ ), however on the average it is off by about  $9 \text{ MeV}/c^2$ . In the framework of the discussed approximation, the struck neutron is never on its mass shell and the minimum deviation from the real mass occurs for vanishing Fermi-momentum and – as can be inferred from equation (6.6) – is equal to the binding energy  $E_B = m_d - m_n - m_p$ . Measurements performed at the CELSIUS and TRIUMF accelerators for the  $pp \rightarrow pp\eta$  [121] and  $pp \rightarrow d\pi^+$  [266] reactions, respectively, have shown that within the statistical errors there is no difference between the total cross section of the free and quasi-free processes. This conjecture is confirmed also by the theoretical investigations [267].

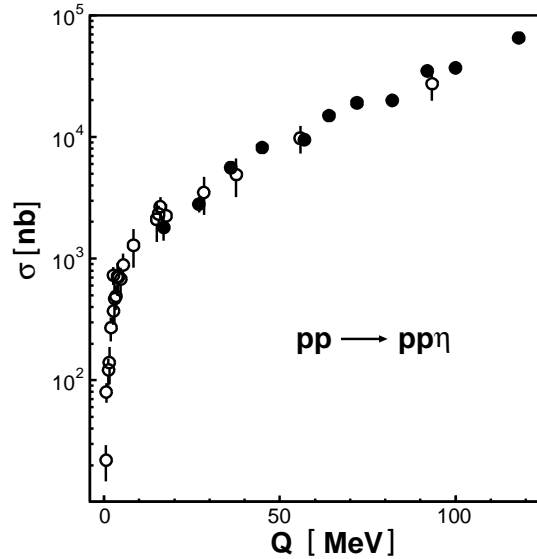


**Figure 6.29:** (a) Total cross sections for the  $pp \rightarrow pp\eta$  reaction as a function of excess energy measured for the scattering of protons in vacuum (open symbols) [10, 18, 50–53] and inside a deuteron (filled symbols) [121].

In figure 6.29 the production of the  $\eta$  meson in free proton-proton collisions is compared to the production inside a deuteron and in the overlapping regions the data agree within the statistical errors. These observations allow to anticipate that indeed the assumption of the identity for the transition matrix element for the meson production off free and quasi-free nucleons bound in the deuteron is correct, at least on the few per cent level. In case of the meson production off the deuteron, one can also justify the assumption of the quasi-free scattering with a geometrical argument, since the average distance between the proton and the

neutron is in the order of <sup>3</sup> 3 fm. Of course, the other nucleon may scatter the incoming proton and the outgoing meson. However, these nuclear phenomena are rather of minor importance in case of the production on the neutron bound in the deuteron, but should be taken into account for derivations of total cross sections from experimental data. Indeed, calculating an influence on the cross section from a possible rescattering of the  $\omega$  meson in the final state of the  $pd \rightarrow d\omega p_{sp}$  reaction, authors of reference [269] found that for the spectator-proton momentum below 100-150 MeV/c the rescattering effects play a minor role. The reduction of the beam flux on a neutron, due to the presence of the proton, referred to as a shadow effect, decreases for example the total cross section by about 4.5 % [270] for the  $\eta$ -meson production. Similarly, the reduction of the total cross section due to the reabsorption of the outgoing  $\eta$  meson on the spectator proton was found to be only about 3 % [270]. The appraisals were performed according to a formula derived in reference [271] which shows that the cross section for the deuteron reduces by a factor of:

$$R = 1 - \sigma_{\eta N}^{inel} \langle r^{-2} \rangle / 4\pi \quad (6.7)$$

compared to the free nucleon cross sections. Here  $\sigma_{\eta N}^{inel}$  denotes the  $\eta N$  inelastic cross section and  $\langle r^{-2} \rangle$  stands for the average of the inverse square nucleon separation in the deuteron taking the nucleon size into account [270]. The latter effect for the production of mesons like  $(\pi, \omega, \eta', \phi)$  is expected to be much smaller, since the s-wave interaction of the  $\eta$ -meson with nucleons is by far stronger than for any of the mentioned ones.

## 6.5 Test measurement of the $pn \rightarrow pn\eta$ reaction

*Nothing is so trivial as treating serious subject  
in a trivial manner [272].*

Erasmus of Rotterdam

As a general commissioning of the extended COSY-11 facility to investigate quasi-free  $pn \rightarrow pnX$  reactions, we have performed a measurement of the  $pn \rightarrow pn\eta$  process at a beam momentum of 2.075 GeV/c [21]. The experiment, carried out in June 2002, had been preceded by the installation of a spectator [158, 273, 274] and neutron detectors [275, 276], and by a series of thorough simulations performed in order to determine

---

<sup>3</sup> The matter radius of the deuteron amounts to  $\approx 2$  fm [268].

the best conditions for measuring quasi-free  $pn \rightarrow pn\eta$  and  $pn \rightarrow pn\eta'$  reactions [20, 28, 230]. Figure 6.30 presents the COSY-11 detection facility with superimposed tracks of protons and neutron originating from the quasi-free  $pn \rightarrow pnX$  reaction induced by a proton beam [62] impinging on a deuteron target [240]. The identification of the  $pn \rightarrow pn\eta$  reaction is based on the measurement of the four-momentum vectors of the outgoing nucleons and the  $\eta$  meson is identified via the missing mass technique. The slow proton stopped in the first layer of the position sensitive silicon detector ( $Si_{spec}$ ) is, in the analysis, considered as a spectator non-interacting with the bombarding particle and moving with the Fermi momentum as possessed at the moment of the collision.

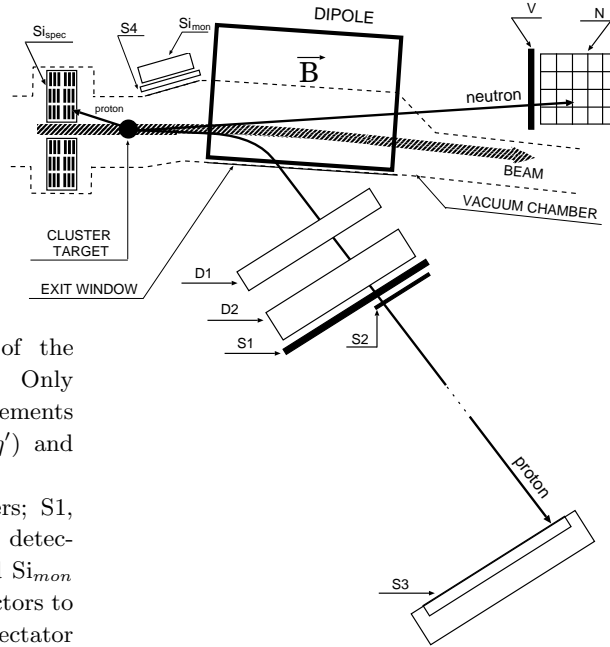


**Figure 6.30:** Schematic view of the COSY-11 detection setup [61]. Only detectors needed for the measurements of the reactions  $pd \rightarrow p_{sp}pn\eta(\eta')$  and  $pd \rightarrow ppn_{sp}$  are shown. D1, D2 denote the drift chambers; S1, S2, S3, S4 and V the scintillation detectors; N the neutron detector and  $Si_{mon}$  and  $Si_{spec}$  [158] silicon strip detectors to detect elastically scattered and spectator protons, respectively.

As we described in subsection 6.4, from the measurement of the momentum vector of the spectator proton  $\vec{p}_{sp}$  one can infer the momentum vector of the struck neutron  $\vec{p}_n = -\vec{p}_{sp}$  at the time of the reaction and hence calculate the total energy of the colliding nucleons for each event. In figures 6.31a and 6.31b the measured and expected distribution of the kinetic energy of the spectator proton is presented. Though still a very rough energy calibration of the detector units was performed, one recognizes a substantial similarity in the shape of both distributions.

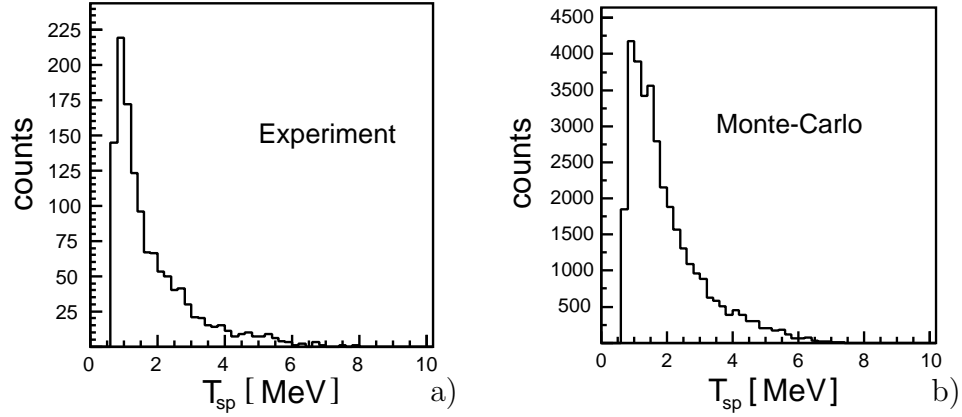


**Figure 6.31:** Distributions of the kinetic energy of the spectator protons. (a) Experiment. (b) Monte-Carlo simulations taking into account the acceptance of the COSY-11 detection system and an analytical parametrization of the deuteron wave function [263] calculated from the PARIS potential [136].

Figure 6.32 shows spectra of the excess energy in respect to the  $pn\eta$  system as obtained in the experiment (6.32a) and the simulation (6.32b) for the  $pn \rightarrow pn\eta$  reaction. The remarkable difference between the distributions comes from the fact that in reality additionally to the  $pn \rightarrow pn\eta$  reaction also the multi-pion production is registered. The  $\eta$  and multi-pion production cannot be distinguished from each other on the event-by-event basis by means of the missing mass technique.

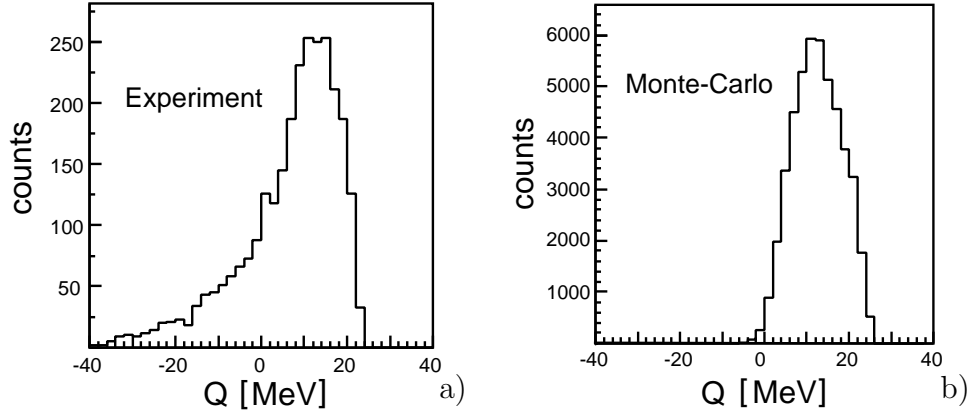


**Figure 6.32:** Distributions of the excess energy  $Q$  for the quasi-free  $pn \rightarrow pnX$  reaction, determined with respect to the  $pn\eta$  threshold. (a) Experiment. (b) Simulation.

However, we can determine the number of the registered  $pn \rightarrow pn\eta$  reactions from the multi-pion background comparing the missing mass distributions for  $Q$  values larger and smaller than zero. Knowing that

negative values of  $Q$  can only be assigned to the multi-pion events we can derive the shape of the missing mass distribution corresponding to these events. This is shown as the dashed line in figure 6.33.

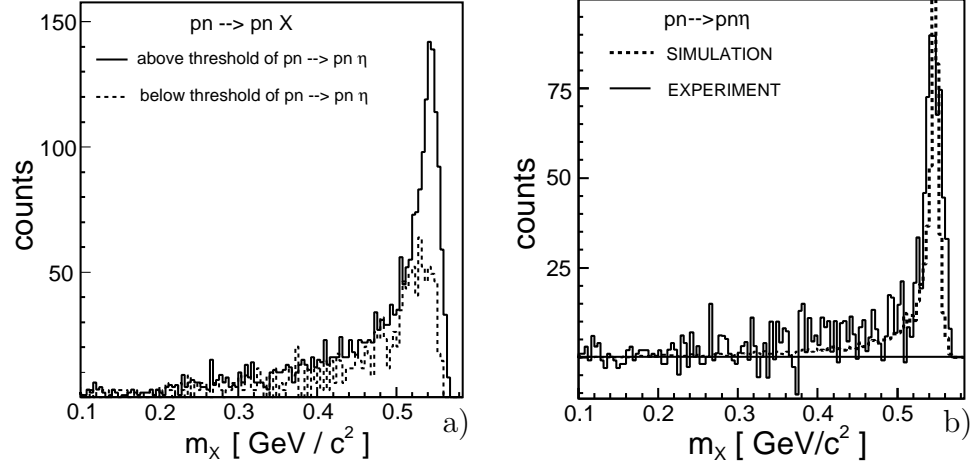


**Figure 6.33:** Missing mass spectra as obtained during the June'02 run:  
a) Event distribution for  $Q < 0$  (dashed line) and for  $Q > 0$  (solid line).  
b) Solid line represents the difference between number of events above and below threshold for the  $pn \rightarrow pn\eta$  reaction, and the dashed line corresponds to the Monte-Carlo simulation.

A thorough evaluation of the background is in progress, however, rough comparison of events for positive and negative  $Q$  yields the promising results with a clear signal from the  $pn \rightarrow pn\eta$  reactions, as can be deduced by inspection of figures 6.33a and 6.33b.

## 6.6 Double quasi-free production

*There is need of a method for investigating the truth about things [207].*

René Descartes

In article [9] we described a method of measuring the close-to-threshold meson production in neutron-neutron collisions, where the momenta of the colliding neutrons could be determined with the accuracy obtainable for the proton-proton reaction. The technique is based on the double quasi-free  $nn \rightarrow nnX^0$  reaction, where deuterons are used as a source of neutrons.

Close-to-threshold meson production in proton-neutron collisions were investigated by means of a technique based on a quasi-free scattering of



the proton off the neutron bound in the deuteron. Thin windowless internal deuterium cluster targets ( $\sim 10^{14}$  atoms/cm<sup>2</sup>) make a detection of an undisturbed spectator proton and a precise determination of the reacting neutron momentum – and hence of the excess energy – possible. Pioneering experiments of the  $\pi^0$  meson creation in the proton-neutron reaction with the simultaneous tagging of the spectator proton resulted in a resolution of the excess energy equal to  $\sigma(Q) = 1.8$  MeV [158]. Similar studies including the production of heavier mesons are carried out at COSY-11 and ANKE facilities [28,278], and we intend to continue them at the forthcoming facility WASA at COSY.

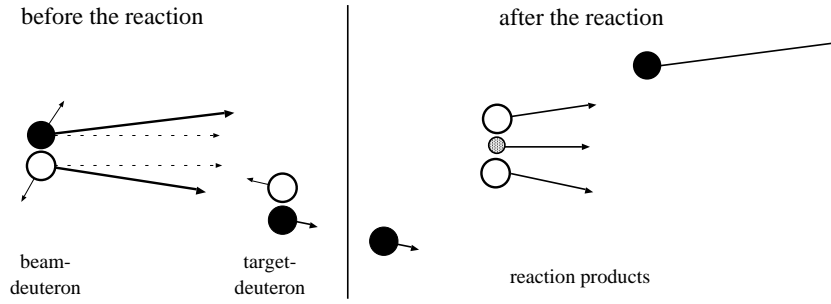


**Figure 6.34:** Schematic depiction of the double quasi-free  $nn \rightarrow nnX$  reaction. During the collisions of deuterons (left hand side of the figure, with the total momentum (solid arrow) resulting from the sum of the beam momentum (dotted arrow) plus the Fermi momentum (short arrow)) a double quasi-free neutron-neutron reaction may lead to the creation of mesons (small gray circle). The spectator protons (black circles) leave the reaction region with their initial momentum plus the Fermi momentum, which they possessed at the moment of the reaction. Neutrons are plotted as open circles. Due to the large relative momenta between spectators and the outgoing neutrons ( $\sim 1$  GeV/c close-to-threshold for the  $\eta$  meson production) a distortion of the  $nnX$  system by the accompanied protons can be neglected.

Experimental investigations of the close-to-threshold production in neutron-neutron collisions, however, have not yet been carried out. A realisation of such studies – which are characterised by typical cross sections of  $\leq \mu\text{b}$  – with high quality neutron beams bombarding a deuterium target is not feasible due to the low neutron beam intensities forcing to use liquid or solid deuterium targets which make the precise determination of the momentum of the spectator proton impossible. In this section a unique possibility of the precise measurement of the close-to-threshold meson production in neutron-neutron collisions is pointed out. The technique is based on the double quasi-free interaction of neutrons originating from colliding deuterons as depicted in Figure 6.34.

Utilizing this method, a precision of  $\sim 1$  MeV can be obtained for determining the excess energy, since it depends only on the accuracy of the momentum or angle reconstruction for the registered spectator protons. At present cooled deuteron beams – available at the facilities CELSIUS and COSY – give the possibility of using this method for the studies of neutron-neutron scattering. Moreover, the usage of a stored beam circulating through an internal cluster target permits the study with high luminosities ( $10^{31} \text{cm}^{-2} \text{s}^{-1}$ ) in spite of very low target densities. These investigations can be realized much more effectively once the WASA detector is installed at COSY. In the double quasi-free interaction, due to the small binding energy of the deuteron ( $E_B = 2.2$  MeV), the colliding neutrons may be approximately treated as free particles in the sense that the matrix element for quasi-free meson production from bound neutrons is identical to that for the free  $nn \rightarrow \text{NNX}$  reaction at the same excess energy available in the NNX system. The measurements at CELSIUS [121, 197] and TRIUMF [266, 277] have proven that the off-shellness of the reacting neutron can be neglected and that the spectator proton influences the interaction only in terms of the associated Fermi motion [266]. The registration of both spectator protons will allow for a precise determination of the excess energy. A possible internal target facility based on the COSY-11 setup [61] is presented in figure 6.35. The energy and the emission angle of the "slow" spectator can be measured by an appropriately segmented silicon detector, whereas the momentum of the "fast" spectator proton can be analysed by the magnetic spectrometer. By means of the detection system shown in figure 6.35, a resolution of the excess energy of 2 MeV can be achieved for excess energies lower than 30 MeV as demonstrated in reference [28]. The double quasi-free  $nn \rightarrow nnX^0$  reaction can be identified by the registration of both outgoing neutrons. For example, in order to measure the production of the  $\eta$  meson, a seven meter distance for the time-of-flight measurement would be enough to obtain 8 MeV (FWHM) missing mass resolution [28] with a calorimeter segmented by  $10 \text{ cm} \times 10 \text{ cm}$  and providing a 0.5 ns ( $\sigma$ ) time resolution, which was obtained in test runs using a scintillator/lead sandwich type of detector. The suggested meson production via a double quasi-free neutron-neutron reaction with precisions achievable for the proton-proton and proton-neutron reactions, opens the possibility of studying for example the charge symmetry breaking by comparing cross sections for the  $pp \rightarrow pp\eta$  and  $nn \rightarrow nn\eta$  reactions, similarly to investigations performed via the  $\pi$ -deuteron reactions [185]. The Dalitz-plot analysis of the  $nn \rightarrow nn$  Meson would allow for the study

of the neutron-neutron and neutron-Meson [279] scattering lengths, the first being still not well established [64] and the second being unknown. In principle when studying the meson production in proton-proton and in proton-neutron collisions one has access to all possible isospin combinations, which can be derived after the correction for the electromagnetic interaction.

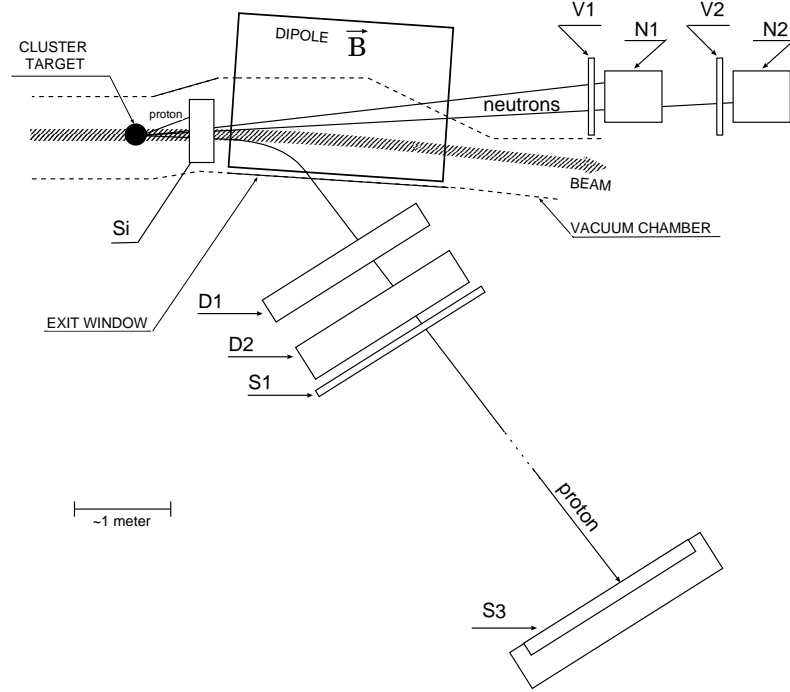


**Figure 6.35:** Schematic view of the extended COSY-11 detection setup [61]. Only detectors needed for the measurements of the  $dd \rightarrow nnp_{sp}p_{sp}X$  reactions are shown. D1,D2 denote the drift chambers used for the track reconstruction of the fast spectator proton; S1,S3 and V1,V2 are the scintillation detectors used as time-of-flight and veto counters, respectively, N1,N2 the neutron detectors, and Si [158] the silicon strip detectors.

Exceptionally, close-to-threshold meson production via the neutron-neutron scattering represents a pure  $T = 1$  isospin channel without accompanying Coulomb interaction and consequently no need for its correction. Investigations of neutron-neutron scattering allow also for the production of  $K^+K^-$  pairs in a system with only two charged particles in the final state ( $nn \rightarrow nnK^+K^-$ ), simplifying the theoretical calculations drastically, which in case of the  $pp \rightarrow ppK^+K^-$  are not feasible due to the difficulty of treating the electromagnetic forces in the system of four

charged particles [280].

At present the COSY synchrotron can accelerate deuterons up to 3.5 GeV/c [62] which, utilizing the Fermi momentum, allows for the  $\pi$  and  $\eta$  meson production in the  $nn \rightarrow nnX^0$  reaction. To investigate the neutron-neutron interaction with the production of heavier mesons like  $\omega$ ,  $\eta'$ , or  $\phi$ , a deuteron beam of  $\sim 7$  GeV/c would be required.

## 7. Conclusion

Using the stochastically cooled proton beam of the cooler synchrotron COSY and the COSY-11 facility we performed measurements of the  $pp \rightarrow pp\eta$  and  $pp \rightarrow pp\eta'$  reaction close to the kinematical threshold. We have succeeded in establishing the energy dependence of the total cross section for both reactions and the probability density of the phase space population for the  $pp \rightarrow pp\eta$  reaction. At present we are pursuing the study by elaborating differential cross sections of the  $pp \rightarrow pp\eta'$  reaction based on the high statistics data from a recently performed experiment [179]. Measuring four-momentum vectors of protons in the entrance and exit channels we determined complete kinematics for each registered event and hence derived all in principle possible empirical information about the studied processes. Thus, the interpretation of the results is limited only by the experimental accuracy and ambiguities of the theoretical approaches.

Inferences of the interaction taking place within the  $pp\eta$  and  $pp\eta'$  systems were based on the comparison between the experimental results and the predictions obtained assuming that all kinematically permitted momentum combinations of the outgoing particles are equally probable. Indeed, we have discovered statistically incontestable deformations of both the excitation function and the phase space abundance. The discrepancies can plausibly be assigned to the influence of the hadronic interaction occurring among ejectiles since the range of excess energy was chosen such that other possible explanations – like variations resulting from the dynamics of the primary production or contributions from larger than zero angular momenta – can be excluded.

A unique precision achieved due to the low emittance of the cooled beam and the high resolution mass spectrometer enabled us to distinguish effects resulting from the  $\eta$ -proton interaction from effects caused by the almost two orders of magnitude stronger proton-proton force. This conclusion was drawn from the phenomenological analysis based on the assumption that the primary production can be separated from the final state interaction and also that the three-body final state can be treated as an incoherent system of pairwise interacting objects. We must admit that these simplifications enabled us to estimate the effects from the proton- $\eta$  and proton- $\eta'$  interaction only qualitatively. Nevertheless, a

remarkable difference between the shape of the excitation functions of the  $pp \rightarrow pp\eta$  and  $pp \rightarrow pp\eta'$  reactions allowed us to conclude that the interaction between the  $\eta'$  meson and the proton is significantly weaker than the analogous interaction between the  $\eta$  meson and the proton. To raise the confidence in the concluded distinction between proton-proton and meson-proton interaction we compared the shapes of the excitation functions of the reactions  $pp \rightarrow pp\eta$  and  $pp \rightarrow pp\eta'$  with the one of  $pp \rightarrow pp\pi^0$ . We could plausibly assert that the differences in shapes are due to the proton- $\eta$ , or correspondingly, to the proton- $\eta'$  interaction since the well known proton- $\pi^0$  interaction is too weak to manifest itself within the current accuracy. Therefore the excitation function for the  $pp \rightarrow pp\pi^0$  reaction reflects the influence of the interaction between protons only. This comparison confirmed – model independently – that the hadronic interaction between the  $\eta'$  meson and the proton is indeed much weaker than the  $\eta$ -proton one. This is the first ever empirical appraisal of this hitherto entirely unknown interaction occurring between the  $\eta'$  meson and the proton.

We minimized a systematic bias of the data performing a multidimensional acceptance correction and the bin-by-bin subtraction of the multi-pion background. In particular, we elaborated invariant mass distributions of two-particle subsystems of the  $pp\eta$  final state independently of the reaction model used in the simulations. We must confess, however, that with the measurement method used and within the achieved statistics it was not possible to determine a background-free occupation density over the Dalitz-plot unless a small number of bins was used, which in turn caused drastic losses in the experimental accuracy. Therefore as a next step of our investigation we proposed a pertinent experiment at a WASA@COSY facility [181].

The experimental technique employed and the developed method of analysis allowed us to achieve an unique precision for the simultaneous determination of the absolute excess energy ( $\sigma(Q) = 0.4$  MeV), missing mass ( $\sigma(m) \approx 0.3$  MeV/ $c^2$ ), and momentum of the outgoing particles ( $\sigma(p) = 4$  MeV/ $c$ ). This unprecedented accuracy enabled us not only to find out that the density of the phase space population is strongly anisotropic but also to discern distortions originating from the proton-proton and proton- $\eta$  interactions. An utterly satisfactory description of the deviations observed at low relative proton-proton momenta was achieved by taking into account the well known hadronic and electromagnetic interactions between the protons. On the contrary, the enhancement at low relative proton- $\eta$  momenta is a few times larger than ex-

pected under the assumption that the mutual interaction among particles in the  $pp\eta$  system can be described by the incoherent pairwise interaction of proton-proton and proton- $\eta$  subsystems. At present many theoretical groups are seeking for an explanation of this effect [79, 82, 122, 128, 141]. Undoubtedly, this and other results presented in this treatise accelerated the development of the formalism of the description of the three-body system in the complex hadronic potential [123, 128] and led to significant progress in the understanding of the production mechanism on both hadronic [81, 141, 228] and quark-gluon levels [223].

Since the interaction between hadrons, their structure, and production dynamics are inseparably connected with each other, in this treatise we have discussed not only the hadronic interaction between the  $\eta$  and  $\eta'$  mesons and the protons but also presented our endeavour to understand the reaction dynamics and the structure of the studied mesons. The observed large difference of the total cross sections between the  $\eta$  and  $\eta'$  meson production shows that these mesons are created via different mechanisms, since comparable coupling constants are expected for both of them, at least in the SU(3) limit. It is well established that close-to-threshold the  $\eta$  meson is produced predominantly through the excitation of the  $S_{11}(1535)$  resonance, and hence the large difference in the observed cross sections suggests that the  $\eta'$  primary production process is nonresonant. Different production mechanisms reflect differences in the structure of these mesons, however, at the present stage we cannot draw any quantitative conclusion.

As far as the meson structure is concerned we focused on the  $\eta'$  meson demonstrating a method which will allow to investigate a gluonic component of its wave function. The study of this very interesting aspect – connected to the search of matter built exclusively out of gluons – will be based on the comparison of the  $\eta'$  meson production via the  $pp \rightarrow pp\eta'$  and  $pn \rightarrow pn\eta'$  reaction. The measurement of the excitation function of the  $pp \rightarrow pp\eta'$  reaction is finished, and in order to accomplish the measurement of the  $pn \rightarrow pn\eta'$  reaction we have extended the COSY-11 detection setup by a neutron and a spectator detectors. The neutron detector was designed and built by us in Cracow [275, 276], and for the registration of the spectator protons we adapted [28, 273, 274] to the COSY-11 facility a silicon pad detector [158] which was previously used by the WASA/PROMICE collaboration at the CELSIUS accelerator. A successful measurement of the  $pn \rightarrow pn\eta$  reaction has proven that it is possible to study quasi-free  $pn \rightarrow pnX$  reactions using the newly accomplished experimental setup.

An exploration of the isospin degrees of freedom in the study of the creation of mesons led us to the entirely novel idea of using quasi-free reactions for the investigations of meson production cross sections as a function of the virtuality of the interacting nucleons. We demonstrated also a method for measuring the close-to-threshold production of mesons in quasi-free neutron-neutron collisions. It is our great hope to conduct these investigations in the near future at the facility WASA@COSY [181].

In parallel we began also to explore spin degrees of freedom. In particular, we have demonstrated that by measuring spin observables it is possible to learn about the very details of the production dynamics of the  $\eta$  meson. Predictions for the analysing power differ so much depending on the assumed mechanism that the determination of this quantity alone will allow to establish whether vector or pseudoscalar meson exchange dominates the production process.

In this treatise we presented results of investigations aiming to determine the interaction of  $\eta$  and  $\eta'$  mesons with nucleons, the structure of these mesons and the mechanism which governs their creation in the collision of nucleons. We have not arrived at the very aim yet. But we have gained a qualitative understanding of the reaction mechanism, estimated the hitherto entirely unknown  $\eta'$ -proton interaction, observed a signal from the  $\eta$ -proton interaction, delivered a sample of high quality data on both total and differential cross sections, and developed novel methods of measurements which should lead to more quantitative statements in the near future.

*So even though my speculations pleased me very much, I believed that other persons had their own speculations which perhaps pleased them even more [281].*

René Descartes

*The approbation of the public I consider as the greatest reward of my labours; but am determin'd to regard its judgment, whatever it be, as my best instruction [183].*

David Hume



# References

- [1] P. Moskal et al., Phys. Rev. **C 69** (2004) 025203.
- [2] P. Moskal et al., Phys. Lett. **B 482** (2000) 356.
- [3] P. Moskal et al., Phys. Lett. **B 474** (2000) 416.
- [4] P. Moskal, M. Wolke, A. Khoukaz, W. Oelert, Prog. Part. Nucl. Phys. **49** (2002) 1.
- [5] A. Khoukaz et al., Eur. Phys. J. **A 20** (2004) 345.
- [6] P. Moskal et al., J. Phys. **G 29** (2003) 2235.
- [7] P. Winter et al., Phys. Lett. **B 544**, 251 (2002); Erratum-ibid. **B 553** (2003) 339.
- [8] P. Moskal et al., Nucl. Instr. & Meth. **A 466** (2001) 448.
- [9] P. Moskal et al., Phys. Lett. **B 517** (2001) 295.
- [10] J. Smyski et al., Phys. Lett. **B 474** (2000) 182.
- [11] P. Moskal et al., Phys. Rev. Lett. **80** (1998) 3202.
- [12] V. Baru et al., Eur. Phys. J. **A 6** (1999) 445.
- [13] P. Moskal et al., Eur. Phys. J. **A 18** (2003) 335.
- [14] P. Moskal et al., Nucl. Phys. **A 721** (2003) 683.
- [15] P. Moskal et al., J. Phys. **G 28** (2002) 1777.
- [16] P. Moskal et al., Acta Phys. Pol. **B 31** (2000) 2277.
- [17] P. Moskal et al., Acta Phys. Pol. **B 29** (1998) 3091.
- [18] P. Moskal et al.,  $\pi N$  Newsletter **16** (2002) 367.
- [19] P. Moskal et al., AIP Conf. Proc. **512** (2000) 65.
- [20] P. Moskal, e-Print Archive: nucl-ex/0110001; Schriften des FZ-Jülich: Matter & Material **11** (2002) 27; Proceedings of the Symposium on Threshold Meson Production in pp and pd Interactions, June 20–24, 2001, Cracow, Poland; Eds. P. Moskal and M. Wolke.
- [21] P. Moskal et al., e-Print Archive: nucl-ex/0311003; Talk presented at Hadron 03: 10th International Conference on Hadron Spectroscopy, Aschaffenburg, Germany, 31 Aug - 6 Sep 2003. AIP Conf. Proc. (2004) in print.
- [22] P. Moskal et al., e-Print Archive: nucl-ex/0208004; Proceedings of the 7th International Workshop on Production, Properties and Interactions of Mesons, Cracow, Poland, 24-28 May (2002). Eds. L. Jarczyk, A. Magiera, C. Guaraldo, H. Machner, World Scientific, Singapore (2003).
- [23] P. Moskal et al., Schriften des FZ-Jülich: Matter & Material **13** (2002), Proceedings of the Workshop on Beam Cooling and Related Topics 2001, 255<sup>th</sup> International WE-Heraeus Seminar, Bad Honnef, Germany, May (2001). Eds. D. Prasuhn.
- [24] W. Oelert, COSY Proposal **No. 11** (1988).

- 
- [25] P. Moskal, COSY Proposal **No. 133** (2003), “Investigation of the  $\eta'$  meson structure and of the isospin dependence of its production in the nucleon–nucleon collisions”, available at <http://ikpe1101.ikp.kfa-juelich.de/>
  - [26] P. Moskal, COSY Proposal **No. 123** (2003), “Comparative study of the interaction in the  $pp\eta$  and  $pp\eta'$  systems”, available at <http://ikpe1101.ikp.kfa-juelich.de/>
  - [27] R. Czyżykiewicz, P. Moskal, COSY Proposal **No. 118** (2002), “Energy dependence of the analyzing power  $A_y(\Theta^*)$  for the  $\bar{p}p \rightarrow pp\eta$  reaction”, available at <http://ikpe1101.ikp.kfa-juelich.de/>
  - [28] P. Moskal, T. Johansson, COSY Proposal **No. 100** (2001), “Investigation of the glue content in the  $\eta'$  meson”, available at <http://ikpe1101.ikp.kfa-juelich.de/>
  - [29] P. Moskal, COSY Proposal **No. 11.7** (1999), “Study of the proton- $\eta'$  and proton- $\eta$  interaction”, available at <http://ikpe1101.ikp.kfa-juelich.de/>
  - [30] P. Moskal, COSY Proposal **No. 11.5** (1997), “Investigation of the  $pp \rightarrow pp\eta'$  reaction at COSY - 11”, available at <http://ikpe1101.ikp.kfa-juelich.de/>
  - [31] P. Moskal, COSY Proposal **No. 11.2** (1996), “Proposal for the investigation of the  $pp \rightarrow pp\eta'$  reaction at the COSY - 11 detection system”, available at <http://ikpe1101.ikp.kfa-juelich.de/>
  - [32] I. Kant, “The Critique of Pure Reason”, available at <http://www.malaspina.com/etext/purekant.htm>.
  - [33] A. Pevsner et al., Phys. Rev. Lett. **7** (1961) 421.
  - [34] G. R. Kalbfleisch et al., Phys. Rev. Lett. **12** (1964) 527.
  - [35] M. Goldberg et al., Phys. Rev. Lett. **12** (1964) 546.
  - [36] A. M. Green, S. Wycech, Phys. Rev. **C 55** (1997) R2167.
  - [37] N. Kaiser, T. Waas, W. Weise, Nucl. Phys. **A 612** (1997) 297.
  - [38] A. M. Green, S. Wycech, e-Print Archive: nucl-th/0009053.
  - [39] A. M. Green, S. Wycech, Phys. Rev. **C 60** (1999) 035208.
  - [40] A. Bramon et al., Eur. Phys. J. **C 7** (1999) 271.
  - [41] C. P. Jessop et al., Phys. Rev. **D 58** (1998) 052002.
  - [42] G. Brandenburg et al., Phys. Rev. Lett. **75** (1995) 3804.
  - [43] K. Hagiwara et al., Phys. Rev. **D 66** (2002) 010001.
  - [44] S. D. Bass, Phys. Lett. **B 463** (1999) 286.
  - [45] D.-M. Li et al., Eur. Phys. J. **C 28** (2003) 335.
  - [46] J. Balewski et al., Phys. Lett. **B 420** (1998) 211.
  - [47] S. Sewerin et al., Phys. Rev. Lett. **83** (1999) 682.
  - [48] R. Bilger et al., Phys. Lett. **B 420** (1998) 217.
  - [49] C. Quentmeier et al., Phys. Lett. **B 515** (2001) 276.
  - [50] H. Calén et al., Phys. Lett. **B 366** (1996) 39.
  - [51] E. Chiavassa et al., Phys. Lett. **B 322** (1994) 270.
  - [52] A. M. Bergdolt et al., Phys. Rev. **D 48** (1993) R2969.
  - [53] F. Hibou et al., Phys. Lett. **B 438** (1998) 41.
  - [54] E. Pickup et al., Phys. Rev. Lett. **8** (1962) 329.
  - [55] L. Bodini et al., Nuovo Cimento **A 58** (1968) 475.
  - [56] W. J. Fickinger et al., Phys. Rev. **125** (1962) 2082.
  - [57] R. I. Louttit et al., Phys. Rev. **123** (1961) 1465.

- 
- [58] E. Bierman et al., Phys. Rev. **147** (1966) 922.
- [59] F. Balestra et al., Phys. Lett. **B 468** (1999) 7.
- [60] D. E. Groom et al., Eur. Phys. J. **C 15** (2000) 1,  
data are available at [http://pdg.lbl.gov/2000/contents\\_plots.html](http://pdg.lbl.gov/2000/contents_plots.html).
- [61] S. Brauksiepe et al., Nucl. Instr. & Meth. **A 376** (1996) 397.
- [62] D. Prasuhn et al., Nucl. Instr. & Meth. **A 441** (2000) 167.
- [63] R. Penrose, “The Emperor’s New Mind, Concerning Computers, Minds, and The Laws of Physics”, Published in Penguin Books (1991).
- [64] R. Machleidt, I. Slaus, J. Phys. G: Nucl. Part. Phys. **27** (2001) R69.
- [65] R. Machleidt, Phys. Rev. **C 63** (2001) 024001.
- [66] K. M. Watson, Phys. Rev. **88** (1952) 1163.
- [67] A. Moalem et al., Nucl. Phys. **A 600** (1996) 445.
- [68] V. Bernard, N. Kaiser, Ulf-G. Meissner, Eur. Phys. J. **A 4** (1999) 259.
- [69] E. Gedalin, A. Moalem, L. Razdolskaja, Nucl. Phys. **A 650** (1999) 471.
- [70] E. Byckling, K. Kajantie, “Particle Kinematics”, John Wiley & Sons, New York (1973).
- [71] C. Hanhart, K. Nakayama, Phys. Lett. **B 454** (1999) 176.
- [72] M. Batinić, A. Švarc, T.-S. H. Lee, Phys. Scripta **56** (1997) 321.
- [73] Plato, “Cratylus”, available at <http://classics.mit.edu/Plato/cratylus.html>
- [74] H. Poincaré, “Science and Method”, St. Augustine’s Press, South Bend, India (2000).
- [75] K. R. Popper, “The Logic of Scientific Discovery”, Routledge Classics, London and New York (2003).
- [76] A. H. Rosenfeld, Phys. Rev. **96** (1954) 130.
- [77] M. Gell-Mann, K. M. Watson, Ann. Rev. Nucl. Sci. **4** (1954) 219.
- [78] H. O. Meyer et al., Phys. Rev. **C 63** (2001) 064002.
- [79] K. Nakayama et al., Phys. Rev. **C 68** (2003) 045201.
- [80] H. O. Meyer et al., Phys. Rev. Lett. **81** (1998) 3096.
- [81] C. Hanhart, Phys. Rept. **397** (2004) 155.
- [82] A. Deloff, Phys. Rev. **C 69** (2004) 035206.
- [83] J. Ritman, Habilitation thesis, Giessen University (2000).
- [84] D. Grzonka, K. Kilian, Schriften des FZ-Jülich: Matter & Materials **11** (2002) 100;  
Proceedings of the Symp. on Threshold Meson Production in pp and pd Interactions,  
June 20-24, 2001, Cracow, Poland; Eds. P. Moskal and M. Wolke.
- [85] B. Russell, “The Problems of Philosophy”, Dover Publications, inc. Mineola,  
New York (1999).
- [86] R. H. Dalitz, Phil. Mag. **44** (1953) 1068.
- [87] J. Dyring, PhD thesis, University of Uppsala, Acta Universitatis Upsaliensis **14** (1997).
- [88] C. Wilkin, University Coll., London, private communication (2003).
- [89] F. Balestra et al., Phys. Rev. Lett. **89** (2002) 092001.
- [90] Aristotle, “Metaphysics”, Ann Arbor Paperbacks The University of Michigan  
Press (2003).
- [91] H. O. Meyer et al., Phys. Rev. Lett. **83** (1999) 5439.
- [92] J. R. Bergervoet et al., Phys. Rev. **C 41** (1990) 1435.
- [93] J. Złomańczuk et al., Phys. Lett. **B 436** (1998) 251.

- 
- [94] R. A. Arndt et al., Phys. Rev. **C 56** (1997) 3005. The Virginia Tech Partial-Wave Analysis Facility (SAID), <http://gwdac.phys.gwu.edu>
  - [95] M. Abdel-Bary et al., Eur. Phys. J. **A 16** (2003) 127.
  - [96] H. Calén et al., Phys. Lett. **B 458** (1999) 190.
  - [97] F. Balestra et al., Phys. Lett. **B 491** (2000) 29.
  - [98] J. S. Mill, “On Liberty, The Subjection of Woman & Utilitarianism”, Modern Library, New York (2002).
  - [99] A. B. Migdal, Sov. Phys. JETP **1** (1955) 2.
  - [100] K. Nakayama, e-Print Archive: nucl-th/0108032; Schriften des FZ-Jülich: Matter and Materials **11** (2002) 119; Proceedings of the Symp. on Threshold Meson Production in pp and pd Interactions, June 20–24, 2001, Cracow, Poland; Eds. P. Moskal and M. Wolke.
  - [101] For the discussion of the FSI effects see e.g.: F. Kleefeld, e-Print Archive nucl-th/0108064; Schriften des FZ-Jülich: Matter & Materials **11** (2002) 51; Proceedings of the Symp. on Threshold Meson Production in pp and pd Interactions, June 20–24, 2001, Cracow, Poland; Eds. P. Moskal and M. Wolke,
  - [102] B. J. Morton et al., Phys. Rev. **169** (1968) 825.
  - [103] J. D. Jackson, J. M. Blatt, Rev. of Mod. Phys. **22** (1950) 77.
  - [104] H. A. Bethe, Phys. Rev. **76** (1949) 38.
  - [105] D. Y. Wong, H. P. Noyes, Phys. Rev. **126** (1962) 1866.
  - [106] R. A. Arndt, R. H. Hackman, L. D. Roper, Phys. Rev. **C 15** (1977) 1002.
  - [107] J. P. Naisse, Nucl. Phys. **A 278** (1977) 506.
  - [108] H. P. Noyes, H. M. Lipinski, Phys. Rev. **C 4** (1971) 995.
  - [109] H. P. Noyes, Ann. Rev. Nucl. Sci. **22** (1972) 465.
  - [110] V. G. J. Stoks et al., Phys. Rev. **C 48** (1993) 792.
  - [111] B. L. Druzhinin et al., Z. Phys. **A 359** (1997) 205.
  - [112] R. Shyam and U. Mosel, Phys. Lett. **B 426** (1998) 1.
  - [113] M. L. Goldberger and K. M. Watson, “Collision Theory”, John Wiley & Sons, New York (1964).
  - [114] A. Bondar et al., Phys. Lett. **B 356** (1995) 8.
  - [115] H. O. Meyer et al., Nucl. Phys. **A 539** (1992) 633.
  - [116] S. Stanislaus et al., Phys. Rev. **C 41** (1990) R1913.
  - [117] R. Bilger et al., Nucl. Phys. **A 693** (2001) 633.
  - [118] G. Fäldt and C. Wilkin, Phys. Lett. **B 382** (1996) 209.
  - [119] G. Fäldt and C. Wilkin, Phys. Rev. **C 56** (1997) 2067.
  - [120] R. Wurzinger et al., Phys. Lett. **B 374** (1996) 283.
  - [121] H. Calén et al., Phys. Rev. Lett. **79** (1997) 2642.
  - [122] A. Fix, Mainz University, private communication (2003).
  - [123] A. Fix, H. Arenhövel, Phys. Rev. **C 69** (2004) 014001.
  - [124] A. Moalem et al., Nucl. Phys. **A 589** (1995), 649.
  - [125] A. Sibirtsev et al., Phys. Rev. **C 65** (2002) 044007.
  - [126] D. Sigg et al., Nucl. Phys. **A 609** (1996) 269; *ibidem* **A 617** (1997) 526.
  - [127] W. Glöckle et al., Phys. Rep. **274** (1996) 107.
  - [128] H. Garcilazo, ESFM Mexico, private communication (2003).

- 
- [129] S. Wycech, Warsaw Ins. Nucl. Studies, private communication (2003).
- [130] U. Schuberth, PhD thesis, Acta Universitatis Upsaliensis **5** (1995).
- [131] V. Hejny et al., Eur. Phys. J. **A 13** (2002) 493; Ch. Elster et al., e-Print Archive: nucl-th/0207052; A. Sibirtsev et al., Phys. Rev. **C 65** (2002) 067002.
- [132] V. Baru et al., Phys. Atom. Nucl. **64** (2001) 579.
- [133] J. A. Niskanen, Phys. Lett. **B 456** (1999) 107.
- [134] J. Haidenbauer et al., Phys. Rev. **C 48** (1993) 2190.
- [135] H. Van Haeringen, Nucl. Phys. **A 253** (1975) 355.
- [136] M. Lacombe et al., Phys. Rev. **C 21** (1980) 861.
- [137] H. W. Fearing, Phys. Rev. Lett. **81** (1998) 758.
- [138] K. Nakayama et al., Phys. Rev. **C 61** (2000) 024001.
- [139] G. Galilei, “Dialogue concerning the two chief world systems”, The Modern Library Paperback Edition, New York (2001).
- [140] The WASA/PROMICE collaboration determined the total cross section of  $2.11 \pm 0.74$  (overall error) at  $Q = 15.0 \pm 0.5$  MeV [50]. This value is by about 30% lower than our result, though the values still agree with each other if one adds the statistical and systematic uncertainties. However, the acceptance correction for this experiment was calculated taking into account the phase space distribution only [130] and this lead to the underestimation of the total cross section which can be deduced from the comparison between the  $s_{pp}$  distribution and the phase space prediction shown in figure 4.11. For the discussion of that issue see also [282]. Our result agrees, however, quite well with the value of  $2.68 \pm 0.54 \mu b$  determined at  $Q = 16 \pm 0.6$  MeV at the SATURNE facility [53].
- [141] V. Baru et al., Phys. Rev. **C 67** (2003) 024002.
- [142] V. Baru, ITEP Moscow, private communication (2003).
- [143] A. Fix, H. Arenhövel, Nucl. Phys. **A 697** (2002) 277.
- [144] J. Haidenbauer, W. Plessas, Phys. Rev. **C 30** (1984) 1822.
- [145] C. Bennhold, H. Tanabe, Nucl. Phys. **A 530** (1991) 625.
- [146] J. Smyrski et al., Ann. Rep. IKP FZ-Jülich, Jül-3640 (1999) 39.
- [147] T. Pratchett, “Sourcery”, HarperCollins Publishers Inc. (2001).
- [148] A. Fix, H. Arenhövel, Eur. Phys. J. **A 9** (2000) 119.
- [149] S. A. Rakityansky et al., Phys. Rev. **C 53** (1996) R2043.
- [150] A. Švarc, S. Ceci, e-Print Archive: nucl-th/0009024.
- [151] B. Mayer et al., Phys. Rev. **C 53** (1996) 2068.
- [152] F. Frascaria et al., Phys. Rev. **C 50** (1994) R537.
- [153] N. Willis et al., Phys. Lett. **B 406** (1997) 14.
- [154] N. V. Shevchenko et al., Eur. Phys. J. **A 9** (2000) 143.
- [155] S. Wycech, Acta Phys. Pol. **B 27** (1996) 2981.
- [156] H. Garcilazo, M. T. Peña, Phys. Rev. **C 63** (2001) 021001.
- [157] H. Calén et al., Phys. Rev. Lett. **80** (1998) 2069.
- [158] R. Bilger et al., Nucl. Instr. & Meth. **A 457** (2001) 64.
- [159] D. A. Hutcheon et al., Phys. Rev. Lett. **64** (1990) 176.
- [160] D. A. Hutcheon et al., Nucl. Phys. **A 535** (1991) 618.
- [161] M. Batinić et al., e-Print Archive: nucl-th/9703023.

- [162] J. Smyrski, Schriften des FZ-Jülich: Matter and Materials **11** (2002) 46; Proceedings of the Symp. on Threshold Meson Production in pp and pd Interactions, June 20–24, 2001, Cracow, Poland; Eds. P. Moskal and M. Wolke.
- [163] H. O. Meyer, J. A. Niskanen, Phys. Rev. **C 47** (1993) 2474.
- [164] T. Ueda, Phys. Rev. Lett. **66** (1991) 297; Phys. Lett. **B 291** (1992) 228.
- [165] T. Ueda, Phys. Scripta **48** (1993) 68.
- [166] S. Wycech, A. M. Green, Phys. Rev. **C 64** (2001) 045206.
- [167] A. Deloff, Phys. Rev. **C 61** (2000) 024004.
- [168] F. Hibou et al., Eur. Phys. J. **A 7** (2000) 537.
- [169] C. Piskor-Ignatowicz, PhD thesis, Jagellonian University, in preparation.
- [170] A. Gillitzer et al., COSY Proposal **No. 102** (2001).  
available at <http://www.fz-juelich.de/ikp/COSY-TOF>
- [171] F. Laue et al., Phys. Rev. Lett. **82** (1999) 1640.
- [172] Q. Haider, L. C. Liu, Phys. Lett. **B 172** (1986) 257.
- [173] L. C. Liu, Q. Haider, Phys. Rev. **C 34** (1986) 1845.
- [174] S. Wycech et al., Phys. Rev. **C 52** (1995) 544.
- [175] V. V. Abaev, B. M. K. Nefkens, Phys. Rev. **C 53** (1996) 385.
- [176] C. Wilkin, Phys. Rev. **C 47** (1993) R938.
- [177] H. C. Chiang, E. Oset, L. C. Liu, Phys. Rev. **C 44** (1991) 738.
- [178] G. L. Li, W. K. Cheung and T. T. S. Kuo, Phys. Lett. **B 195** (1987) 515.
- [179] J. Przerwa, R. Czyżykiewicz, P. Moskal, Ann. Rep. 2003 IKP FZ-Jülich,  
available at <http://ikpe1101.ikp.kfa-juelich.de/>
- [180] J. Zabierowski et al., Phys. Scripta **T99** (2002) 159.
- [181] P. Moskal for the COSY-11 collaboration, Letter of Intent **No. 14** for an experiment with an  $4\pi$  electro-magnetic calorimeter at COSY. Presented at Finuphy Workshop on Advanced Electromagnetic Calorimetry (2004).  
available at <http://ankecv.s.ikp.kfa-juelich.de/femc04/en/index.shtml>
- [182] W. Heisenberg, Physics Today / March (1976) 32.
- [183] D. Hume, “A Treatise of Human Nature”, LONDON: Printed for JOHN NOON, at the White-Hart, near Mercers-Chapel, in Cheapside. *MDCCXXXIX*.
- [184] G. Rappenecker et al., Nucl. Phys. **A 590** (1995) 763.
- [185] W. B. Tippens et al., Phys. Rev. **D 63** (2001) 052001.
- [186] P. Moskal, Ann. Rep. 2000, IKP, FZ-Jülich, Jül-3852 (2001) 48.
- [187] N. Copernicus, Minor Works III, Letter against Wagner, Polish Scientific Publishers, Warsaw-Cracow (1985).
- [188] S. Capstick et al., e-Print Archive: hep-ph/0012238; Hadronic Physics White Paper, proceedings of the APS Division of Nuclear Physics Town Meeting on Electromagnetic and Hadronic Physics, December 1–4, 2000, Newport News, Virginia; available at [http://www.jlab.org/intralab/calendar/dnp\\_tm](http://www.jlab.org/intralab/calendar/dnp_tm)
- [189] K. Maltman, N. Isgur, Phys. Rev. **D 29** (1984) 952.
- [190] R. Descartes, “The Passions of the Soul”, Hackett Publishing Company, Indianapolis/Cambridge (1989).
- [191] J. F. Germond, C. Wilkin, Nucl. Phys. **A 518** (1990) 308.
- [192] J. M. Laget, F. Wellers, J. F. Lecolley, Phys. Lett. **B 257** (1991) 254.

- [193] G. Fäldt and C. Wilkin, Phys. Scripta **64** (2001) 427.
- [194] T. Vetter, A. Engel, T. Biró, U. Mosel, Phys. Lett. **B 263** (1991) 153.
- [195] K. Nakayama, J. Speth, T.-S. H. Lee, Phys. Rev. **C 65** (2002) 045210.
- [196] B. L. Alvaredo, E. Oset, Phys. Lett. **B 324** (1994) 125.
- [197] H. Calén et al., Phys. Rev. **C 58** (1998) 2667.
- [198] M. T. Peña, H. Garcilazo, D. O. Riska, Nucl. Phys. **A 683** (2001) 322.
- [199] F. Kleefeld, M. Dillig, Acta Phys. Polon. **B 29** (1998) 3059.
- [200] S. Ceci, A. Švarc, e-Print Archive: nucl-th/0301036.
- [201] R. Czyżykiewicz, P. Moskal, Ann. Rep. (2003) IKP FZ-Jülich, available at <http://ikpe1101.ikp.kfa-juelich.de/>
- [202] R. Czyżykiewicz, PhD thesis, Jagellonian University, in preparation.
- [203] P. Winter, diploma thesis, University of Bonn (2001), Berichte des FZ-Jülich, Jül-3943 (2002), available at <http://ikpe1101.ikp.kfa-juelich.de>
- [204] R. Czyżykiewicz et al., e-Print Archive: nucl-ex/0312006; Talk presented at Hadron 03: 10th International Conference on Hadron Spectroscopy, Aschaffenburg, Germany, 31 Aug - 6 Sep (2003).
- [205] P. Winter, R. Czyżykiewicz et al., e-Print Archive: nucl-ex/0406034, Letter of Intent **No. 17** for an experiment with an  $4\pi$  electro-magnetic calorimeter at COSY. Presented at Finuphy Workshop on Advanced Electromagnetic Calorimetry (2004).
- [206] M. P. Rekalo, J. Arvieux, E. Tomasi-Gustafsson, Phys. Rev. **C 55** (1997) 2630.
- [207] R. Descartes, “Rules For The Direction of The Mind”, Descartes Philosophical Writings. Thomas Nelson and Sons Ltd., London (1954). available at <http://faculty.uccb.ns.ca/philosophy/kbryson/rulesfor.htm>.
- [208] H. Machner, J. Haidenbauer, J. Phys. **G 25** (1999) R231.
- [209] M. Altmeier et al., Phys. Rev. Lett. **85** (2000) 1819.
- [210] A. Sibirtsev, W. Cassing, Eur. Phys. J. **A 2** (1998) 333.
- [211] R. Plötzke et al., Phys. Lett. **B 444** (1998) 555.
- [212] P. Ball, J.-M. Frère and M. Tytgat, Phys. Lett. **B 365** (1996) 367.
- [213] S. D. Bass, S. Wetzell and W. Weise, Nucl. Phys. **A 686** (2001) 429.
- [214] S. D. Bass, e-Print Archive: hep-ph/0006348; Proceedings of the 8th Int. Workshop On Deep Inelastic Scattering And QCD (DIS 2000), April 25–30, 2000, Liverpool, England; Eds. J. A. Gracey and T. Greenshaw, World Scientific, Singapore (2001) 206.
- [215] S. D. Bass, Eur. Phys. J. **A 5** (1999) 17.
- [216] N. Nikolaev, CosyNews **No. 3** May 1998, Published by the FZ-Jülich in Cooperation with CANU, the COSY User Organisation of the Universities
- [217] E. Kou, Phys. Rev. **D 63** (2001) 054027.
- [218] S. D. Bass, Innsbruck University, private communication (2001).
- [219] S. D. Bass, e-Print Archive: hep-ph/0108187, Schriften des FZ-Jülich: Matter and Materials **11** (2002) 11. Proceedings of the Symp. on Threshold Meson Production in pp and pd Interactions, June 20–24, 2001, Cracow, Poland; Eds. P. Moskal and M. Wolke.
- [220] M. Dillig, e-Print Archive: hep-ph/0202067.
- [221] N. I. Kochelev, V. Vento, A.V. Vinnikov, Phys. Lett. **B 472** (2000) 247.
- [222] F. Kleefeld, M. Dillig, F. Pilotto, Acta Phys. Pol. **B 27** (1996) 2867.
- [223] M. Dillig, e-Print Archive: nucl-th/0201050.

- [224] H. von Bingen, "Scivias", Bear & Company, Santa Fe, New Mexico (1986).
- [225] B. Magee, "Confessions of a Philosopher", Phoenix Paperback, London (2002).
- [226] Proceedings of the Workshop on the Structure of the  $\eta'$  Meson. New Mexico State University and CEBAF, Las Cruces, New Mexico, March 8, 1996, World Scientific (1996), Eds. M. Burkardt, J. Goity, V. Papavassiliou, S. Pate.
- [227] G. Fäldt, T. Johansson, C. Wilkin, *Physica Scripta* **T 99** (2002) 146.
- [228] K. Nakayama, H. Haberzettl, *Phys. Rev.* **C 69** (2004) 065212.
- [229] B. Krusche, S. Schadmand, *Prog. Part. Nucl. Phys.* **51** (2003) 399.
- [230] R. Czyżykiewicz, diploma thesis, Jagellonian University (2002), Berichte des FZ-Jülich, Jül-4017 (2002). available at <http://ikpe1101.ikp.kfa-juelich.de/>
- [231] K. Kilian, caffee break lecture, Jülich (2004).
- [232] B. Maglich, HADRON'03: X International Conference on Hadron Spectroscopy August 31 - September 6, 2003, Aschaffenburg, Germany. AIP Conf. Proc. (2004) in print.
- [233] B. Maglich, *Schriften des FZ-Jülich: Matter & Materials* (2004) in print; Proceedings of the Second Symposium on Threshold Meson Production in pp and pd Interaction, June 1-3, 2004, Cracow, Poland.
- [234] H. Stockhorst, *Schriften des FZ-Jülich: Matter & Materials* **11** (2002) 176; Proceedings of the Symp. on Threshold Meson Production in pp and pd Interactions, June 20-24, 2001, Cracow, Poland; Eds. P. Moskal and M. Wolke.
- [235] B. Russell, "Religion and Science", Oxford University Press, New York (1997).
- [236] M. Wolke, PhD thesis, University of Bonn (1998); Berichte des FZ-Jülich, Jül-3532 (1998), available at <http://ikpe1101.ikp.kfa-juelich.de/>
- [237] P. Moskal, PhD thesis, Jagellonian University (1998), Berichte des FZ-Jülich, Jül-3685 (1999), available at <http://ikpe1101.ikp.kfa-juelich.de/>
- [238] K. R. Popper, "Conjectures and Refutations", Routledge and Kegan Paul Ltd., London (1963).
- [239] R. Maier, *Nucl. Instr. & Meth.* **A 390** (1997) 1.
- [240] H. Dombrowski et al., *Nucl. Instr. & Meth.* **A 386** (1997) 228.
- [241] A. Khoukaz, PhD thesis, Westfälische Wilhelms-Universität Münster (1996).
- [242] B. Gugulski et al., Berichte des FZ Jülich, KFA-IKP(I)-1992-3 (1992).
- [243] P. Moskal, diploma thesis, Jagellonian University (1993), Berichte des FZ Jülich; Jül-2825 (1993).
- [244] M. Wolke, diploma thesis, Westfälische Wilhelms-Universität Münster, Berichte des FZ Jülich; Jül-2852 (1993).
- [245] G. Anton et al., *Nucl. Instr. & Meth.* **A 310** (1991) 631.
- [246] M. Köhler et al., Berichte des FZ Jülich; Jül-3071, 1995
- [247] B. Maglič, G. Costa, *Phys. Lett.* **18** (1965) 185.
- [248] P. Moskal, Ann. Rep. 1997, IKP FZ-Jülich, Jül-3505 (1998) 41. available at <http://ikpe1101.ikp.kfa-juelich.de/>
- [249] K. R. Popper, "In Search of a Better World", Routledge, London and New York (2000).
- [250] P. Moskal, Ann. Rep. 1996, IKP, FZ Jülich, Jül-3365 (1997) 36. available at <http://ikpe1101.ikp.kfa-juelich.de/>
- [251] A. Khoukaz et al., *Eur. Phys. J.* **D 5** (1999) 275.
- [252] M. Schulz-Rojahn, PhD thesis, Rheinische Friedrich-Wilhelm-Universität Bonn (1998).
- [253] D. Albers et al., *Phys. Rev. Lett.* **78** (1997) 1652.



- [254] S. Baker, R.D. Cousins, Nucl. Instr. & Meth. **221** (1984) 437.
- [255] G. J. Feldman, R. D. Cousins, Phys. Rev. **D 57** (1998) 3873.
- [256] S. van der Meer, Rev. Mod. Phys. **57** (1985) 689.
- [257] D. Möhl, CERN **84-15** (1984) 97.
- [258] C. F. Gauss, Abhandlungen zur Methode der kleinsten Quadrate, Königl. Geodätisches Institut (1887).
- [259] G. A. Bürger, Münchhausen, Tosa Verlag, Wien.
- [260] Z. Herbert, "The power of taste", Selected Poems, Wydawnictwo Literackie, Kraków (2003).
- [261] E. Roderburg et al., Acta Phys. Pol. **B 31** (2000) 2299.
- [262] R. J. Slobodrian, Rep. Prog. Phys. **34** (1971) 175.
- [263] M. Lacombe et al., Phys. Lett. **101B** (1981) 139.
- [264] S. Häggström, PhD thesis, Acta Universitatis Upsaliensis **13** (1997).
- [265] I. Lehmann et al., Nucl. Instr. & Meth. **A**, in print.
- [266] F. Duncan et al., Phys. Rev. Lett. **80** (1998) 4390.
- [267] L. P. Kaptari, B. Kämpfer, S. S. Semikh, e-Print Archive: nucl-th/0212066.
- [268] M. Garçon, J.W. Van Orden, Adv. Nucl. Phys. **26** (2001) 293.
- [269] Y.S. Golubeva et al., Eur. Phys. J. **A 7** (2000) 271.
- [270] E. Chiavassa et al., Phys. Lett. **B 337** (1994) 192.
- [271] R. Smith and C. Wilkin, Nuovo Cimento Lett. **IV** (1970) 647.
- [272] Erasmus of Rotterdam, "Praise of Folly", Prefatory Letter to Thomas More, Penguin Books, London (1993).
- [273] M. Janusz, P. Moskal, Ann. Rep. 2003, IKP, FZ-Jülich, Germany (2004); E. Białkowski, J. Majewski, P. Moskal, J. Uehlemann, Ann. Rep. 2001, IKP, FZ-Jülich, Jül-3978 (2002) p.22; J. Majewski, E. Białkowski, R. Czyżykiewicz, O. Felden, G. Friori, P. Moskal, Ann. Rep. 2001, IKP, FZ-Jülich, Jül-3978 (2002) p.21.
- [274] M. Janusz, diploma thesis, Jagellonian University (2004).  
available at <http://ikpe1101.ikp.kfa-juelich.de/>
- [275] P. Moskal, Ann. Rep. 2001, IKP, FZ-Jülich, Jül-3978 (2002) p.19; P. Moskal, Ann. Rep. 1996, IKP, FZ-Jülich, Jül-3365 (1997) p.35; M. Janusz, R. Czyżykiewicz, W. Migdał, P. Moskal, Ann. Rep. 2002, IKP, FZ-Jülich, Germany (2003); T. Rożek, P. Moskal, Ann. Rep. 2002, IKP, FZ-Jülich, Germany (2003).
- [276] J. Przerwa, e-Print Archive: hep-ex/0408016; diploma thesis, Jagellonian University (2004), Berichte des FZ-Jülich, Jül-4141 (2004).
- [277] H. Hahn et al., Phys. Rev. Lett. **82** (1999) 2258.
- [278] S. Barsov et al., e-Print Archive: nucl-ex/0305031.
- [279] A. Kudriavtsev, ITEP Moscow, private communication (2001).
- [280] Ch. Hanhart, FZ-Jülich, private communication (2001).
- [281] R. Descartes, "Discourse on Method", The Liberal Arts Press, inc. New York (1956).
- [282] S. AbdEl Samad et al., Eur. Phys. J. **A 17** (2003) 595.